



Renilson, M.R. (1981) The broaching of ships in following seas. PhD thesis

<http://theses.gla.ac.uk/6615/>

Copyright and moral rights for this thesis are retained by the author

A copy can be downloaded for personal non-commercial research or study, without prior permission or charge

This thesis cannot be reproduced or quoted extensively from without first obtaining permission in writing from the Author

The content must not be changed in any way or sold commercially in any format or medium without the formal permission of the Author

When referring to this work, full bibliographic details including the author, title, awarding institution and date of the thesis must be given.

THE BROACHING OF SHIPS
IN FOLLOWING SEAS

by

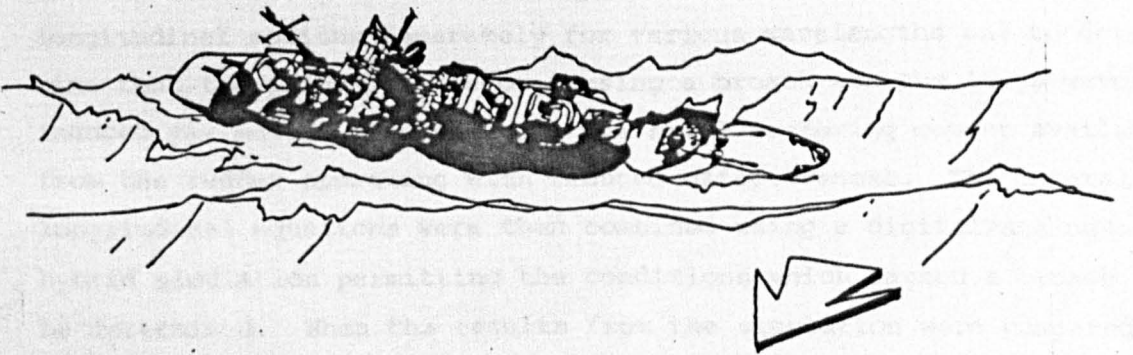
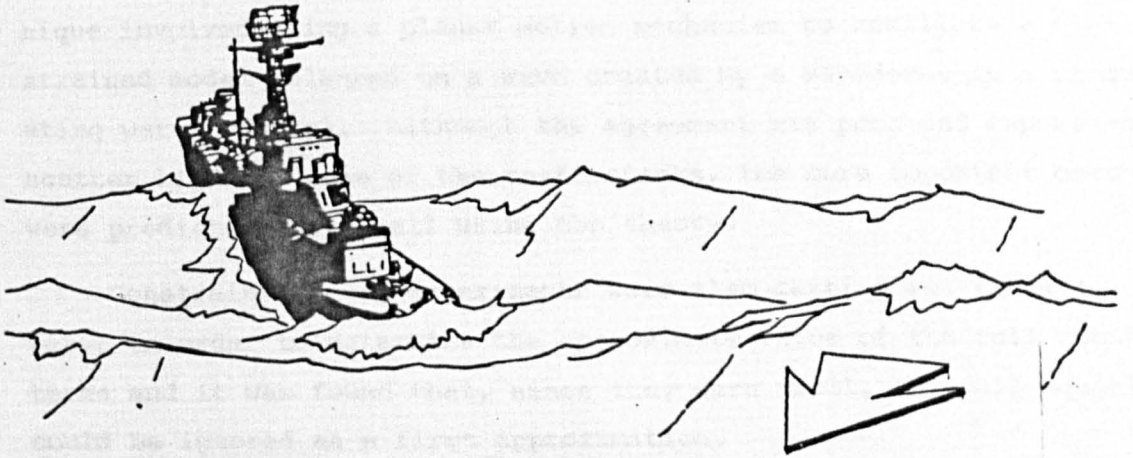
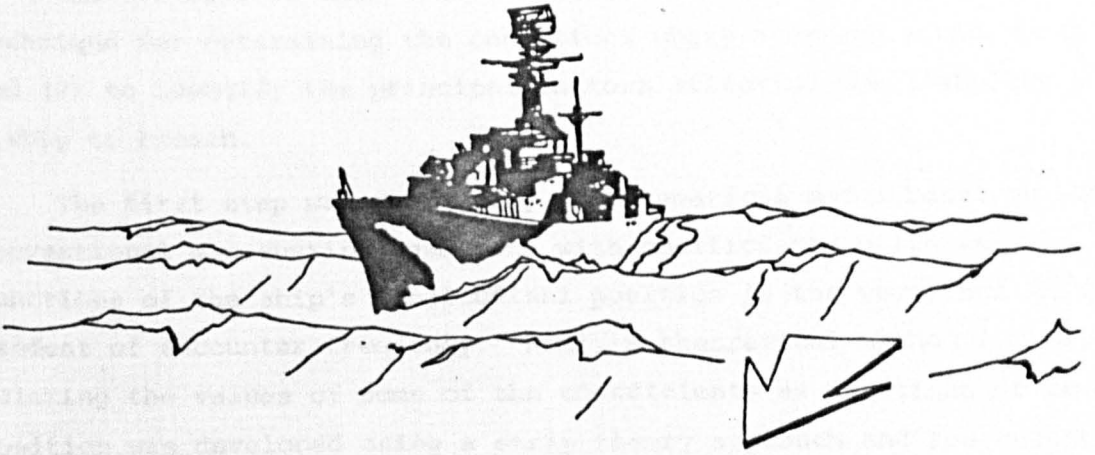
M.R. Renilson

A thesis submitted for the Degree of Doctor
of Philosophy in the Department of Naval
Architecture and Ocean Engineering at the
University of Glasgow

December 1981

BEST COPY AVAILABLE.

VARIABLE PRINT QUALITY



Frontispiece "Broaching-to" (Taken from Ref. 2)

SUMMARY

The two aims of this work were: (1) to develop a theoretical technique for determining the conditions where a broach would occur, and (2) to identify the principal factors affecting the liability of a ship to broach.

The first step was to develop a mathematical model based on the conventional manoeuvring equations with coefficients which were functions of the ship's longitudinal position in the wave, but independent of encounter frequency. Next, a theoretical method for calculating the values of some of the coefficients as functions of wave position was developed using a strip theory approach and the results compared with those obtained experimentally. The experimental technique involved using a planar motion mechanism to oscillate a constrained model balanced on a wave created by a wavedozer in a circulating water channel. Although the agreement was poor and experimental scatter high for some of the coefficients, the more important ones were predicted quite well using the theory.

Constrained model experiments were also carried out in calm water in order to determine the approximate value of the roll coupling terms and it was found that, since they were small, the roll equation could be ignored as a first approximation.

It was then possible to study the stability of the lateral and longitudinal motions separately for various wavelengths and to determine that the principal factor causing a broach was the large wave-induced yaw moment combined with the small restoring moment available from the rudder operating with reduced effectiveness. The lateral and longitudinal equations were then combined using a digital/analogue hybrid simulation permitting the conditions which caused a broach to be determined. When the results from the simulation were compared with experimental results which had already been carried out by the Admiralty Marine Technology Establishment at Haslar there was fairly good agreement, implying that this method could be used to determine whether a proposed design would meet an acceptable standard.

Finally, possible improvements to the simulation were suggested and guidelines for reducing the liability to broach were given both for the operator and the designer.

ACKNOWLEDGEMENTS

This thesis is based on work carried out at the University of Glasgow which was funded by the SRC, and the author is indebted to Professor D. Faulkner and Dr. A.M. Ferguson who made this possible.

The experiments carried out at the National Maritime Institute were funded by the Admiralty Marine Technology Establishment, and the author is very grateful to the staff of both of these organisations without whose help the experiments could not have been completed. In particular, Mr. B.N. Steele, Dr. A.M. Ferguson and Mr. J.A.H. Paffett are to be thanked for making this possible.

The encouragement and interest shown by Mr. P.D. Marshall (previously at AMTE(H)), Dr. A.R.J.M. Lloyd, Mr. J.F.W. Anslow and Professor R.K. Burcher of AMTE(H), and Dr. R.C. McGregor of the University of Glasgow is gratefully acknowledged.

The author would like to record a special thanks to Mr. A. Driscoll who acted as liaison officer at AMTE(H) during the whole period of the project, and without whom the co-operation between the University of Glasgow and the Admiralty Marine Technology Establishment would not have gone nearly so smoothly.

Finally, the author would like to thank Mrs. H. Taylor and Mrs. M. Frieze for typing the manuscript, Mr. G. Kerr for drawing the figures, and all his colleagues in the Department for their useful comments and helpful advice.

DECLARATION

*Except where reference is made to
the work of others this thesis is
believed to be original.*

* * *

CONTENTS

	Page
FRONTISPIECE	(ii)
SUMMARY	(iii)
ACKNOWLEDGEMENTS	(iv)
DECLARATION	(v)
LIST OF FIGURES	(ix)
Chapter 1 <u>INTRODUCTION</u>	1
Previous Work on Broaching	1
<i>Physical Model Approach</i>	1
<i>Mathematical Model Approach</i>	2
Background to the Present Study	4
Definition of a Broach	8
Objectives and Scope of the Present Study	10
Chapter 2 <u>MATHEMATICAL MODEL</u>	12
The Equations of Motion	14
<i>The Conventional Manoeuvring Equations</i>	14
<i>The Equations for the Broaching Model</i>	14
<i>Autopilot Equation</i>	15
Stability	16
<i>Calm Water Stability Criteria</i>	16
<i>Stability Criteria in the Following Sea</i>	17
<i>Addition of Rudder Terms</i>	18
<i>Equilibrium Rudder Angle</i>	19
<i>Longitudinal Stability</i>	20
Chapter 3 <u>CALCULATION OF THE HYDRODYNAMIC COEFFICIENTS</u>	22
Introduction	22
Sway Force and Yawing Moment due to Heading Angle	23
<i>Pressure Force</i>	24
<i>Acceleration Force</i>	27
Longitudinal Force	30
<i>Pressure Force</i>	31
<i>Acceleration Force</i>	32
Rudder Derivatives	37
Manoeuvring Derivatives	40

<u>CONTENTS, Contd.</u>		Page
Chapter 4	<u>CONSTRAINED MODEL EXPERIMENTS</u>	43
	Introduction	43
	Heel-Induced Yaw Moment and Sway Force Experiments	43
	<i>Free Running Experiments</i>	43
	<i>Constrained Model Experiments</i>	45
	The Development of the Wavedozer	47
	<i>General</i>	47
	<i>Preliminary Experiments</i>	51
	<i>Design/Manufacture</i>	52
	<i>Calibration</i>	52
	<i>Results</i>	55
	Planar Motion Mechanism Experiments	57
	<i>General</i>	57
	<i>Experiment Specification</i>	57
	<i>Experiment Procedure</i>	61
	<i>Analysis</i>	62
	<i>Results</i>	66
Chapter 5	<u>COMPARISON BETWEEN THEORETICAL AND EXPERIMENTAL DETERMINATION OF THE COEFFICIENTS</u>	68
	Conclusions	70
Chapter 6	<u>THE EFFECT OF THE VARIATION OF THE COEFFICIENTS OF THE EQUATIONS OF MOTION</u>	78
	The Wave-Induced Longitudinal Force	78
	Wave-Induced Yaw Moment	80
	The Calm Water Stability Criteria	80
	Rudder Effectiveness	80
	Equilibrium Rudder Angle	83
	Solution of the Lateral Equations of Motion	86
	Conclusions	88

<u>CONTENTS</u> , <i>Contd.</i>		Page
Chapter 7	<u>SIMULATION</u>	90
	Surging	90
	Lateral Simulation	92
	Simulation of Longitudinal and Lateral Motions Combined	94
	Comparison of Simulation with Free Running Model Experiments	98
	Discussion	101
Chapter 8	<u>DISCUSSION AND CONCLUSIONS</u>	108
	Simulation	108
	<i>Possible Improvements to the Mathematical Model</i>	108
	<i>Possible Improvements to the Coefficient Prediction Method</i>	109
	<i>Conclusions</i>	109
	Factors Affecting a Broach	110
	<i>Guidelines for Reducing the Liability to Broach at the Operating Stage</i>	111
	<i>Guidelines for Reducing the Liability to Broach at the Design Stage</i>	112
	Closure	113
APPENDIX (A)	- CO-ORDINATE SYSTEMS	114
APPENDIX (B)	- NOTATION	116
APPENDIX (C)	- SUMMARY OF COMPUTER PROGRAMS	121
APPENDIX (D)	- PLANAR MOTION MECHANISM ANALYSIS	123
	<i>Data Handling</i>	123
	<i>Conventional PMM Analysis</i>	123
	<i>Modified Analysis</i>	128
REFERENCES		135
BIBLIOGRAPHY		139

LIST OF FIGURES

	Page
Frontispiece "Broaching to"	(ii)
 CHAPTER 1	
1.1 Plot of steered run	5
1.2 Plot of broached run	5
1.3 Broaching zone for standard rudder	6
1.4 Broaching zone for $\frac{1}{2}$ depth rudder	7
 CHAPTER 2	
2.1 Profile of the ship in two different positions	12
2.2 Illustrative plot of X force along wavelength	21
 CHAPTER 3	
3.1 Profile of the hull in a wave	22
3.2 Schematic view of the hull in a wave	23
3.3 Pressure against depth for 3 positions in a wave calculated using equation 3.1	25
3.4 Comparison of C_H obtained using the Frank Close Fit Method with the Schwarz-Christoffel Transformation for a rectangular cross-section	28
3.5 Comparison of C_H obtained using the Frank Close Fit Method with the Schwarz-Christoffel Transformation for a triangular cross-section	29
3.6 Longitudinal forces acting on the hull	31
3.7 Schematic view of a transverse strip showing a trapezohedron δ_z thick	33
3.8 Rhombus formed from trapezium	34
3.9 Z-plane for Schwarz-Christoffel transformation	35
3.10 Position of wave waterline relative to rudder	39
 CHAPTER 4	
4.1 Schematic diagram of experiments in CWC	44
4.2 Arrangement of model for heel-induced yaw moment and sway force experiments	48
4.3 Sway force against heel angle	48
4.4 Yaw moment against heel angle	49

LIST OF FIGURES, Contd.

	Page	
4.5	Sway force and yaw moment against speed	50
4.6	Final design of wavedozer	53
4.7	Fully assembled wavedozer	54
4.8	λ/h against running water depth	56
4.9	Body plan of fine form model	58
4.10	General arrangement of fine form model	59
4.11	Diagrammatic arrangement of instrumentation	60
4.12	Model in a wave	63
4.13	Rudder ventilation in a wave	64
CHAPTER 5		
5.1	Trim as a function of ξ	71
5.2	Non-dimensional X-force as a function of ξ	71
5.3	Y'_{α} as a function of ξ	72
5.4	N'_{α} as a function of ξ	72
5.5	Y'_{δ} as a function of ξ	73
5.6	N'_{δ} as a function of ξ	73
5.7	Y'_v as a function of ξ	74
5.8	N'_v as a function of ξ	74
5.9	$(Y'_r - m)'$ as a function of ξ	75
5.10	$(N'_r - mx'_G)'$ as a function of ξ	75
5.11	$(Y'_v - m)'$ as a function of ξ	76
5.12	$(N'_v - mx'_G)'$ as a function of ξ	76
5.13	$(Y'_r - mx'_G)'$ as a function of ξ	77
5.14	$(N'_r - I'_z)'$ as a function of ξ	77
CHAPTER 6		
6.1	X' force as a function of ξ for various λ/L 's	79
6.2	N'_{δ} as a function of ξ for various λ/L 's	79
6.3	Calm water stability criteria, C, as a function of ξ	81
6.4	N'_{δ} as a function of ξ for various λ/L 's	82
6.5	N'_{δ} as a function of ξ for various ship conditions	82
6.6	δ_{eq}/α_0 as a function of ξ for $\lambda/L = 0.9$ $\lambda/h = 28$	84
6.7	δ_{eq}/α_0 as a function of ξ for $\lambda/L = 1.0$ $\lambda/h = 28$	84

LIST OF FIGURES, Contd.

	Page
6.8 δ_{eq}/α_0 as a function of ξ for $\lambda/L = 1.4$, $\lambda/h = 28$	85
6.9 δ_{eq}/α_0 as a function of ξ for various wavelengths	85
6.10 The real part of the principal root as a function of ξ	87
6.11 The real part of the principal root as a function of ξ	87
CHAPTER 7	
7.1 Digital simulation of surging; varying ξ_0	91
7.2 Comparison of digital and analogue simulation of surging	93
7.3 Stability in lateral plane only; varying P_1	95
7.4 Patch diagram for complete hybrid simulation	97
7.5 Comparison between predicted and experimental results for standard rudder	99
7.6 Comparison between predicted and experimental results for $\frac{1}{2}$ depth rudder	100
7.7 Record from simulation	102
7.8 Record from simulation	104
7.9 Record from simulation	105
7.10 Record from simulation	107
APPENDIX (A)	
A1 Wave fixed co-ordinate system	115
A2 Body fixed co-ordinate system	115
APPENDIX (D)	
D1 Pure sway in calm water	124
D2 Pure sway in calm water	125
D3 Pure yaw in calm water	126
D4 Pure sway in waves	127
D5 $Y^{(v)}$ for varying v	131
D6 $Y^{(v)}/y_0 \omega$ for varying ω^2	132
D7 $Y^{(\dot{v})}$ for varying \dot{v}	133
D8 $Y^{(\dot{v})}/y_0 \omega^2$ for varying ω^2	134

Chapter 1

INTRODUCTION

Considerable difficulties have often been experienced with steering when travelling in severe following seas^[1]. The danger is that the ship will suddenly yaw from its desired course, ending up almost beam on to the wave direction despite application of maximum opposite rudder. This is known as broaching-to and the associated large heel angles can cause considerable damage and possibly even a capsize. The danger has been appreciated for many years by mariners, who can give graphic but unscientific descriptions of the behaviour of their ships under extreme conditions. The fact that the frequency of encounter is low and that surging velocities can be high makes the problem extremely non-linear and hence very difficult to investigate scientifically^[2].

Previous Work on Broaching

The work done on broaching can be divided into two separate approaches. There is the physical approach where full-scale incidents are studied in depth and where free running models are used in regular or irregular waves, in order to simulate a broach, and there is the theoretical approach which involves the setting up of a mathematical model and solving for stability. This can involve the use of constrained physical models to help determine the coefficients for the equations.

Physical Model Approach:

In 1957 Du Cane included following sea tests in an experimental programme to compare the seakeeping performance of four high speed hull forms^[3]. He used a fishing line control in a conventional towing tank and initiated a yaw by deflecting the bow of the model by hand. If the rudders could respond and return the model to its original path then the run was considered "steered". On the other hand, if the model continued to yaw, it was prevented from capsizing by a safety line and the run was considered "broached". Although this

technique seems very crude it has often been used since for investigating the liability to broach of particular ships. [For example Refs. 4 and 5.]

Boese^[6] improved upon this technique by using a radio controlled model in a large towing tank fitted with an autopilot and means of determining its exact path throughout the run. He recognised the importance of surging and concluded that it was necessary for the ship to be forced to travel at wave speed before a broach could occur.

The experiments discussed above were all carried out in regular waves in a towing tank. Paulling, et al.^[7,8] went a stage nearer the full-scale situation by using radio controlled models in San Francisco Bay. These extensive experiments involved two models about five and a half metres long running for around 200 wave encounters on a fixed heading controlled by an autopilot. The study was not one of broaching specifically, but investigated the three different modes of capsizing in following seas. Films were taken of some of the runs and it can be seen that the surging affected the motions quite considerably. Loss of directional control was found to occur either due to a succession of steep waves or due to the fact that the "vessel accelerated on the face of a wave". If the yaw was caused by one wave only it was much more dynamic and this was thought to be more likely with smaller, faster craft than those used in these experiments. (A "conventional dry cargo ship" and a "large fine high speed container ship".)

In 1962 Du Cane and Goodrich^[1] gave a comprehensive summary of the factors involved in broaching and presented a number of accounts of full-scale incidents. They showed how complex the situation was, particularly in irregular seas, and concluded that the surging motion was very important. Conolly^[2] also described a number of full-scale incidents and reviewed the work done so far, in particular pointing out the inadequacies of existing mathematical model approaches.

Mathematical Model Approach:

As early as 1948 Davidson^[9] investigated the problem of broaching using conventional manoeuvring equations with additional terms for the lateral wave forces. He calculated the value of the loss in

rudder effectiveness and obtained the value of the wave force terms from constrained model experiments in following sea conditions. Unfortunately, however, since he assumed that the sway force and yaw moment due to drift angle remained constant at their calm water value in the wave condition, the results he obtained were incorrect. In addition, he assumed that the ship was travelling at wave speed and neglected the effect of the surge equation.

This idea of using conventional manoeuvring equations with constant coefficients was continued by other authors^[10-15] with improvements in the calculation of the lateral wave forces and with contributions due to autopilot terms. Using linearised small waves, Rydill found that a stable ship could not be made unstable in a following sea. However, Wahab and Swaan found that if the waves were not considered small it was possible to obtain longitudinal positions in the wave where the ship became unstable. Since the surge equation had not been included in the above analysis it was not possible to say if the ship would spend much time in the unstable regions or if it would pass from them before a broach could be built up.

Grim recognised the importance of surging and devised an experimental method of obtaining the wave induced-surge forces^[16]. He also devised a theoretical method for obtaining the condition where the ship could be forced to travel at wave speed and stated that this was a pre-requisite for a broach to occur^[17]. He was later able to compare his theoretical results with the experimental ones given by Du Cane and Goodrich in Ref. 1. (See Grim's discussion to Ref. 1.) Boese^[6] also investigated the surging motion and, in addition to measuring its magnitude using a free running model, he studied the effect it would have on the behaviour of the ship depending on the ratio of ship speed to wave speed.

Hamamoto was the first to consider that all the coefficients in the lateral manoeuvring equations should vary in the following sea condition^[18,19]. However, he neglected the surge equation. He devised an experimental method for determining the variation of some of the coefficients and compared the results obtained with those from an adaption of a calm water theoretical method. Unfortunately,

the comparison was not favourable and he did not go on further to examine the resulting lateral stability.

Background to the Present Study

In order to investigate the liability to broach of current fine form designs the Admiralty Marine Technology Establishment at Haslar (AMTE (H)) undertook two series of free running model experiments in regular waves in their large manoeuvring basin. (This work was carried out by Nicholson^[20] and by Lloyd.) The models were steered manually by radio control from the shore on a course of about 20° to the wave direction. Since the optical tracking method gave the position of the wave with respect to the model at each time interval, the plots of the model trajectories can give a good idea of the behaviour of the model in the waves (Figures 1.1 and 1.2). The effect of the surging velocities can be seen, as can the fact that in the broaching run the model was being forced to travel at wave speed when the severe yaw was initiated^[21]. From analysing these path records it was possible to obtain a plot of λ/L against nominal F_n for a constant wave steepness. The area on this plot where broaching occurs can be denoted "broaching zone" and this is shown in Figure 1.3. The second series of experiments involved investigating the effect of altering the depth of the rudders, and the broaching zone obtained using half depth rudders can be seen in Figure 1.4. If this is compared with Figure 1.3 it can be seen that the rudder depth has a significant effect on the liability to broach of a certain ship. When the depth of the rudder was increased by 50% the model did not broach in any of the conditions tested.

The line $\omega_e = 0$ is shown in Figures 1.3 and 1.4 since this corresponds to the case where model speed equals wave speed. It is suggested that, since the model is accelerated to wave speed before being broached, the upper boundary of the broaching zone is the line corresponding to the minimum self-propulsion speed to enable the model to be surged to wave speed. Grim^[17] calculated this line theoretically and the result obtained using his method is compared with the experimental results in Ref. 20.

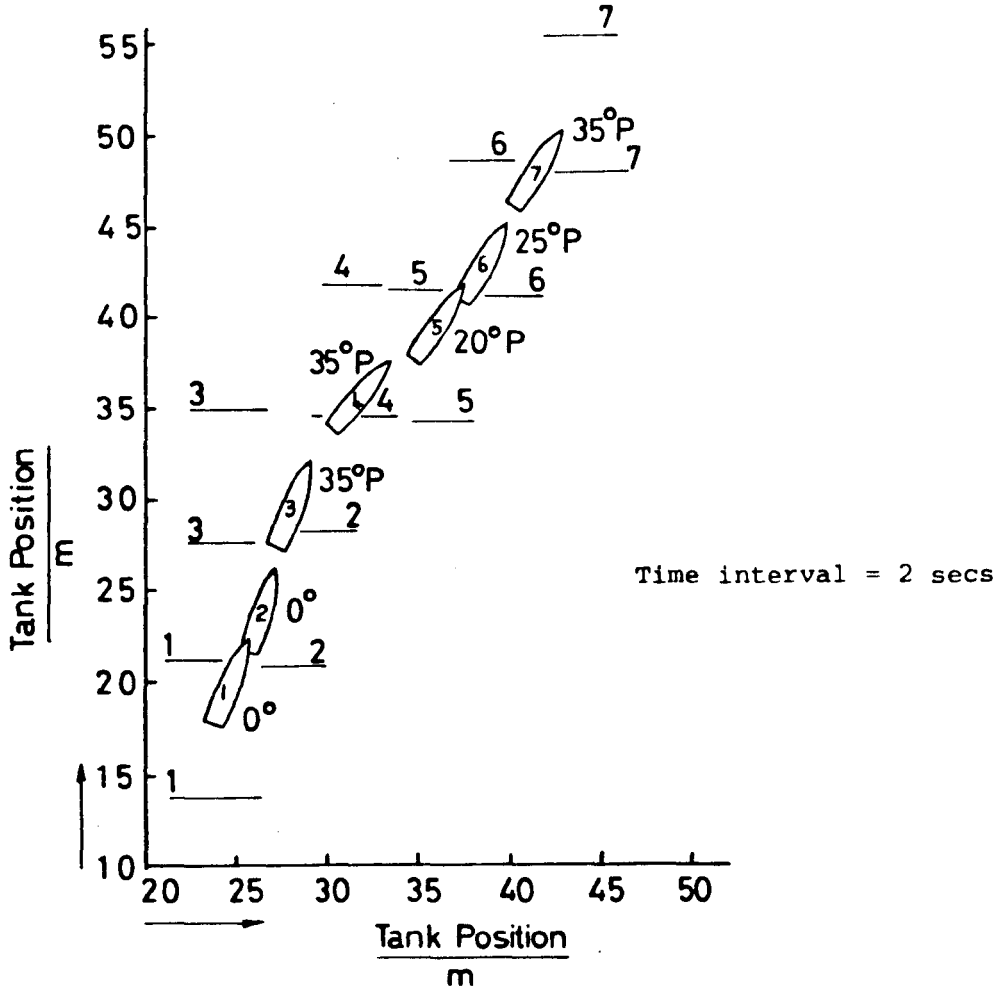


Figure 1.1 Plot of steered run (taken from Ref. 20)

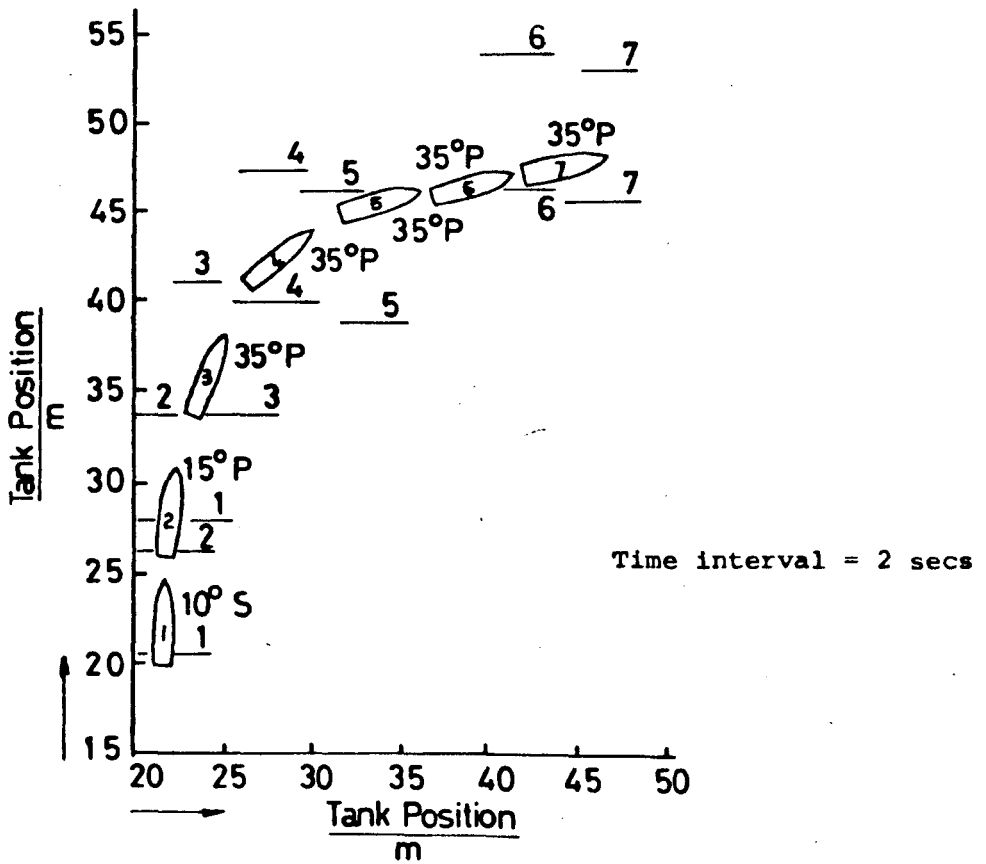


Figure 1.2 Plot of broached run (taken from Ref. 20)

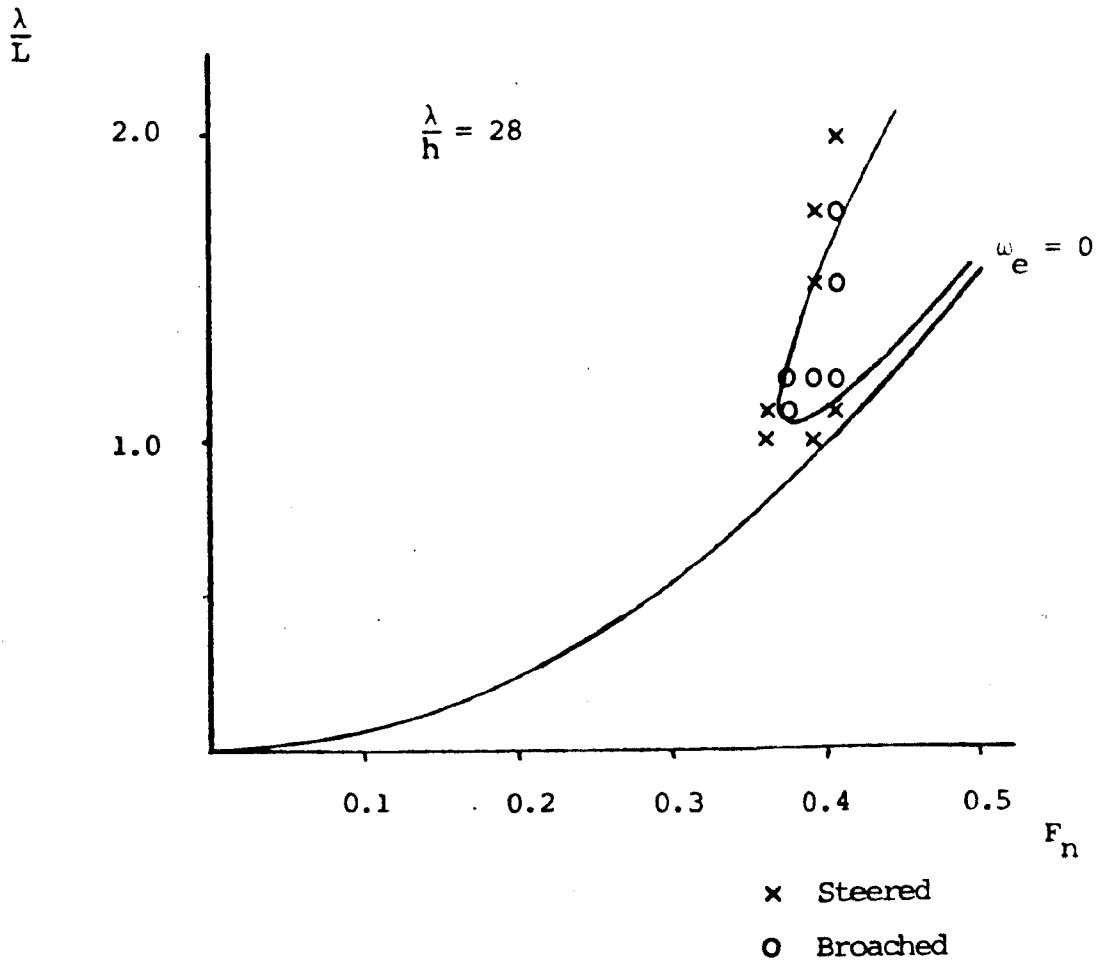


Figure 1.3 Broaching zone for standard rudder
(From an unpublished report by Lloyd)

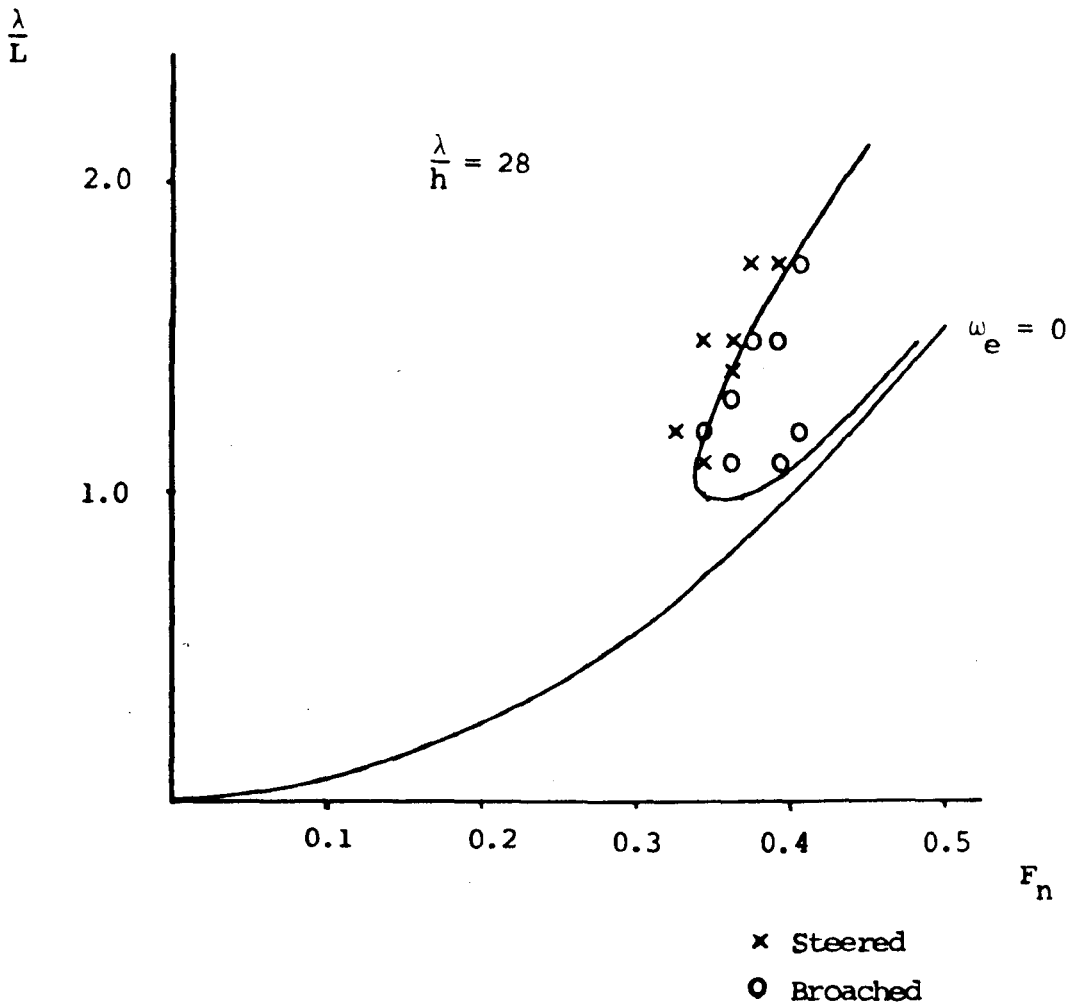


Figure 1.4 Broaching zone for $\frac{1}{2}$ depth rudder
 (From an unpublished report by Lloyd)

From these experiments Lloyd proposed a simple method of obtaining the probability of broaching in an irregular sea and a standard criteria for future ships. He suggested that, since the size of the rudders played such an important role in determining the liability to broach, it should be increased until this acceptable criteria was met. Although the work by Nicholson and Lloyd had clarified many points about broaching and had achieved "a reasonable qualitative understanding of the mechanism of broaching-to", it was still "not yet possible to quantify the forces and moments involved". Lloyd, therefore, recommended that a theoretical study of broaching be commenced in order that it might be possible to determine the minimum rudder size without recourse to experiment. In addition, it was pointed out that this approach might also lead to identification of the features of hull form which make a ship susceptible to broaching.

Definition of a Broach

Before going on to set up a mathematical model to describe the broaching condition, it is worth defining exactly what is meant by a broach. Loss of control in a following sea can occur in several ways, depending roughly on the speed of the ship compared to the speed of the waves. On one extreme, when the ship speed is much less than the wave speed, the ship will be subject to a fluctuating yawing moment as the waves pass. This moment, combined with the non-linearities introduced by the surging of the ship will, at best, result in a zig-zag path about the correct mean heading or, at worst, in a gradual shift of the mean heading, ending with the ship beam on to the waves. This worst case occurs when the ship cannot recover its original heading before the next crest strikes it, and is termed "cumulative yawing motion"^[22]. On the other extreme, when the ship speed is much greater than the waves, it will be slowed down by climbing up the back of a wave and then accelerating down its face into the trough in front. Since the ship will now have a considerable downward speed in addition to its increased forward speed, it will bury its bow in the back of the next crest, causing a sudden forward shift in the centre of lateral area and a sudden high increase in bow resistance which may cause a loss in directional stability.

This mode of loss of control is termed "bow rooting"^[22] and will occur only with very fast craft.

As has already been noted, a ship travelling slower than the waves can be accelerated to a considerably higher speed. Now, if this results in the ship travelling at the same speed as the waves, it will take up a steady state position with respect to the waves, and the periodic fluctuations will be replaced by a constant moment with a value dependent on the heading angle. For a heading angle of zero there can be no moment, and for small angles this will increase linearly.

This wave-induced yawing moment will be a function of the ship's longitudinal position in the wave, the wave length and the wave height. As can be seen from Figures 1.3 and 1.4 the length of the waves which can cause broaching will be of the order of ship length or greater, and for a steepness of $\lambda/h = 28$ the ship must have a calm water speed of $F_n = 0.35$ or greater. Therefore, since shorter ships are more likely to encounter waves of ship length or greater they are more prone to broaching than longer ships provided they are travelling fast enough. For example, a 25m long fishing boat travelling at 12 knots has a Froude number equal to 0.38 and could be in danger of broaching in a severe following sea, whereas a 200m long container ship travelling at 24 knots has a Froude number of 0.27 and is very unlikely to broach. This is because of the relative rarity of 200m plus long waves which would need to be steeper than $\lambda/h = 28$ in order to accelerate the ship to wave speed. A 100m long frigate has been known to broach while travelling at 10 knots^[23]. ($F_n = 0.16$.) However, the exact wave condition at the time is unknown.

If the moment applied by the waves is greater than that applied by the rudder then the ship will yaw, increasing the wave-induced moment and causing further yawing. If the rudder does not control the ship quickly then it will spin round till it is almost beam on to the waves. This loss of control occurs suddenly with a high rate of turn, and the centrifugal forces combined with the high heel angles can cause considerable damage or even total loss. This is known as a "true broach"^[24] and is the subject of the present investigation. For convenience, the true broach has been defined as occurring due to

one wave only and if it takes successive waves to yaw the ship then the condition is deemed to be "cumulative yawing motion".

Thus, although "cumulative yawing motion" can result in the ship ending up beam on to the waves, and possibly even capsizing, it is not being included in this present study which is involved only with a true broach as defined above. This simplifies the analysis considerably as the frequency of encounter will be almost zero during the critical phase and the ship can be assumed to be in its steady state position in the vertical plane. This is very important since, as will be seen later, it permits the coefficients of motion to be determined assuming zero encounter frequency - thus reducing the complexities of both the experimental procedure and the theoretical calculation method.

Objectives and Scope of the Present Study

The two objectives of this work are: (1) to develop a technique for theoretically predicting the broaching zones discussed above, and (2) to identify the principle factors affecting the liability of a ship to broach. The result of successfully accomplishing both these aims would be an acceptable standard against which proposed designs could be compared and sound guidelines for reducing the liability to broach, both for the design and operating stages.

In order to tackle these two objectives a simulation will be set up to predict the broaching zones. This can be used to obtain the values of the forces and moments during a broach and hence the factors affecting the liability to broach can be found.

First, a mathematical model will be developed in Chapter 2, and then a theoretical method for obtaining some of the coefficients developed in Chapter 3. Chapter 4 describes two sets of constrained model experiments. The purpose of the first set was to obtain the approximate magnitude of some of the coefficients to see if they could be ignored in order to simplify the mathematical model, while the second set provided experimental results of the coefficients calculated in Chapter 3. The experimental and theoretical coefficients are compared in Chapter 5, and Chapter 6 uses the theoretical method to obtain the coefficients for a range of wave lengths and hence to investigate

stability and the effect of small changes over the range. The complete simulation is developed in Chapter 7 and the results are compared with those obtained using the free running model experiments. The conclusions for both objectives are given in Chapter 8.

Chapter 2

MATHEMATICAL MODEL

In order to study theoretically the behaviour of a ship in a following sea at or near to the broaching condition, it is necessary to develop a mathematical model. The more complex this model the more accurate any predictions will be, but the more difficult it will be to isolate the predominant factors due to difficulties in handling the complex equations. In order to benefit from the large amount of work done on manoeuvring in calm water, it would be of great advantage to base any model on the conventional manoeuvring equations.

When a ship is travelling in a following sea and is in danger of broaching, the encounter frequency will be low, as discussed in the previous chapter. The waves will be slowly overtaking the ship and the relative longitudinal position of the ship to the wave will be important. From looking at Figure 2.1 it can easily be seen that the hydrodynamic forces will vary with longitudinal position and therefore the longitudinal equation will be required.

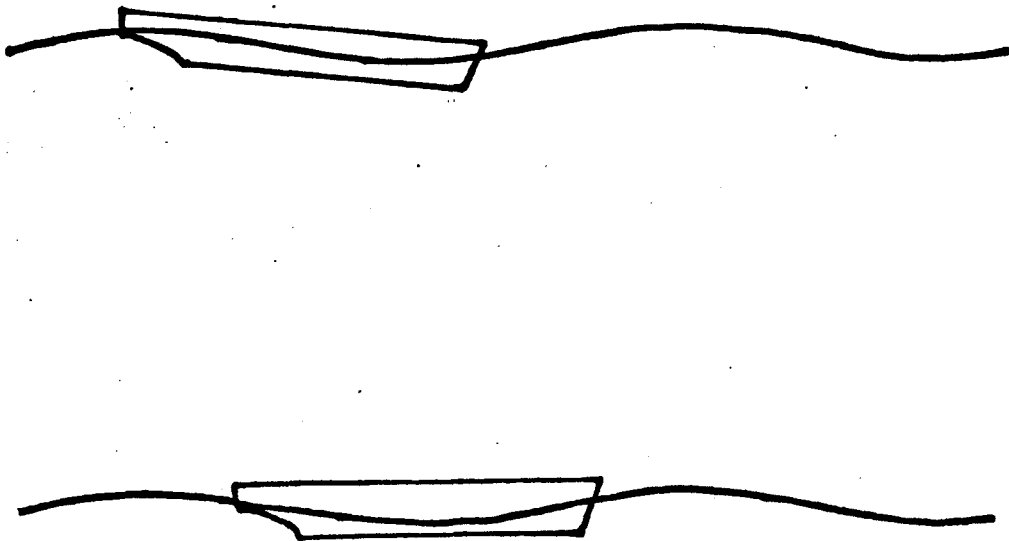


Figure 2.1 Profile of the ship in two different positions.

Since the waves are slowly overtaking the ship it is reasonable to assume that the hydrodynamic coefficients of motion will not depend on encounter frequency. That leads to the important assumption upon which all subsequent analysis is based. This is that the motion of the ship can be determined using the conventional lateral motion manoeuvring equations, with coefficients dependent on longitudinal wave position, coupled to a longitudinal equation to obtain the relative position between the ship and the wave. It is thus possible to obtain the values of the coefficients for any given longitudinal position by assuming zero frequency of encounter and hence that the ship will be in its steady state position in the vertical plane. This is important because it allows the values of the coefficients to be obtained experimentally using a constrained model held in a fixed longitudinal position with respect to the wave, and it also makes it possible to calculate the ship's position in the vertical plane for the theoretical calculation of the coefficients.

The coefficients, then, are all functions of the relative longitudinal position of the ship to the wave but are assumed to be independent of encounter frequency. The main reason for this assumption is that because the encounter frequency is sufficiently low the ship can be assumed to be in its equilibrium position in the vertical plane all the time. Obviously, as the encounter frequency increases this assumption will become less accurate so the present investigation is restricted to the very low encounter frequency case of a "true broach" as defined in the previous chapter. It may be that the method can be extended to cover the slightly higher encounter frequency of the "cumulative yawing motion" and "bow rooting" conditions and this could be the subject of a future investigation.

Although the relationship between motion and force will be far from linear in the latter stages of a broach, it is considered that linear equations could predict a broach/no broach situation during the transient phase. For this reason, together with the motivation to reduce complexity as discussed above, the present analysis is restricted to the linear equations of motion.

The Equations of Motion

The Conventional Manoeuvring Equations:

The development of these equations can be found in many places in the literature, for example Refs. 25 and 26, so it is not intended to repeat it here. It is usual to neglect the longitudinal equation, the roll coupling and, hence, the roll equation and to use right-handed body-fixed axis with origin amidships. If the resulting equations are non-dimensionalised they become

$$\begin{aligned} Y'_v v' + (Y'_\dot{v} - m') \dot{v}' + (Y'_r - m') r' + (Y'_\dot{r} - m' x'_G) \dot{r}' + Y'_\delta \delta' &= 0 \\ N'_v v' + (N'_\dot{v} - m' x'_G) \dot{v}' + (N'_r - m' x'_G) r' + (N'_\dot{r} - I'_z) \dot{r}' + N'_\delta \delta' &= 0 \\ &\dots\dots 2.1 \end{aligned}$$

As discussed in Ref. 26 these equations are based on a linearised Taylor expansion and are adequate to determine stability characteristics in calm water. Fluid memory effects have been ignored as it has been shown^[27] that they are negligible for usual ship manoeuvres.

The Equations for the Broaching Model:

As has already been discussed, the longitudinal equation must be added to the above equations if they are to be used in the following sea conditions. This is required in order to determine the wave position, denoted x_{ws} which is the x^* co-ordinate of the stern and can be non-dimensionalised as $\xi = x_{ws} / \lambda$ (see Appendix A).

The roll equation is neglected from the conventional equations because large merchant ships moving in fairly calm water remain approximately upright. It has already been shown in the previous chapter, however, that ships can adopt significant heel angles during a broach. Little work has been done on the roll coupling coefficients (Y'_ϕ, N'_ϕ) and the need to include the roll equation will depend on their value compared to the other forces and moments. If interest were to be extended to the possibility of a broach resulting in a capsize, obviously the roll equation would be required; however, the assumption of linearity in the lateral motions would probably not hold this far and non-linearities would need to be introduced as in Ref. 28. For completeness, therefore, the roll equation will be included but, as yet, with no knowledge of the relative size of the coefficients, conclusions as to how important it is cannot be made.

In calm water Y and N will be functions of: $v, \dot{v}, r, \dot{r}, \phi$ and δ . However, in the following sea condition there will be the additional dependence on heading angle to the direction of wave travel, α . Thus for the wave condition, Eqs. 2.1 become

$$\begin{aligned}
 Y'_v v' + (Y'_v - m') \dot{v}' + (Y'_r - m') r' + (Y'_r - m' x'_G) \dot{r}' \\
 + Y'_\phi \phi' + Y'_\delta \delta' + Y'_\alpha \alpha' = 0 \\
 N'_v v' + (N'_v - m' x'_G) \dot{v}' + (N'_r - m' x'_G) r' + (N'_r - I'_z) \dot{r}' \\
 + N'_\phi \phi' + N'_\delta \delta' + N'_\alpha \alpha' = 0 \\
 K'_v v' + (K'_v - m' z'_G) \dot{v}' + (K'_r - m' z'_G) r' + (K'_r - m' x'_G z'_G) \dot{r}' \\
 + (K'_p - I'_x) \dot{p}' + (K'_p - m' z'_G) p' \\
 + K'_\delta \delta' + K'_\alpha \alpha' + \Delta' GM' \phi' = 0 \\
 X'_u u' + X'_v v' + X'_r r' + (X'_u - m') \dot{u}' + X'_\delta \delta' + X'_\xi \xi = 0
 \end{aligned}
 \tag{2.2}$$

In order to reduce complexity Eqs. 2.2 are not written in functional form. However, it is important to remember that all the coefficients ($Y'_v, (Y'_v - m')$, etc.) are functions of ξ as described above.

The dependence on heading angle, α , in Eqs. 2.2 in the horizontal plane has its analogy in the vertical plane as a dependence on pitch angle, θ , when considering the submarine equations^[29].

Autopilot Equation:

Equations 2.2 contain terms dependent on the rudder angle, δ . This rudder angle is often prescribed by a helmsman but, for the model being developed, some means of determining it is required. The most convenient way to do this is to adopt the standard autopilot equation discussed in Ref. '30

$$\delta_d = P_1 \psi + P_2 \dot{\psi} \tag{2.3}$$

where P_1 and P_2 are known as the autopilot constants, and ψ is the heading error ($\psi = \alpha - \alpha_d$).

The problem with simply substituting 2.3 into 2.2 is that of time lags since neither the control system nor the rudder respond instantaneously. There are essentially two types of lag, that due to the control system (constant lag) and that due to the rudder response (exponential lag). When a desired rudder angle is called for there will be a delay before the rudder starts to move, and it will reach its maximum rate fairly quickly. It will then continue to move at this rate until it approaches the desired angle, whereupon it will slow down and stop.

Describing this procedure analytically is not simple; however, it can be set up on an analogue computer relatively easily and that is described in Chapter 7.

Stability

Before looking at the stability of the motion resulting from these equations it is worth noting that there are essentially three different classes of stability^[26]:

- (1) Straight line stability,
- (2) Directional stability, and
- (3) Positional motion stability.

If a ship possesses (1) alone it will end up travelling in a straight line with a new heading after a small disturbance. If it possesses (2) it will return to its original heading, whereas if it possesses (3) it will return to its original path. It is possible to subdivide (2) into those with complex stability roots (oscillations) and those with real roots (no oscillations).

Calm Water Stability Criteria:

Ships in calm water with rudders fixed amidships can only possess (1) at best. (Many of them do not even do this.) The criteria for rudder fixed straight line stability developed from 2.1 is

$$C = Y'_v (N'_r - m'x'_G) - N'_v (Y'_r - m') > 0 \quad \dots \quad 2.4$$

i.e. C must be positive for stability.

Comparing different ships for degree of stability on the basis of their values of C is quite common in calm water and it was suggested that ships which were more stable using this criteria would be less liable to broach. The assumption made was that the effect of the wave would be to alter the coefficients in Eq. 2.4 in order to make C negative and hence result in a broach. This assumption will be tested in Chapter 6, but for the meantime it is worth noting that many ships (notably supertankers) possess negative values of C and are easily made controllable by correct use of the rudder.

Stability Criteria in the Following Sea:

If the last two equations in 2.2 are neglected and the stability in yaw/sway only is considered, a cubic is obtained

$$A\lambda^3 + B\lambda^2 + C\lambda + D = 0 \quad \dots\dots \quad 2.5$$

where:

$$A = (Y'_V - m')(N'_R - I'_Z) - (N'_V - m'x'_G)(Y'_R - m'x'_G)$$

$$B = Y'_V(N'_R - I'_Z) + (Y'_V - m')(N'_R - m'x'_G) - N'_V(Y'_R - m'x'_G) - (N'_V - m'x'_G)(Y'_R - m')$$

$$C = Y'_V(N'_R - m'x'_G) + (Y'_V - m')N'_\alpha - N'_V(Y'_R - m') - (N'_V - m'x'_G)Y'_\alpha$$

$$D = Y'_V N'_\alpha - N'_V Y'_\alpha$$

For stability it is necessary that D/A be positive and, since A is always positive, this reduces to that of D being positive.

Since N'_V is very small and Y'_V is always large and negative, the over-riding factor is the sign of N'_α . If it is positive, the ship will be unstable, whereas if it is negative the ship will be stable. In other words, when the wave-induced yaw moment is positive a small positive heading angle will result in a positive moment, increasing the heading angle and hence causing an instability. This is intuitively correct and the addition of the roll equation will not alter the conclusions which are that, with the rudder fixed, an instability is bound to occur over that part of the wavelength which has positive N'_α . The above argument applies only to the case when the desired heading angle is zero and, in fact, results in a directional stability test.

If the desired heading angle is other than zero a negative wave-induced moment will reduce the actual angle to zero, whereas a positive yawing moment will increase the angle, resulting in a broach. Thus, the positions on the wave which are going to be important in relation to broaching are those where N'_α is positive.

Addition of Rudder Terms:

As was discussed above, when the rudder is fixed there will be regions of instability, therefore it is necessary to look at how addition of the rudder terms can reduce this.

Again neglecting the last two equations of 2.2, but now including the autopilot equation, 2.3, with no allowance for time lag gives

$$A_1 v' + B_1 \dot{v}' + (D_1 + H_1 P_1) \alpha' + (E_1 + H_1 P_2) \dot{\alpha}' + F_1 \alpha' - H_1 P_1 \alpha'_d = 0$$

$$A_2 v' + B_2 \dot{v}' + (D_2 + H_2 P_1) \alpha' + (E_2 + H_2 P_2) \dot{\alpha}' + F_2 \alpha' - H_2 P_1 \alpha'_d = 0$$

..... 2.6

where:

$$A_1 = Y'_v$$

$$A_2 = N'_v$$

$$B_1 = (Y'_v - m')$$

$$B_2 = (N'_v - m'x'_G)$$

$$D_1 = Y'_\alpha$$

$$D_2 = N'_\alpha$$

$$E_1 = (Y'_r - m')$$

$$E_2 = (N'_r - m'x'_G)$$

$$F_1 = (Y'_r - m'x'_G)$$

$$F_2 = (N'_r - I'_z)$$

$$H_1 = Y'_\delta$$

$$H_2 = N'_\delta$$

and P_1, P_2 are the autopilot constants.

If the desired heading angle is taken to be zero, Eqs. 2.6 can be written

$$(A_1 + B_1 D) v' + (D_1 + H_1 P_1 + (E_1 + H_1 P_2) D + F_1 D^2) \alpha' = 0$$

$$(A_2 + B_2 D) v' + (D_2 + H_2 P_1 + (E_2 + H_2 P_2) D + F_2 D^2) \alpha' = 0$$

..... 2.7

where D is the differential operator operating on v or α with respect to time. It can be shown^[25] that this results in the cubic

$$\lambda^3 + a_2 \lambda^2 + a_1 \lambda + a_0 = 0 \quad \dots \quad 2.8$$

where:

$$a_2 = \frac{B_1(F_2 + H_2P_2) + A_1F_2 - B_2(E_1 + H_1P_2) - A_2F_1}{B_1F_2 - B_2F_1}$$

$$a_1 = \frac{A_1(E_2 + H_2P_2) + B_1D_2 + B_1H_2P_1 - A_2(E_1 + H_1P_2) - B_2D_1 - B_2H_1P_1}{B_1F_2 - B_2F_1}$$

$$a_0 = \frac{A_1D_2 + A_1H_2P_1 - A_2D_1 - A_2H_1P_1}{B_1F_2 - B_2F_1}$$

Equation 2.8 can be solved for each position along the wavelength and the stability roots examined. This will give an indication of the effect of varying P_1 and P_2 . However, it must be remembered that this has many important simplifications. These are: neglect of time lag in the rudder response, no maximum rudder angle, no coupling with the roll equation and, perhaps most important of all, no coupling to the longitudinal equation. The effect of the longitudinal equation is important because, if the ship only spends a short time on certain parts of the wave, it may well be able to suffer being very unstable in the lateral plane for this short period of time.

Equilibrium Rudder Angle:

Another approach to the problem of lateral stability is to consider the rudder angle that would be required to keep the ship on a desired heading angle. This rudder angle is brought about by the wave-induced yawing moment causing a moment on the ship, dependent on heading angle. In order to balance this moment there will be a required rudder angle which may be termed the equilibrium rudder angle. Since there is a maximum angle permitted by the steering gear, it can be seen that if the equilibrium angle exceeds this then it is impossible for the ship to travel at the required heading angle. This analysis ignores dynamic effects but allows different parameters, such as rudder dimensions, trim angle, stern shape, etc., to be readily compared. From Eqs. 2.2, again neglecting the last two equations, the ratio of equilibrium rudder angle to heading angle can be obtained as

$$\frac{\delta_{eq}}{\alpha_0} = \frac{Y'_v N'_\alpha - N'_v Y'_\alpha}{N'_v Y'_\delta - N'_\delta Y'_v} \quad \dots \quad 2.9$$

Longitudinal Stability:

If the coupling from the lateral equations is neglected from the last equation in 2.2 it becomes

$$X'_u u' + (X'_u - m') \dot{u}' + X'_\xi = 0 \quad \dots\dots \quad 2.10$$

Now, if the change in resistance with speed and the longitudinal added mass can be considered independent of ξ , then the only term dependent on wave position in 2.10 is X'_ξ . This will be a cyclic function repeated every wavelength and can be considered as a sine curve for now. For longitudinal stability

$$X'_u u + X'_\xi = 0$$

which requires a large enough wave-induced force (X'_ξ) to counteract the increased resistance that the ship has when travelling at wave speed over that when travelling at self-propulsion speed. Figure 2.2 shows an idealised plot of X'_ξ against ξ . The lower dashed line indicates the increased resistance of a ship initially travelling at U , when travelling at wave speed. The points where this intersects the wave force indicate the equilibrium positions. The position at $\xi = 0.94$, however, is one of unstable equilibrium, since a small disturbance which produces an increase in forward force will cause a positive acceleration resulting in a larger ξ which, in turn, results in a further increase in X' . The position at $\xi = 0.32$ will be one of stable equilibrium, as any disturbance produces a contrary force.

For the same ship travelling at a different self-propulsion speed there will be a different increase in resistance when travelling at wave speed, resulting in different equilibrium positions as indicated by the chain dotted line in Figure 2.2. (This is an example of a ship initially travelling at a lower self-propulsion speed.)

A ship slowly being overtaken by waves will be accelerated and may eventually settle down into its longitudinal steady state position. Before doing this, however, it will spend more time over a certain length of the wave than on another and lateral instability may cause a broach. In order to study this possibility it is necessary to know which region of the wave the ship will spend most of its time in, and how laterally stable it will be over this region. Thus, it is neces-

ary to know the values of the coefficients in Eqs. 2.2 and how they vary with ξ .

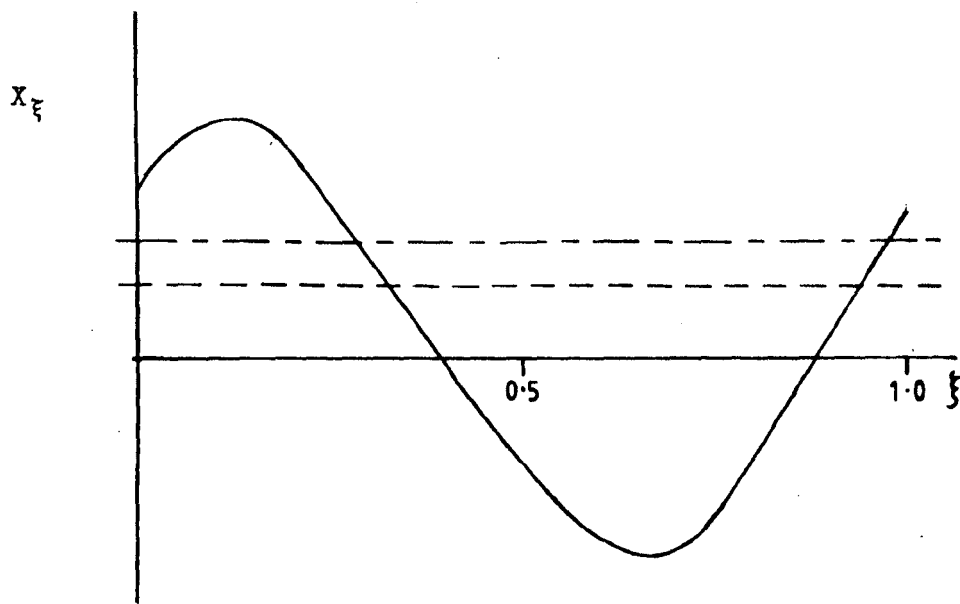


Figure 2.2 Illustrative plot of X force along wavelength.

Chapters 3 and 4 deal with obtaining these coefficients, while Chapters 6 and 7 cover the subsequent stability analysis.

Chapter 3

CALCULATION OF THE HYDRODYNAMIC COEFFICIENTSIntroduction

This chapter deals with the theoretical calculation of the coefficients used in the model developed in Chapter 2.

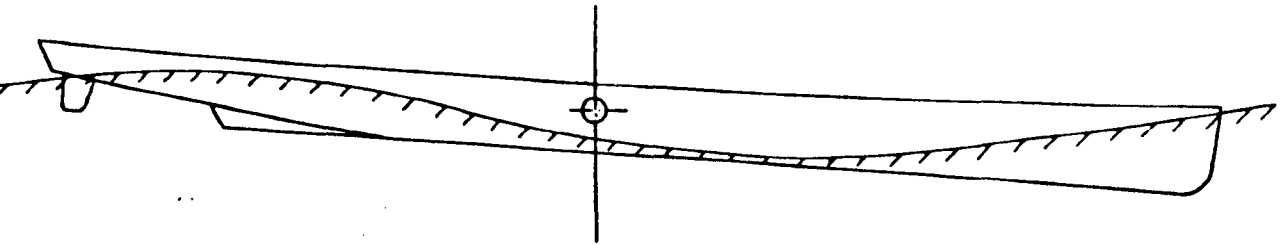


Figure 3.1 Profile Of The Hull In A Wave

Figure 3.1 shows the ship in the wave and it can be seen that the wave height will not be small compared to the draft. In addition, the wave length will be of the order of the ship length, or greater, and so it is not possible to assume infinitesimal wave height or that the ship will remain in its undisturbed position in the vertical plane. Since the coefficients are assumed to be independent of encounter frequency they can be calculated for the zero frequency of encounter condition. For this case the ship will be in its equilibrium position in the vertical plane so the pitch angle (τ) and vertical displacement (z^*) will be functions of wave position only. They are calculated by a trial and error method which adjusts the position of the ship in the vertical plane until the displacement in the wave equals that in calm

water, and the longitudinal centres of buoyancy (LCB) and gravity (LCG) are in the same longitudinal position. This has the effect of ignoring the vertical component of the Froude-Kryloff and inertia forces and assumes that the pressure varies linearly with depth from the surface of the wave. Since the vertical position of the ship in the wave is only used for calculating the lateral and longitudinal coefficients and will be altered by the fact that the ship adopts an additional trim angle due to the high speed it is thought that the above approximation is sufficiently accurate for the present purpose.

Sway Force and Yawing Moment due to Heading Angle

As described in Chapter 2, the wave-induced sway force and yawing moment are assumed to be linear functions of heading angle for small angles. They are denoted by Y_α and N_α respectively, where Y_α and N_α are functions of ξ .

In order to calculate $Y_\alpha(\xi)$ and $N_\alpha(\xi)$ it is convenient to consider the ship with a small heading angle α_0 . The ship is then divided into transverse strips δx wide, distance x from the origin (Figure 3.2).

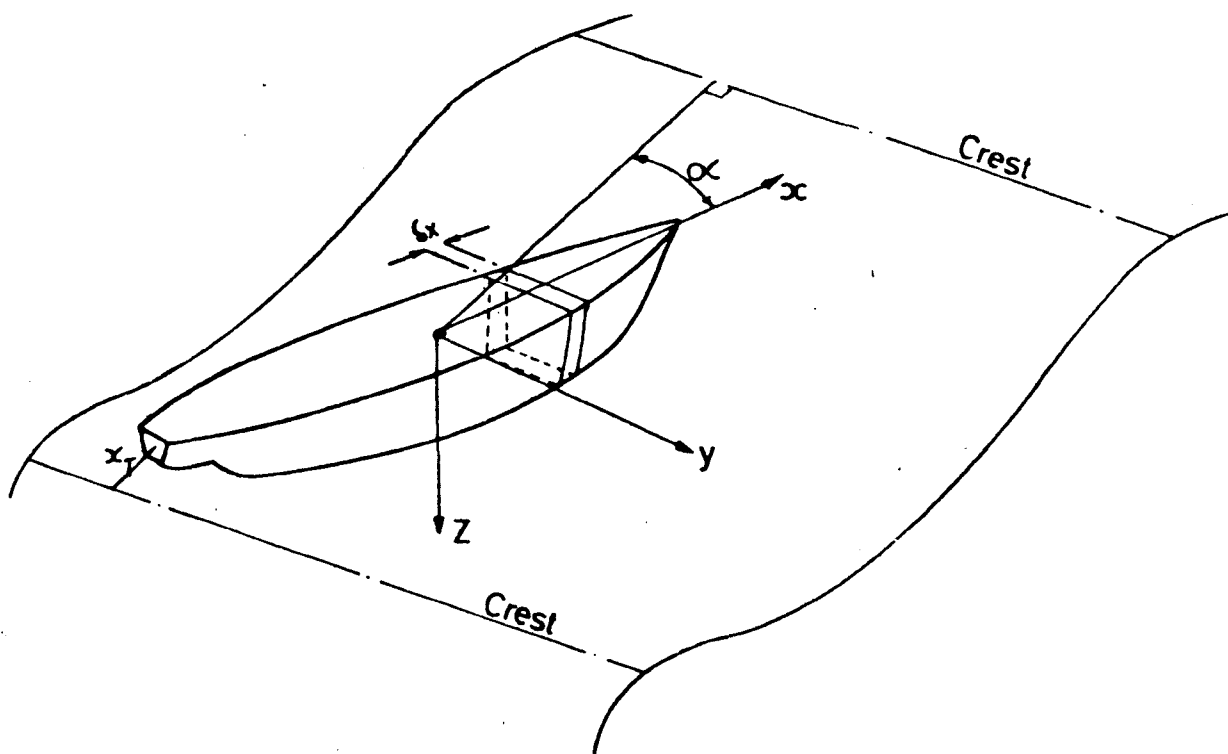


Figure 3.2 Schematic View Of The Hull In A Wave

Using the slender body assumption, the side force can be obtained by integrating the horizontal component of the force on each strip along the length of the hull. (Since the x component of the force is assumed to be negligible compared to the y component.)

The velocity forces are ignored throughout the wave force calculations as they were found to be negligibly small compared to the pressure and acceleration terms.

Pressure Force:

The pressure at any point in the wave is given by

$$P = \rho g e^{-Kz^*} \cos Kx^* + \rho g z \quad \dots \quad 3.1$$

Thus, the lateral pressure force on each strip is

$$Y_{\text{STRIP}}^P = \int_{S_P} P \, dz \, dx - \int_{S_S} P \, dz \, dx \quad \dots \quad 3.2$$

where S_S is the wetted surface on the starboard side of the strip, and S_P the wetted surface on the port side. Using

$$\eta = -A \cos Kx^* \quad \dots \quad 3.3$$

it can easily be shown that Eq. 3.1 gives a non-zero pressure on the wave surface. In other words, it does not satisfy the dynamic boundary condition on the free surface. This is because 3.1 is obtained from the linear velocity potential derived by neglecting second order terms and by applying the boundary conditions to the undisturbed plane of the free surface, $z^* = 0$.

Figure 3.3 gives a plot of pressure against depth for three wave positions; crest, node and trough. The lateral pressure force will depend on the difference in forces on each side caused by different wave positions due to the heading angle. Thus, the important factor in determining the pressure force at a depth z^* on a transverse strip is the local rate of change of pressure with respect to x^* . As can be seen from Figure 3.3, the small error in the pressure calculation resulting in a non-zero pressure at the free surface will have only a second order effect on the rate of change of pressure. It is, there-

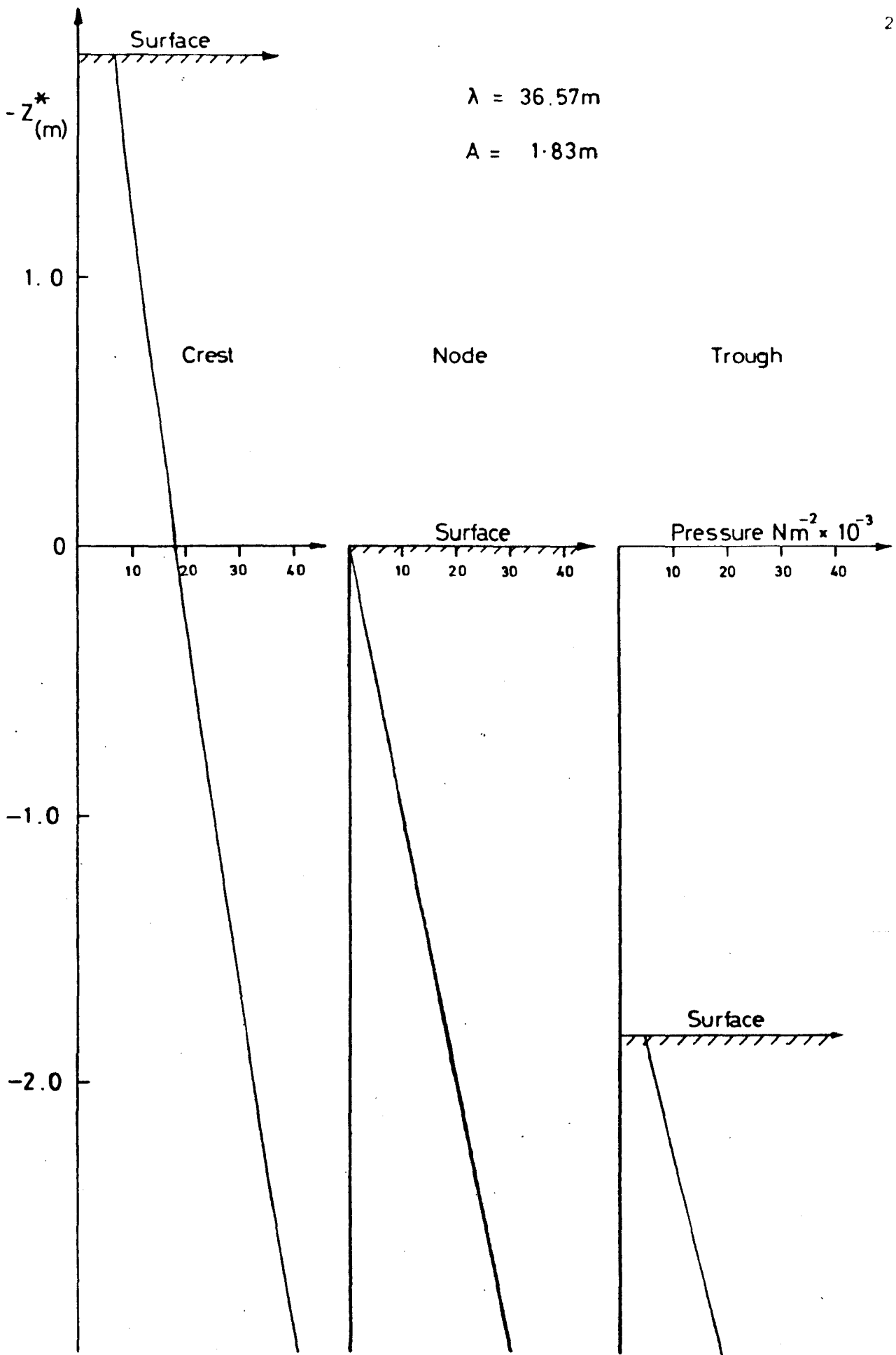


Figure 3.3 Pressure Against Depth For Three Positions In A Wave
Calculated Using Equation 3.1

fore, considered accurate enough for the present purposes to calculate the pressure using 3.1 and integrate to the free surface obtained by 3.3

Thus, the Y force on each strip will be

$$\begin{aligned}
 Y_{\text{STRIP}}^P = & - \int_{D_T}^{-A \cos Kx_{Pf}^*} \rho g (A e^{-Kz^*} \cos Kx_P^* + z^*) \delta x dz \\
 & + \int_{D_T}^{-A \cos Kx_{Sf}^*} \rho g (A e^{-Kz^*} \cos Kx_S^* + z^*) \delta x dz \quad \dots\dots \quad 3.4
 \end{aligned}$$

however, because the ship is not wall-sided but has some shape, x_S^* and x_P^* are functions of z

$$\begin{aligned}
 x_S^* &= x_T^* + x \cos \alpha + \frac{L}{2} \cos \alpha - b(z) \sin \alpha \\
 x_P^* &= x_T^* + x \cos \alpha + \frac{L}{2} \cos \alpha + b(z) \sin \alpha \quad \dots\dots \quad 3.5
 \end{aligned}$$

x_{Sf}^* and x_{Pf}^* are the values of x_S^* and x_P^* respectively on the free surface. Equations 3.5 simplify to

$$\begin{aligned}
 x_S^* &= x_T^* + x + \frac{L}{2} - b(z) \alpha \\
 x_P^* &= x_T^* + x + \frac{L}{2} + b(z) \alpha \quad \dots\dots \quad 3.6
 \end{aligned}$$

for small α and, in addition, for small pitch angle, τ , $z^* = z$.

In order to integrate 3.4 analytically, $b(z)$ must be known for each strip; therefore, it is preferred to perform the integration numerically using the values of b given as functions of z in the form of the offset tables.

Hence, the total lateral pressure force and yawing moment can be found using

$$Y^P = \int_{-\frac{L}{2}}^{\frac{L}{2}} Y_{STRIP}^P dx \quad \dots \quad 3.7$$

$$N^P = \int_{-\frac{L}{2}}^{\frac{L}{2}} Y_{STRIP}^P x dx$$

Acceleration Force:

The acceleration force can be calculated by

$$F = acc^n \times AVM \quad \dots \quad 3.8$$

Now, in order to calculate the transverse force and yawing moment, the ship is divided into strips as before. The acceleration is assumed to be constant over the width of the strip with the value at its centre-line. It will, however, vary with depth. The method used here, therefore, for calculating the acceleration force on each strip, is to obtain a mean transverse acceleration and then multiply this by the added mass for the strip.

$$acc^n = \frac{\alpha 2\pi g}{\lambda} A e^{-Kz^*} \sin Kx_C^* \quad \dots \quad 3.9$$

Integrating and dividing by the depth the mean acceleration becomes

$$\overline{acc^n} = \frac{\alpha g A}{D_{WC}} \sin Kx_C^* (e^{-KD_T} - e^{KA} \cos Kx_C^*) \quad \dots \quad 3.10$$

Thus,

$$Y_{STRIP}^a = \frac{AVM_{STRIP} \alpha g A}{D_{WC}} \sin Kx_C^* (e^{-KD_T} - e^{KA} \cos Kx_C^*) \delta x \quad \dots \quad 3.11$$

AVM_{STRIP} is the two-dimensional added mass value for the strip and can be calculated using the Schwarz-Christoffel transformation^[32] for straightsided sections, or by the Frank-Close-Fit method for ship shapes. Figures 3.4 and 3.5 show comparisons between these two

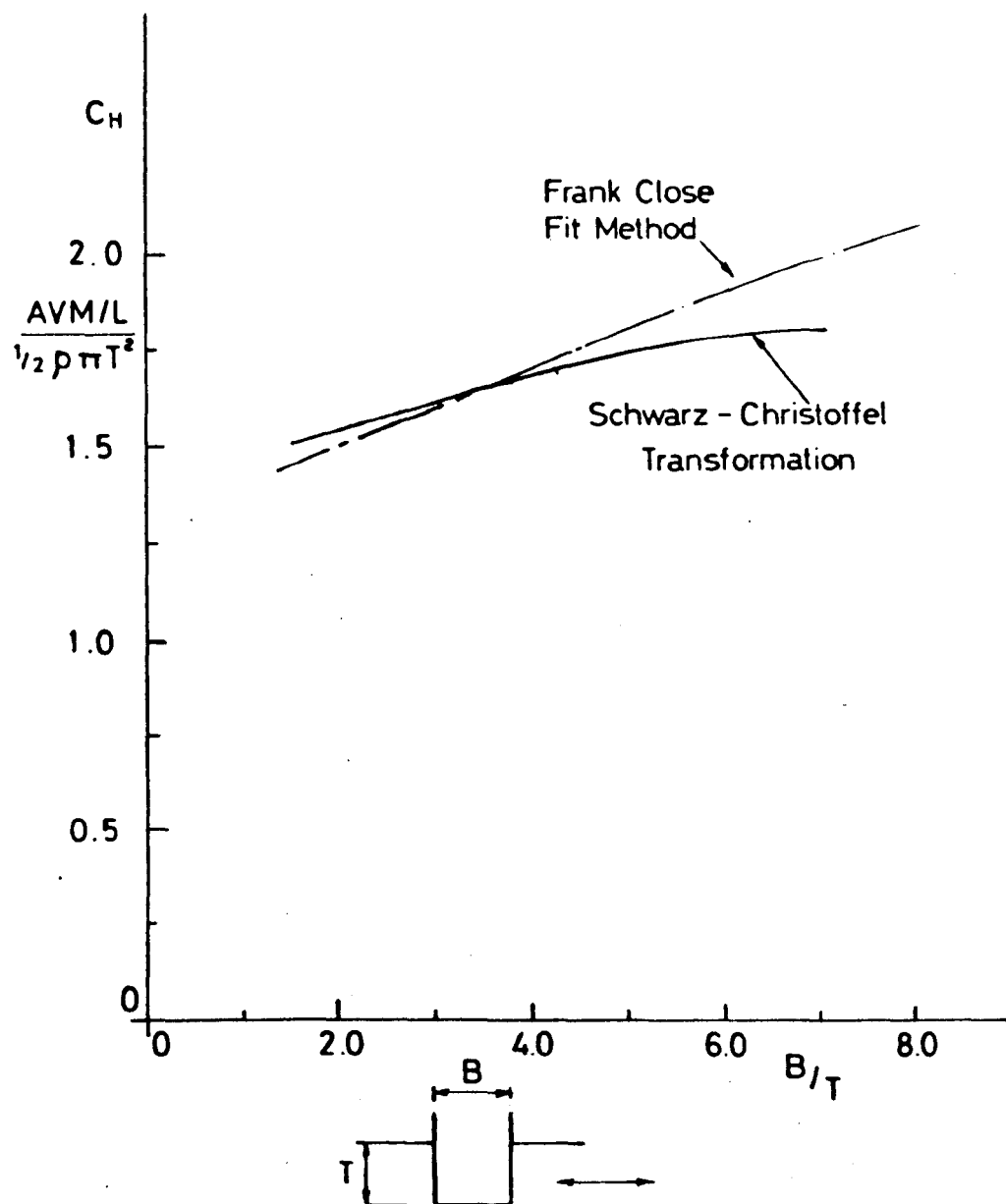


Figure 3.4 Comparison Of C_H Obtained Using The Frank Close Fit Method With The Schwarz - Christoffel Transformation For A Rectangular Cross Section

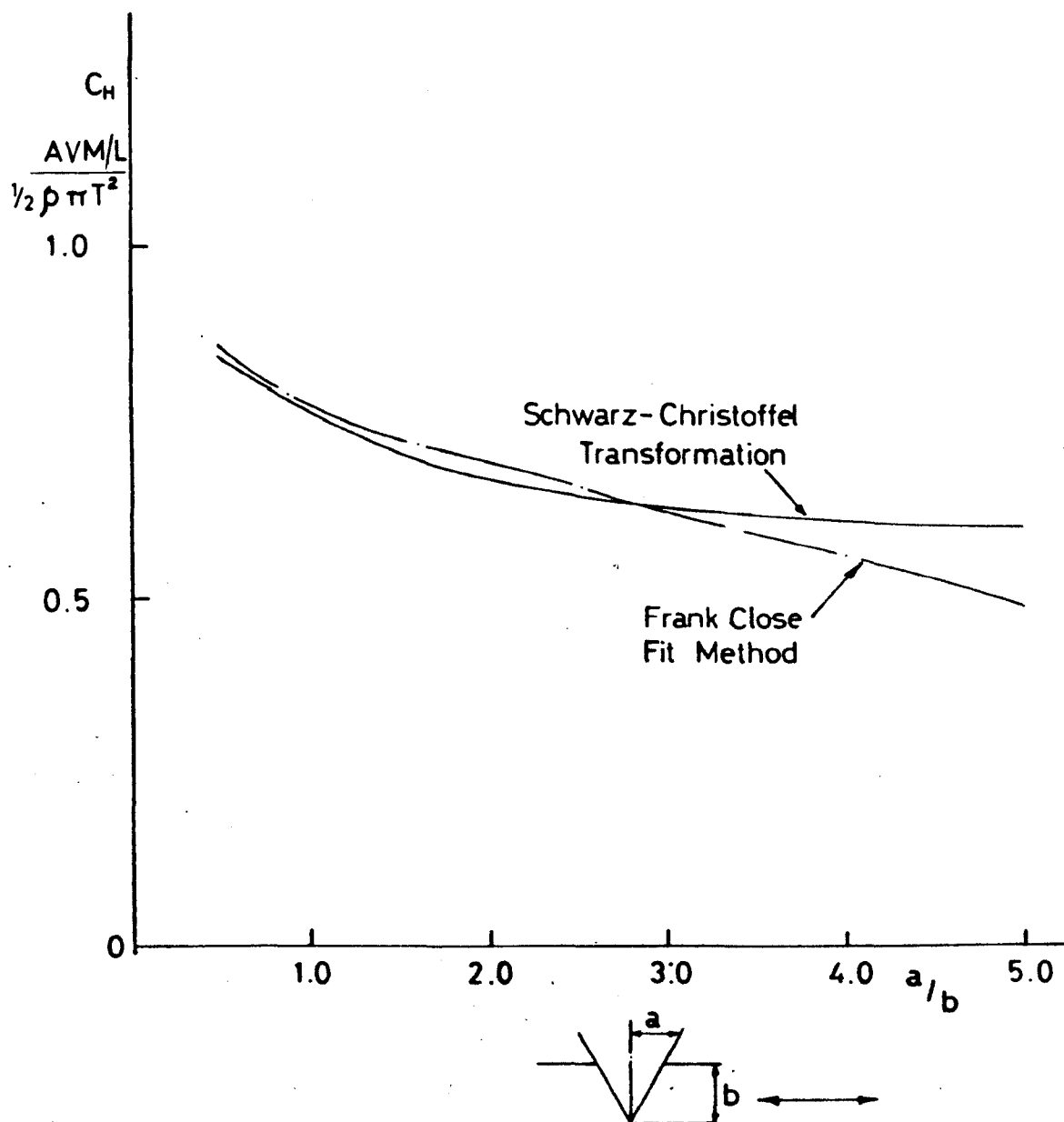


Figure 3.5 Comparison Of C_H Obtained Using The Frank Close Fit Method With The Schwarz-Christoffel Transformation For A Triangular Cross Section

methods for simple shapes. (Reference 32 gives the Schwarz-Christoffel results, while Ref. 33 outlines the Frank-Close-Fit method.)

Longitudinal Force

As described in Chapter 2, there will be a wave-induced longitudinal force acting on the ship's hull as a function of wave position. This is denoted X_{ξ} and is assumed to be constant for small heading angles.

The slender body assumption does not hold for longitudinal motions since the gradient dy/dx cannot be assumed to be zero. A further complication is the trim angle which introduces a component of the vertical gradient, dy/dz , into the required gradient on the $x^* - y^*$ plane, dy^*/dx^* . It can easily be shown that

$$\frac{dy^*}{dx^*} = \frac{dy}{dx} \cos \tau + \frac{dy}{dz} \sin \tau \quad \dots\dots \quad 3.12$$

In principle it should be possible to make use of Eq. 3.12 when computing the X force on the hull. It was found, however, that the numerical errors introduced by this method were considerable and an alternative approach was used.

Instead of attempting to calculate the force in the x^* direction directly, the forces in the x and z directions were found and resolved to obtain the x^* and z^* forces. This procedure involved less error, as the z^* force is known to equal $-mg$ for equilibrium and the x force is small.

Figure 3.6 shows the forces acting on a ship with a trim angle of τ . Z and X are the hydrodynamic and hydrostatic forces acting; mg is the gravitational force on the body and X_{ξ} is the resultant wave force.

For equilibrium

$$X \sin \tau = Z \cos \tau + mg \quad \dots\dots \quad 3.13$$

$$X_{\xi} + X \cos \tau + Z \sin \tau = 0 \quad \dots\dots \quad 3.14$$

Giving

$$X_{\xi} = mg \tan \tau - \frac{X}{\cos \tau} \quad \dots\dots \quad 3.15$$

which, when τ is small, simplifies to

$$X_{\xi} = mg \tau - X \quad \dots\dots \quad 3.16$$

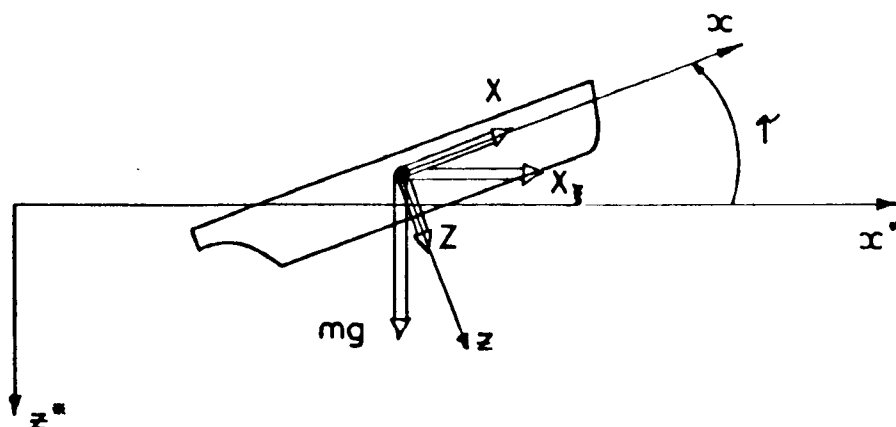


Figure 3.6 Longitudinal Forces Acting On The Hull

As mg and τ are known, only X is required to be calculated and this can be done as follows.

Pressure Force:

As for the sway force and yawing moment, the longitudinal pressure force is calculated by integrating the pressure over the entire wetted surface of the hull. The essential difference between the calculation for the longitudinal force and the lateral force is that, in the case of the lateral force the longitudinal component of the normal to the ship's hull is neglected, whereas for the longitudinal calculation it must be taken into account.

Thus, the longitudinal component of the pressure force on a transverse strip will be

$$X_{\text{STRIP}}^P = -2\rho g \int_{D_T} \left(A e^{-Kz^*} \cos Kx_C^* + z^* \right) \theta \delta x dz \quad \dots \quad 3.17$$

for small θ ,

where θ is a function of z as well as of x .

In addition to the pressure force contribution to the X force from the longitudinal component of the pressure at the sides of the ship, there will be a contribution due to the transom stern. Here $\theta = \pi/2$ and the contribution to the X pressure force will be

$$X_{\text{TRANSOM}}^P = -2\rho g \int_{D_T} \left(A e^{-Kz^*} \cos Kx_T^* + z^* \right) b dz \quad \dots \quad 3.18$$

Thus, the total longitudinal pressure force is given by

$$X^P = \int_{-\frac{L}{2}}^{\frac{L}{2}} X_{\text{STRIP}}^P dx + X_{\text{TRANSOM}}^P \quad \dots \quad 3.19$$

Acceleration Force:

The problem with calculating the longitudinal acceleration force is in obtaining the longitudinal added mass and, in particular, since the acceleration will be varying over the ship's length, in obtaining the longitudinal spread of the added mass.

The method used is to divide the ship into transverse strips as before. These transverse strips are further divided into horizontal strips resulting in regular trapezohedrons as shown in Figure 3.7. Each of these trapezohedrons can be considered in two dimensions as a trapezium which forms part of a rhombus as shown in Figure 3.8. Now,

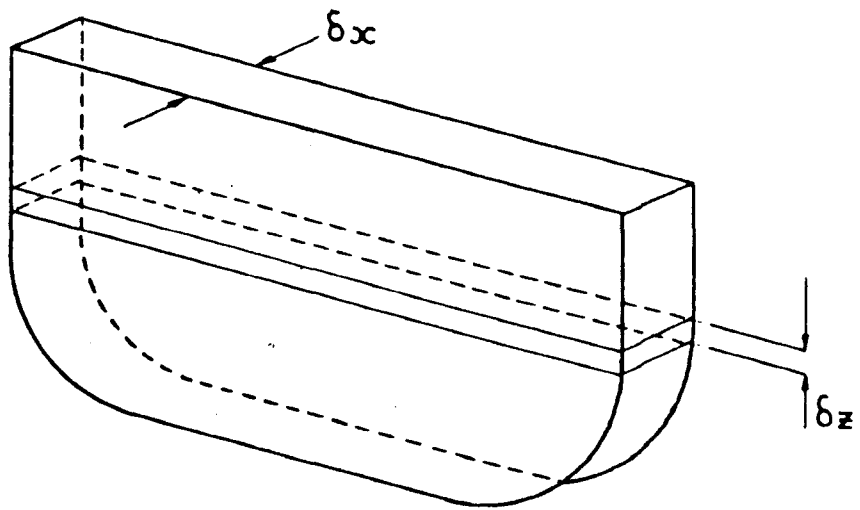


Figure 3.7 Schematic View Of A Transverse Strip Showing
A Trapezohedron δ_z Thick

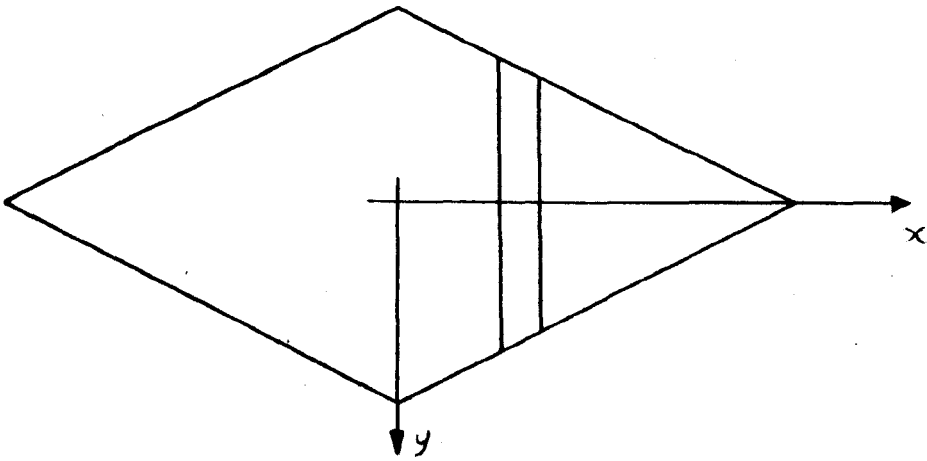


Figure 3.8 Rhombus Formed From Trapezium

using the Schwarz-Christoffel transformation, the AVM of this rhombus can be obtained and, assuming that this is spread evenly over the entire shape, the AVM of the trapezium can be found. Thus, what in fact is being obtained is the AVM due to an element of the ship's surface. It is then assumed that the acceleration is constant over this element in order to calculate the acceleration force.

Using the Schwarz-Christoffel transformation, which is explained fully in Ref. 34, the added mass coefficient of half a rhombus, as shown in Figure 3.9 is given by

$$C_{al} = \frac{2\pi^2 (1 - \gamma)}{\Gamma^2\left(\frac{3}{2} - \gamma\right) \Gamma^2(\gamma) \sin^2 \gamma\pi} + 2 \cot(\gamma\pi) \quad \dots \quad 3.20$$

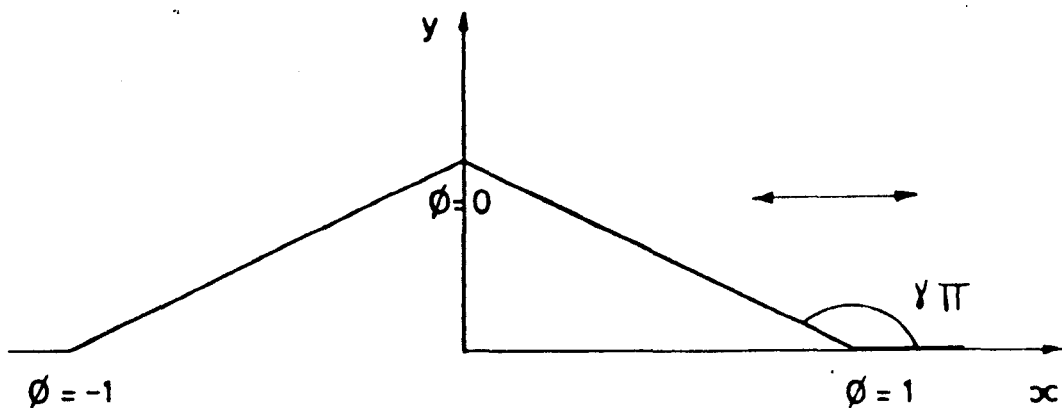


Figure 3.9 Z-Plane For Schwarz - Christoffel Transformation

Thus, the two-dimensional added mass of the rhombus containing the required trapezium will be

$$2\text{-D AVM} = \rho\pi B_1^2 C_{al} \quad \dots \quad 3.21$$

where B_1 is the local half breadth.

Now the two-dimensional AVM/unit length which is, in fact, the added mass due to the ends of an elemental trapezohedron, can be calculated by dividing Eq. 3.21 by the length of the rhombus to obtain

$$2\text{-D AVM/unit length} = \frac{1}{2}\rho\pi B_1 C_{al} \tan [(1-\gamma)\pi] \quad \dots \quad 3.22$$

Hence the longitudinal acceleration force at a point on the ship's hull can be expressed as

$$X_{\text{POINT}}^a = \frac{\rho\pi^2 B_1 C_{al} A e^{-Kz^*} \tan [(1-\gamma)\pi] \sin Kx_C^*}{\lambda} \quad \dots \quad 3.23$$

Thus, the longitudinal acceleration force on a strip will be

$$X_{\text{STRIP}}^a = \int_{D_T} \left(-A \cos Kx_T^* \right) X_{\text{POINT}}^a \delta x dz \quad \dots \quad 3.24$$

In a similar way to the pressure force there will be a contribution due to the force on the transom. This will depend on the AVM of the transom which can be calculated using half of the value of an equivalent flat plate. Thus, the total longitudinal acceleration force is given by

$$X^a = \int_{-\frac{L}{2}}^{\frac{L}{2}} X_{\text{STRIP}}^a dx + X_{\text{TRANSOM}}^a \quad \dots \quad 3.25$$

It is interesting to note that if this modification of the Schwarz-Christoffel transformation is applied to a semi-submerged

circular cylinder using ten evenly-spaced ordinates, the value of the AVM coefficient obtained is 1.09. This compares quite well with the idealised value of 1.0 for this case.

Rudder Derivatives

The rudder derivatives, N_δ and Y_δ , are both dependent on the side force generated by the rudders operating at an angle to the centreline of the ship. The rudders operate as low aspect ratio hydrofoils with a limited groundboard effect, caused by their proximity to the hull, in a complex flow which is affected by the hull and screws upstream. For this reason an absolute theoretical calculation of the rudder derivatives will be complex and inaccurate, so the method used here is to calculate the ratio between calm water and wave derivatives. This is then used together with the experimental calm water value to obtain Y_δ and N_δ in the wave. In order to simplify the procedure the effect the vertical component of the orbital velocity will have on the rudder derivatives is ignored.

For simplicity, the velocity at the rudders can be calculated from

$$V_R = \eta V_S \quad \dots \quad 3.26$$

where η is assumed constant for small changes in speed.

From Ref. 26 the lift coefficient of a low aspect ratio foil is given by

$$C_L = \left(\frac{\partial C_L}{\partial \delta} \right) \delta + \frac{C_{Dc}}{R} \delta^2 \quad \dots \quad 3.27$$

where δ is the angle of attack in radians and R is the effective aspect ratio. C_{Dc} is the crossflow drag coefficient which is dependent on both tip shape and taper ratio. The second term on the right-hand side of Eq. 3.27 is a small non-linear contribution and can be neglected in the present analysis, which is aimed at finding the ratio between calm water and wave conditions, as opposed to the absolute value of the derivatives.

Considering only rectangular geometry rudders with no sweepback, the lift slope can be expressed as

$$\frac{\partial C_L}{\partial \delta} = \frac{0.9 (2\pi) R}{[(\sqrt{R^2 + 4}) + 1.8]} \quad \dots \quad 3.28$$

Now, the lift on the rudder is given by

$$\frac{dL}{d\delta} = \frac{1}{2} \rho S_R V_R^2 \frac{dC_L}{d\delta} \quad \dots \quad 3.29$$

giving

$$Y'_\delta = \frac{1}{L^2 V_S^2} S_R V_R^2 \frac{dC_L}{d\delta} \quad \dots \quad 3.30$$

and

$$N'_\delta = \frac{l_R}{L^3 V_S^2} S_R V_R^2 \frac{dC_L}{d\delta} \quad \dots \quad 3.31$$

$$\frac{Y'_\delta}{Y'_\delta} = \frac{N'_\delta}{N'_\delta} = \frac{S_{R_w} V_{R_w}^2 R_w [\sqrt{(R_c^2 + 4)} + 1.8]}{S_{R_c} V_{R_c}^2 R_c [\sqrt{(R_w^2 + 4)} + 1.8]} \quad \dots \quad 3.32$$

$$= \frac{d_w^2 (\eta V_S - V_o)^2 \Lambda_c \mu_w}{d_c^2 (\eta V_S)^2 \Lambda_w \mu_c} \quad \dots \quad 3.33$$

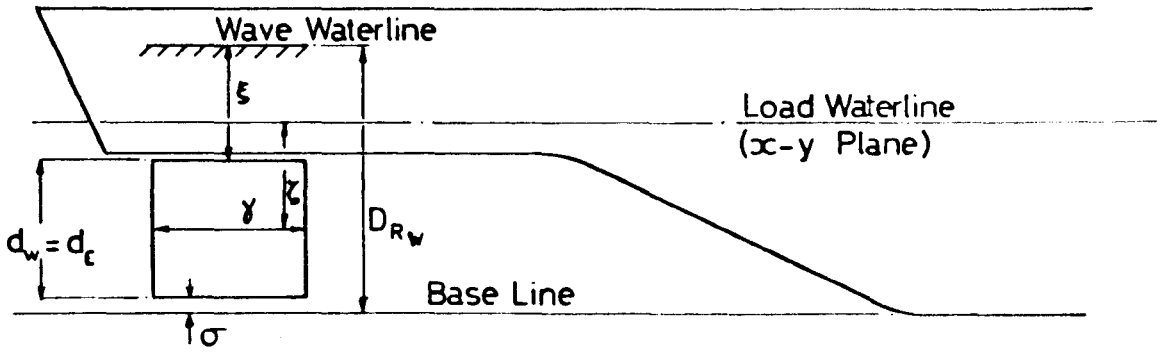
where

$$\Lambda_c = \sqrt{\left(\mu_c^2 \frac{d_c^2}{\gamma^2} + 4\right) + 1.8}$$

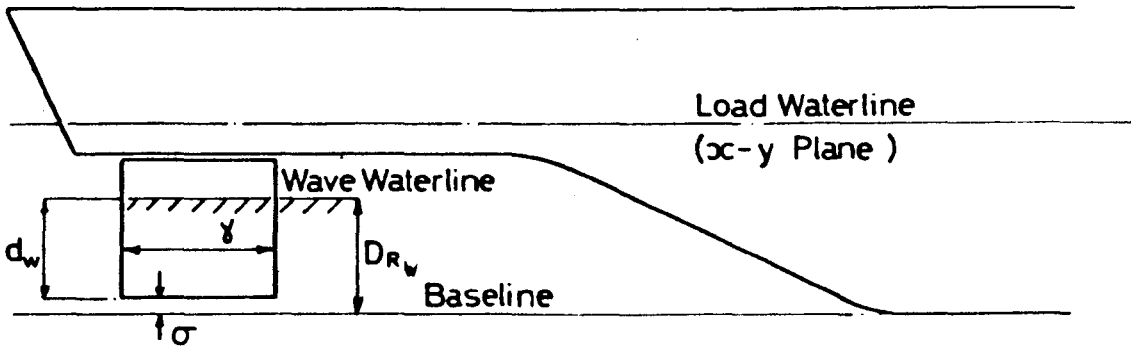
$$\Lambda_w = \sqrt{\left(\mu_w^2 \frac{d_w^2}{\gamma^2} + 4\right) + 1.8}$$

$$V_o = KAC e^{-Kz} \cos Kx^*$$

and μ_c , μ_w are the aspect ratio factors caused by the proximity of the rudders to the hull in the calm water and the wave conditions respectively. V_o is the horizontal component of the orbital velocity which is assumed to be constant over the rudder with the value taken at its centre of area.



a. Wave Waterline Above The Rudder



b. Wave Waterline Below The Rudder

Figure 3.10 Position Of Wave Waterline Relative To Rudder

There are two separate possibilities for the wave condition dependent on the position of the wave waterline as shown in Figure 3.10(a) and (b). In the first case the aspect ratio and rudder area are unchanged from the calm water condition to the wave condition and hence Eq. 3.33 simplifies to

$$\frac{Y'_{\delta_w}}{Y'_{\delta_c}} = \frac{N'_{\delta_w}}{N'_{\delta_c}} = \frac{(\eta v_s - v_o)^2}{(\eta v_s)^2} \quad \dots \quad 3.34$$

In the second case both the aspect ratio and the rudder area will be reduced from the calm water condition to the wave condition. μ_w will equal one, since the hull will now no longer have a ground-board effect on the rudder in the wave condition, and $d_w = D_{R_w} - \sigma$. Thus Eq. 3.33 becomes

$$\frac{Y'_{\delta_w}}{Y'_{\delta_c}} = \frac{N'_{\delta_w}}{N'_{\delta_c}} = \frac{(D_{R_w} - \sigma)^2 (\eta v_s - v_o)^2 \Lambda_c}{d_c^2 (\eta v_s)^2 \Lambda_w \mu_c} \quad \dots \quad 3.35$$

The rudder derivatives are then obtained from

$$Y'_{\delta} = Y'_{\delta_E} \left(\frac{Y'_{\delta_w}}{Y'_{\delta_c}} \right) \quad \dots \quad 3.36$$

and

$$N'_{\delta} = N'_{\delta_E} \left(\frac{N'_{\delta_w}}{N'_{\delta_c}} \right) \quad \dots \quad 3.37$$

where Y'_{δ_E} and N'_{δ_E} are the calm water values obtained experimentally.

Manoeuvring Derivatives

It is not possible, using the present state-of-the-art, accurately to predict theoretically the sway velocity or rotational velocity derivatives even at low speeds in calm water. For this reason no attempt has been made here to try to do so at high speeds in waves. Instead, a calculation of the change in the derivatives caused by the wave is made and applied to the derivative obtained experimentally in calm water. The method used here is based on the assumption that the derivatives

are made up of potential and viscous flow components which are independent. The potential flow component is that which exists in an ideal fluid and hence can be calculated using strip theory, whereas the viscous flow component is related to lift and crossflow drag effects and cannot be readily calculated theoretically. The assumption made here is that the viscous component will remain unchanged in the wave condition and hence it is only required to calculate the change in the potential flow component.

Considering the derivative Y_v we have

$$Y_{v\text{TOTAL}} = Y_{v\text{POTENTIAL}} + Y_{v\text{VISCIOUS}} \quad \dots \quad 3.38$$

If $Y_{v\text{TOTAL}}$ is assumed to be known from model experiments in calm water and $Y_{v\text{POTENTIAL}}$ can be calculated using strip theory, then $Y_{v\text{VISCIOUS}}$ can be calculated for calm water. Since $Y_{v\text{VISCIOUS}}$ is assumed constant and $Y_{v\text{POTENTIAL}}$ can be calculated, $Y_{v\text{TOTAL}}$ can be found for any desired wave condition. This method is applied to the derivatives Y'_v , N'_v , Y'_r and N'_r .

The acceleration derivatives can be calculated directly using strip theory as they comprise entirely of potential flow contributions. The cross coupling acceleration derivatives are calculated here although it is recognised that they are very small and often assumed to be zero.

The strip theory used is due to Clarke^[32,35] with the added mass values obtained from the Frank-Close-Fit method as for the transverse force calculation. The rudders are assumed to be at the stern so that an addition due to their added mass is made to the added mass coefficient of the stern.

Thus

$$Y'_v = -\pi \left(\frac{1}{L}\right)^2 \int_{\text{STERN}}^{\text{BOW}} T^2 C_H dx' \quad \dots \quad 3.39$$

$$N'_v = -\pi \left(\frac{1}{L}\right)^2 \int_{\text{STERN}}^{\text{BOW}} T^2 C_H x' dx' \quad \dots \quad 3.40$$

$$Y_{\dot{r}}' = -\pi \left(\frac{1}{L}\right)^2 \int_{\text{STERN}}^{\text{BOW}} T^2 C_H x' dx' \quad \dots \quad 3.41$$

$$N_{\dot{r}}' = -\pi \left(\frac{1}{L}\right)^2 \int_{\text{STERN}}^{\text{BOW}} T^2 C_H x' dx' \quad \dots \quad 3.42$$

$$Y'_{\text{V POTENTIAL}} = -\pi \left(\frac{1}{L}\right)^2 T_{\text{STERN}}^2 C_{H \text{STERN}} \quad \dots \quad 3.43$$

$$N'_{\text{V POTENTIAL}} = Y'_{\text{V POTENTIAL}} x'_{\text{STERN}} + Y'_{\dot{v}} \quad \dots \quad 3.44$$

$$Y'_{\dot{r} \text{ POTENTIAL}} = Y'_{\text{V POTENTIAL}} x'_{\text{STERN}} \quad \dots \quad 3.45$$

$$N'_{\dot{r} \text{ POTENTIAL}} = Y'_{\text{V POTENTIAL}} x'_{\text{STERN}} + Y'_{\dot{r}} \quad \dots \quad 3.46$$

using the generally accepted assumption that $C_{H \text{BOW}} = 0$, since a finite value of kinetic energy cannot be instantaneously imparted to the fluid at the bow.

Chapter 4

CONSTRAINED MODEL EXPERIMENTS

Introduction

In order to test the validity of the theoretical technique for determining the coefficients developed in the previous chapter, and in order to obtain the approximate magnitude of the roll coupling terms constrained model experiments were carried out both in the University of Glasgow's Hydrodynamics Laboratory^[36] and in the National Maritime Institute's (NMI) Circulating Water Channel (CWC)^[24].

Initial experiments at Glasgow were conducted on a 2.9m Series 60 model. These comprised of (a) investigating the loss of GM in a following sea (described fully in Ref. 37), and (b) investigating the magnitude of the heel-induced yaw moment in calm water.

The experiments at NMI used a 3.66m fine form model constrained to remain upright and were devised to obtain the change in the coefficients in the following sea condition. Originally it was intended to test at various heel angles also, but this was prevented due to lack of time. The model was oscillated using a planar motion mechanism (PMM) whilst remaining in the same longitudinal position in the wave. This was obtained by using a wave created by a wanedozer travelling at the same speed as the carriage (Figure 4.1). In order to reduce experimental difficulties and to permit additional PMM oscillations, this experiment was carried out in a CWC. In this facility the model, carriage and wanedozer all remained fixed with respect to the earth, while the water flowed past at the required velocity. The dynamics are identical to those of the more conventional water-fixed, model-moving towing tank facilities.

Heel-Induced Yaw Moment and Sway Force Experiments

Free Running Experiments:

Prior to carrying out the constrained experiments a selection of models was projected down the tank with given heel angles and their trajectories observed. The models were not self-propelled and, since

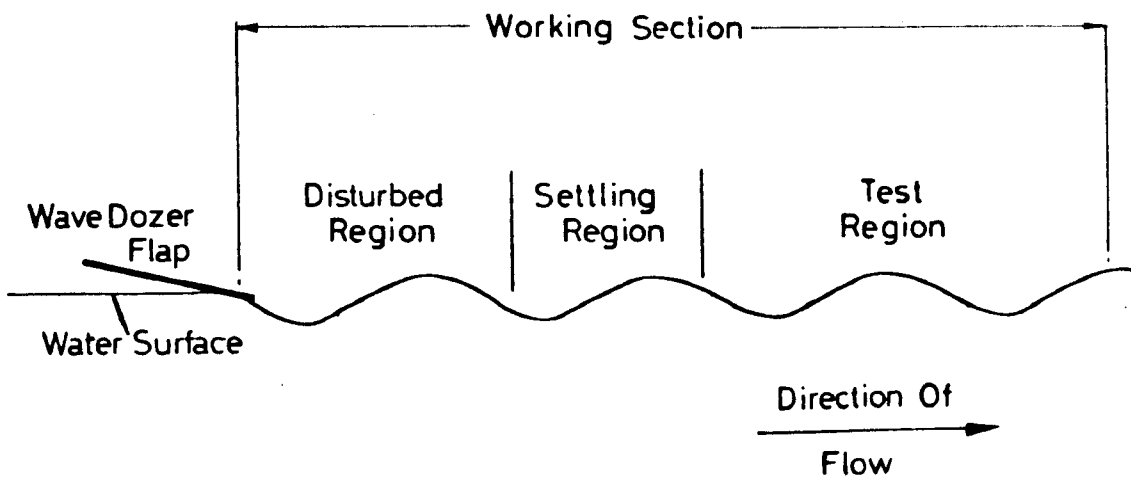


Figure 4.1 Schematic Diagram Of Experiments In C.W.C

they relied purely on momentum for motion, their speed was not constant. For some of the runs a rudder angle was applied in an attempt to counteract the heel-induced yaw moment and result in a straight line motion of the model. This was extremely difficult as it appeared that the relation between the yawing caused by the heel and that caused by the rudder varied with speed. The only conclusions that could be drawn from these *ad hoc* experiments, therefore, was that, in general, a starboard heel angle caused a yaw to port (and vice versa), which could be counteracted by a port rudder angle. The required rudder angle appeared to vary from model to model and over the Froude number range tested, which was from 0 to about 0.2.

Constrained Model Experiments:

Three series of constrained model experiments were carried out using a 2.9m long Series 60 form with a block coefficient of 0.65, principle dimensions of which are given in Table 4.1 [36,38]. The model was not self-propelled, but was towed using the arrangement shown in Figure 4.2. For the first series of experiments a solid towing rod was used instead of the wire shown in Figure 4.2, but it was found that this could apply an additional moment and hence these results were discarded. The remaining two series of experiments used the towing wire and it was found that correlation between them was very good. The first of these involved running at a constant speed with various heel angles in order to obtain plots of side force and yawing moment against heel angle. This was repeated for six separate speeds and gave an indication of the range of linearity, together with values of Y'_ϕ and N'_ϕ for the different speeds tested.

The final series investigated the effect of a constant heel angle over the Froude number range $0.22 < F_n < 0.37$ giving plots of sway force and yaw moment against speed.

The experimental set-up was as shown in Figure 4.2. The model was free to heave and pitch. The guides permitted heel angles up to 45° and were fitted close to the centre of lateral resistance in the vertical plane. The attachment of the model to the guide incorporated a cantilever bar which was fitted with a strain gauge bridge for measuring side force. The signals from the strain gauges were fed through

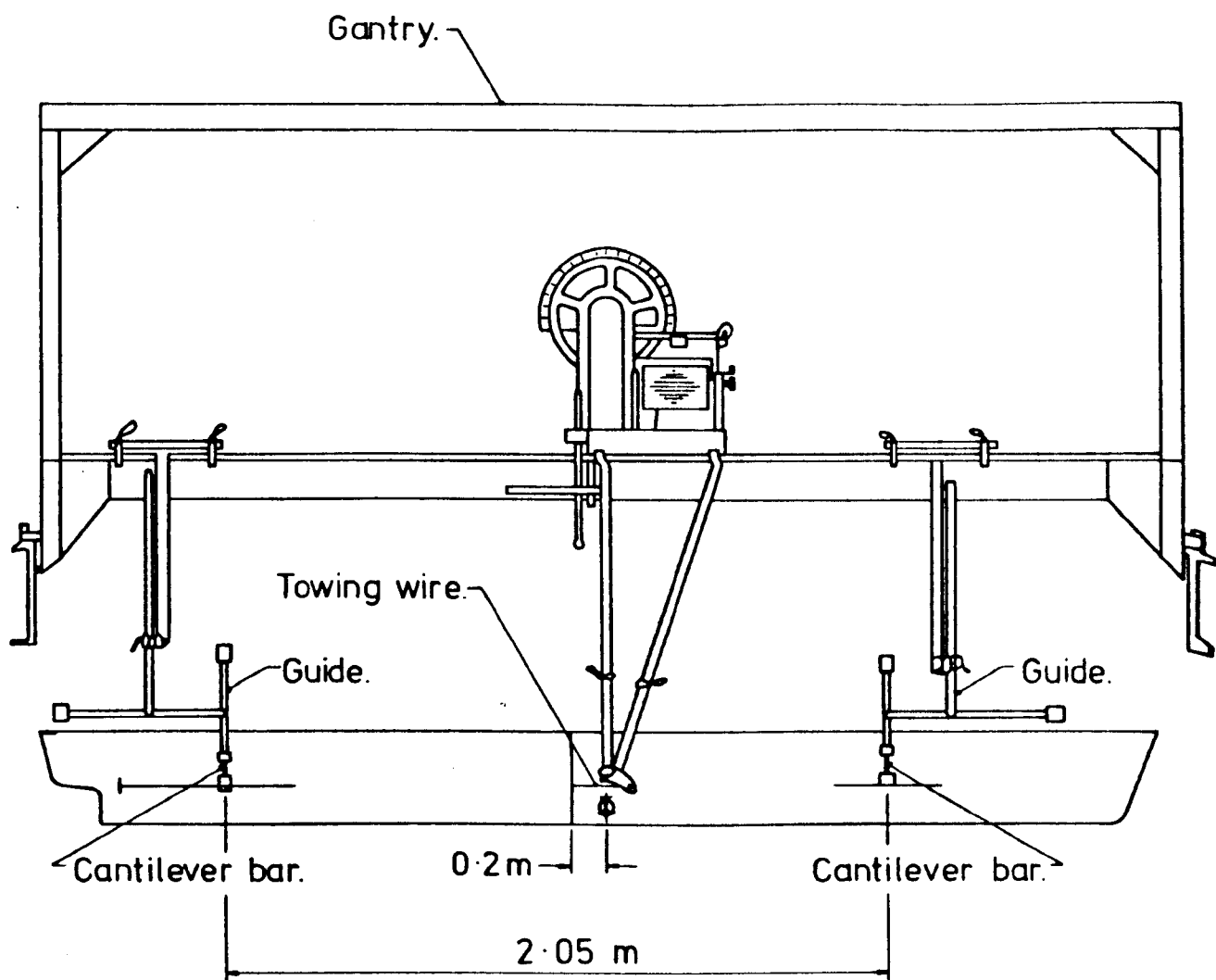


Figure 4.2 Arrangement Of Model For Heel Induced
Yaw Moment And Sway Force Experiments

suitable amplifiers to a pen recorder. All analysis was done manually. The yawing moment due to heel angle can be split up into two components:

- (1) A component due to the aerofoil effect of the asymmetrical waterplane causing a varying side force along the length of the hull which induces a moment.
- (2) The transverse displacement of the centre of longitudinal resistance from the tow position forming a couple in the horizontal plane.

The first component can be considered as a pure moment, with the second component being an induced moment, caused by the fact that the centre of longitudinal resistance (CLR) will move transversely due to the heel angle. Since the CLR will be in the same vertical plane as the tow point in the upright condition and will shift an amount dependent on heel angle and independent of tow height, the induced moment will be dependent on tow height. Further, since the tow height used in the experiments is above the propeller position a self-propelled ship would be expected to have a more positive heel-induced yaw moment than the model used in the experiments. The proportion of the total measured yaw moment due to induced moment will vary with speed. For $F_n = 0.24$ it will be about 20% and for $F_n = 0.32$ it will be about 50%. Since the induced moment is caused by the resistance forming a couple with the propulsion the usual Froude scaling considerations will apply.

The non-dimensional results are given in Figures 4.3 to 4.5, where it can be seen that both Y'_ϕ and N'_ϕ vary considerably with speed. Since the Series 60 form is not intended to travel at very high Froude numbers, the additional wavemaking produced may have affected the results somewhat.

The Development of the Wavedozer

General:

The wavedozer was pioneered by Hogben^[39] and Standing^[40] who used it to create waves behind a carriage in a conventional towing tank. The carriage stopped before the test area and waves were projected on towards the model. For the experiments described here the

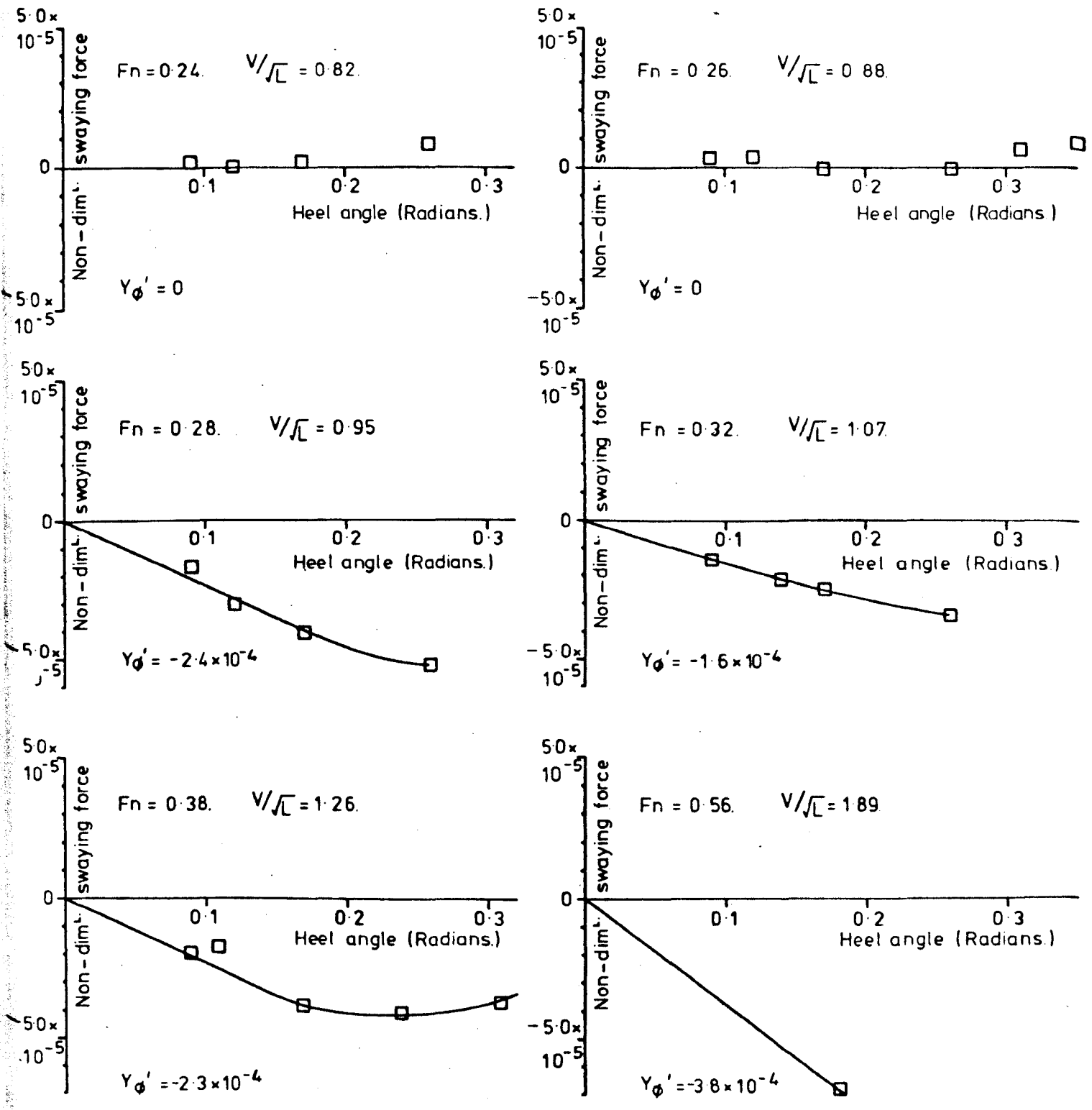


Figure 4.3 Sway Force Against Heel Angle

— Mean line through experimental points.
 - - - Corrected to propeller position.

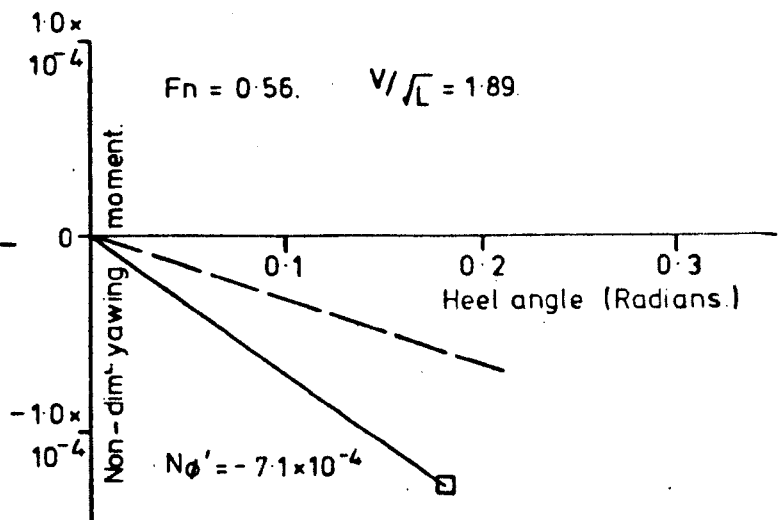
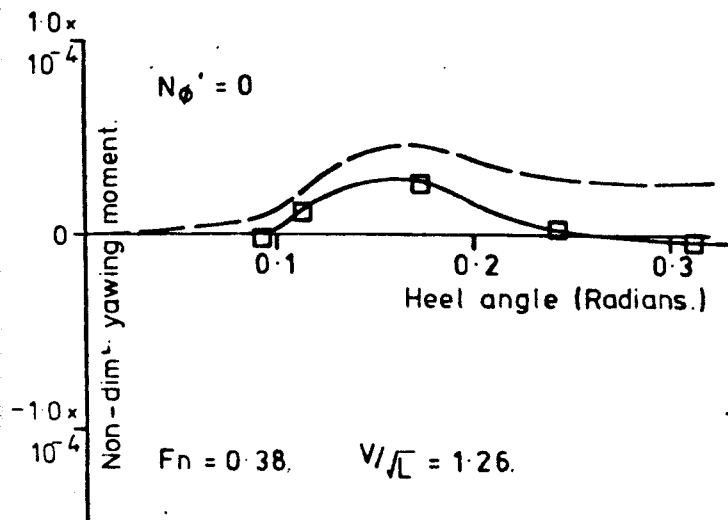
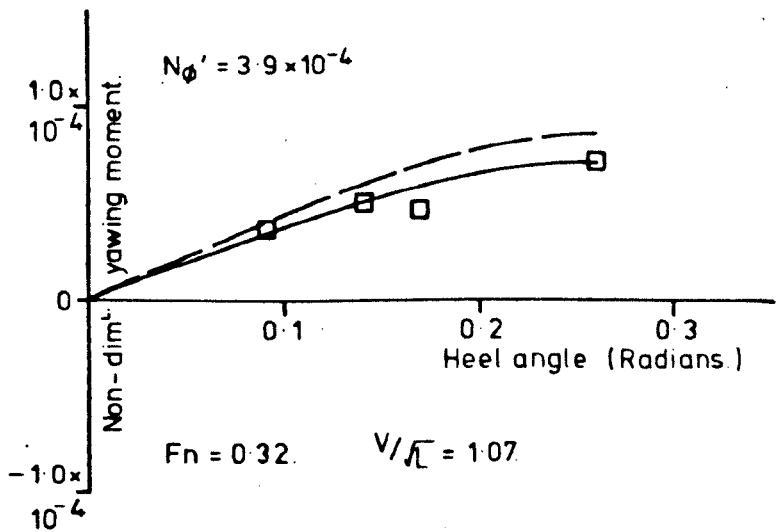
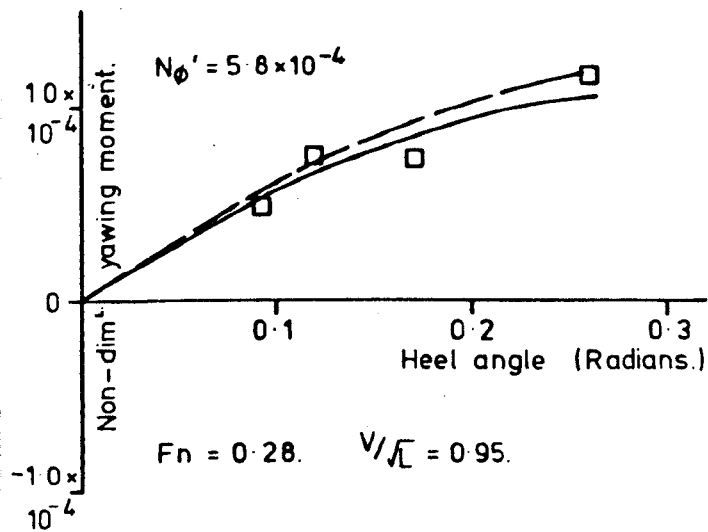
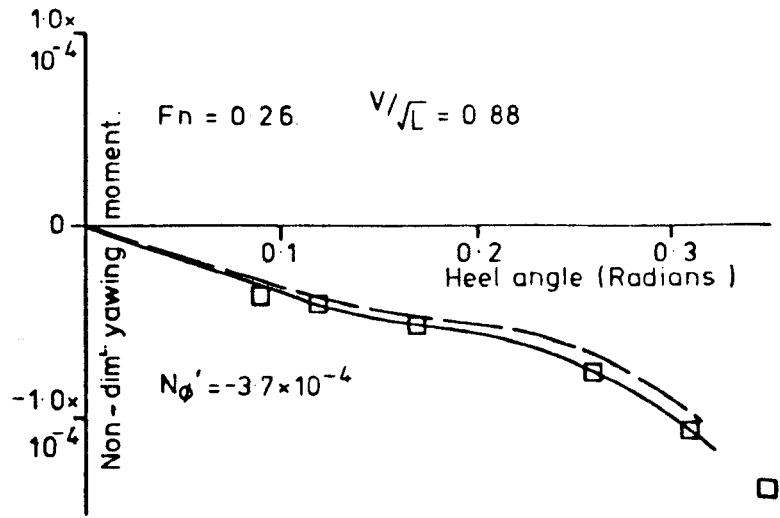
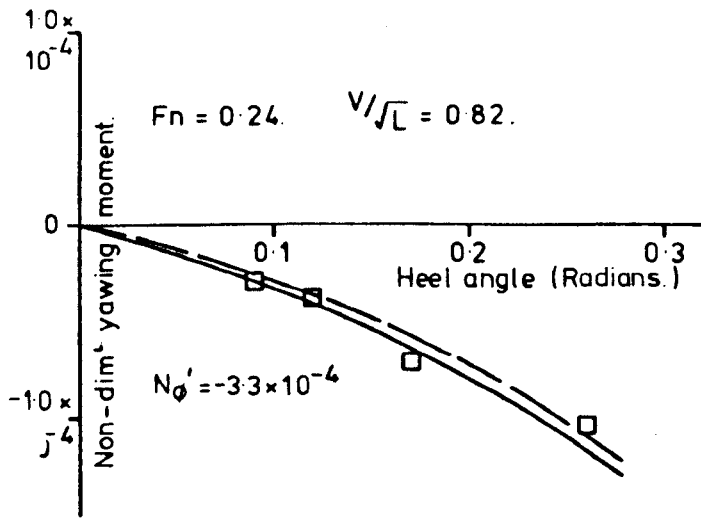


Figure 4.4 Yaw Moment Against Heel Angle

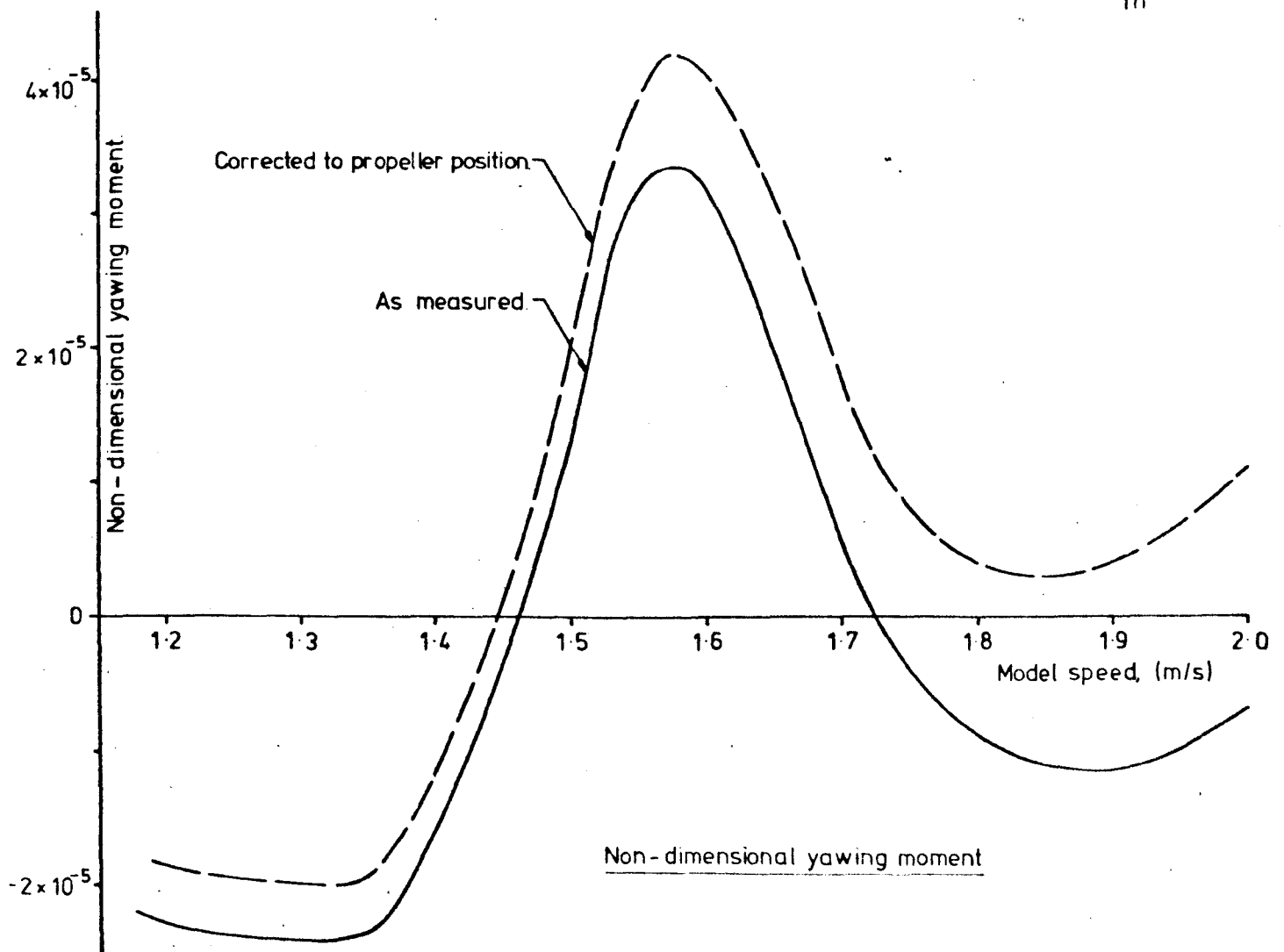
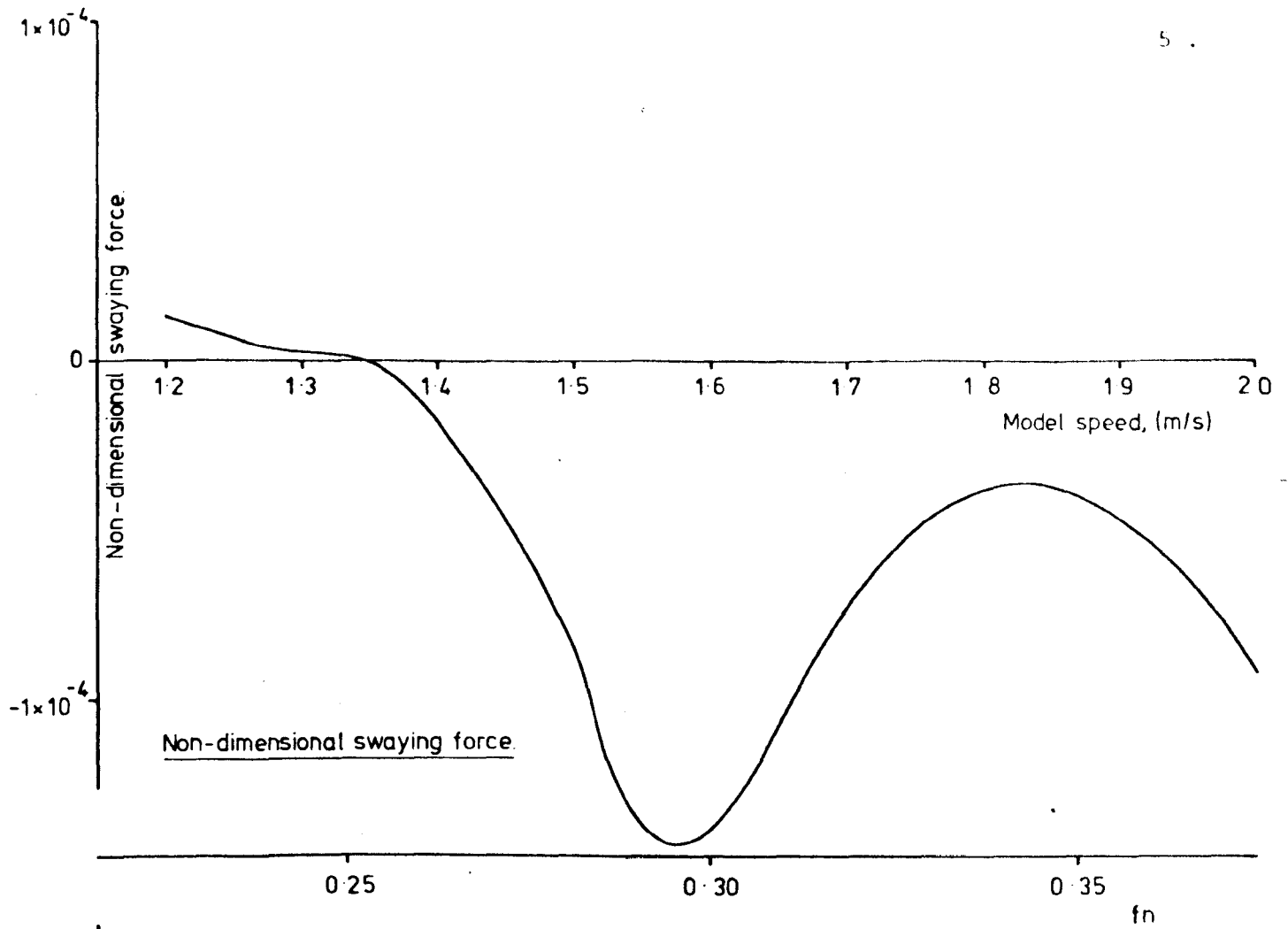


Figure 4.5 Sway Force And Yaw Moment Against Speed (For 10° Of Heel)

the model was tested in the waves behind the wanedozer and a CWC was used to overcome the difficulty of towing a large flap and a model with the prescribed separation in a conventional towing tank. The CWC at NMI was chosen for the experiment as being the largest in the country, but a wanedozer had to be designed and built to fit it^[41]. The main requirements were:

- (1) As smooth a wave as possible.
- (2) The ability to vary the separation distance between the flap and the model.
- (3) As large a separation between the model and the flap as possible.

In order to get a smooth wave it was essential that the flap was as smooth as possible and had a straight trailing edge. It was also important that the tank wall and the flap be tight-fitting - using a CWC helped greatly here since the flap was not required to move with respect to the wall. The separation distance was easily altered in the CWC as the carriage which mounted the PMM and the model was on rails and could be moved very exactly by hand. Finally, the separation distance possible, over two wave lengths ($\approx 8\text{m}$) at the desired speed, was adequate to allow the disturbances from the wavemaker to die down.

Preliminary Experiments:

Before designing the full-scale wanedozer some preliminary experiments were carried out. First, using the 1/10th scale CWC at NMI (an exact hydrodynamic scale model of the large CWC^[42]) the optimum position and flap angle were obtained. This was level with the join between the constriction zone and the working section at an angle of 14° to the horizontal.

Next, the CWC at AMTE(H) was used to test the idea that oblique waves could be created using an oblique flap. The conclusions drawn from these experiments were:

- (1) The wave profile at the upstream side of the flap disappeared after the first wave.

- (2) The wave gradually became more normal to the direction of flow in the channel, although this was difficult to observe due to the effects of (1).
- (3) The first wave was quite well-defined and parallel to the flap.

From these conclusions it was obvious that the oblique wavedozer would not be suitable for the PMM experiments.

Design/Manufacture:

The detailed design and manufacture of the wavedozer was undertaken by AMTE(H). For ease of handling, the final design (Figure 4.6) was arranged to consist of four sections. Each section consisted of a quarter of the flap, a vertical support frame and a heavy channel which spanned two of the 305mm × 457mm concrete beams which span the CWC in the constriction section.

The flap was manufactured from 6mm thick mild steel (MS) plate, suitably stiffened transversely, each plate being joined to its neighbour by nuts and bolts passing through MS angles welded to the edges of the plates. Each plane was bolted to its support frame which was manufactured from 50mm × 50mm × 6mm MS angle. The frames were bolted to support channels spanning the beams.

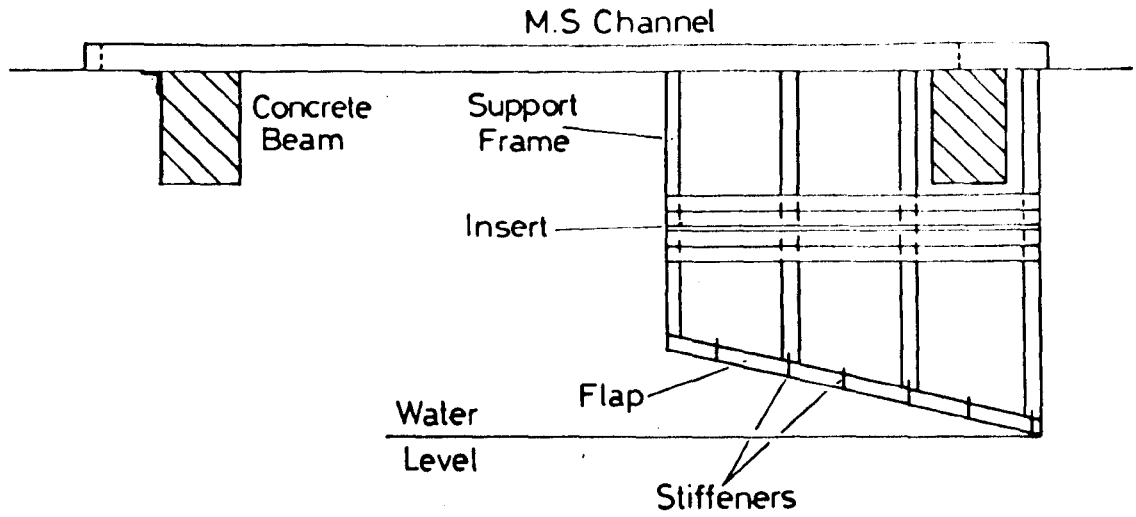
The edges of the flaps adjacent to the channel walls had glass reinforced plastic (GRP) extensions moulded to the shape of the channel walls. The outer edges of these GRP inserts had plastic tubing covering them to give a good fit to the channel walls.

An adjustable stiffened extension was fitted to the trailing (downstream) edge of the flap.

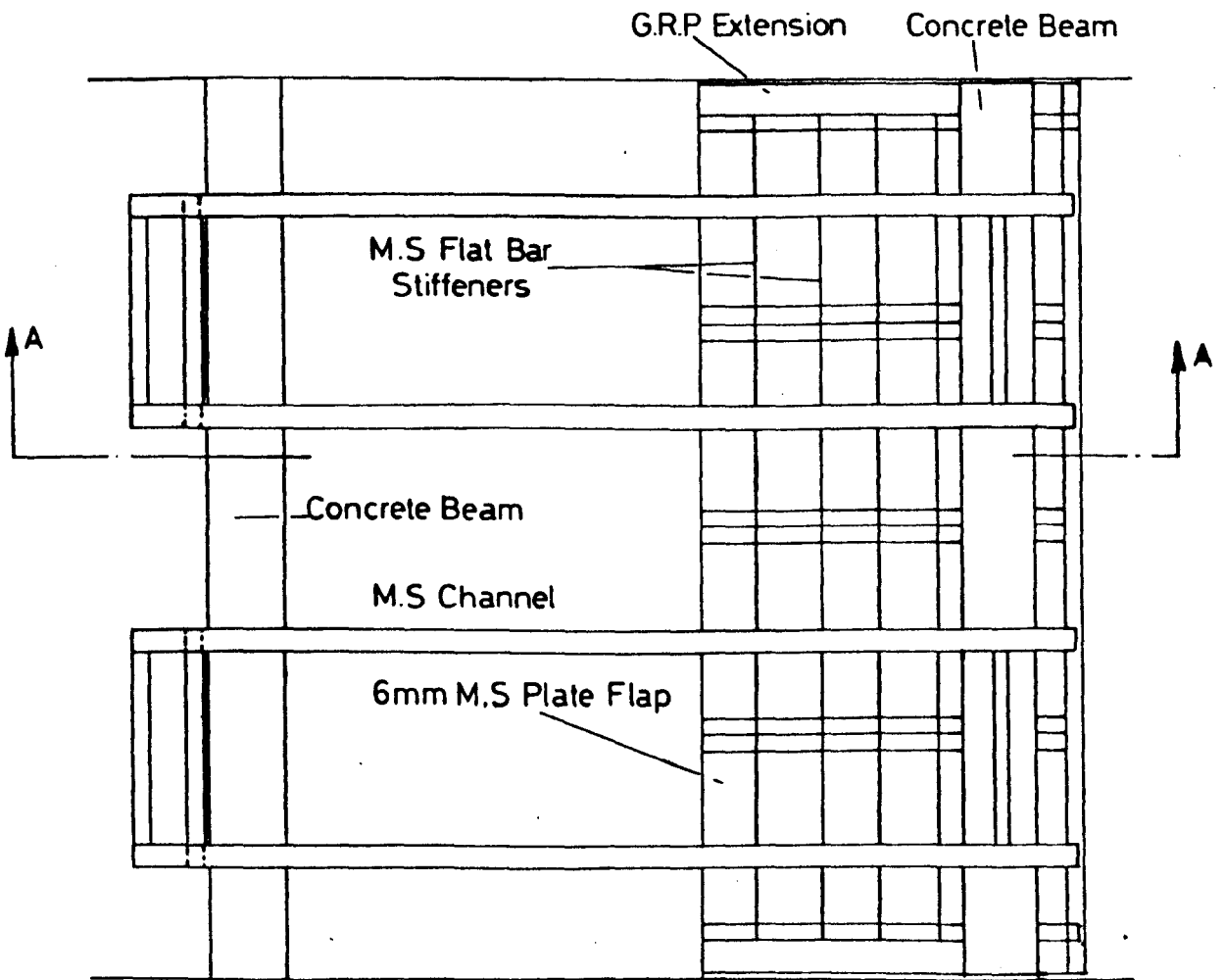
A photograph of the fully assembled wavedozer is shown in Figure 4.7.

Calibration:

Prior to conducting the model experiments the wavedozer was calibrated for a range of speeds and wave steepnesses. References 39 and 40 indicated that wave steepness depended almost entirely on the depth of immersion of the flap and that the wavelength depended on the speed



SECTION A-A



PLAN

Figure 4.6 Final Design Of Wavedozer

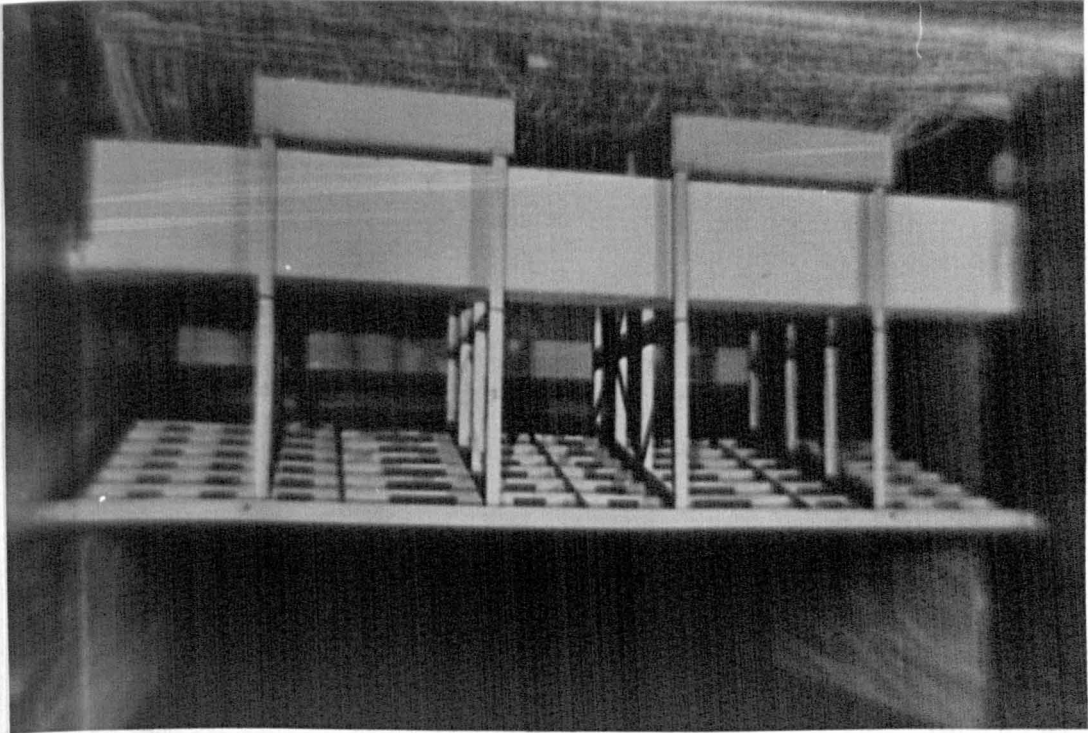


Figure 4.7 Fully assembled wadedozer

of the water. This was also borne out in both the preliminary experiments.

In the CWC, an increase in water speed causes an increase in water depth, thereby increasing flap immersion as the flap position was fixed. It was not possible, therefore, to vary the water speed independently of flap immersion and the following technique had to be used.

The depth of water at zero speed (D_0) was measured and then the water speed was slowly increased (raising the water depth) until the water level touched the flap. The resultant wave conditions were allowed to settle for 10 - 15 minutes when wave height and length were recorded. (The third and fourth crests were used as this was the region in which the model was to be tested.) The depth of water (D_R) in the running condition was also recorded. The water speed was then slightly increased and once the conditions had settled another record was taken. This procedure was repeated for further speeds until the first generated wave broke and the wave system became disturbed. The technique was repeated for several initial water depths D_0 .

Results:

Figure 4.8 gives a plot of λ/h obtained for various running depths of water D_R . Because the vertical position of the wavedozer flap was fixed, any variation in D_R was effectively a variation in the depth of flap immersion, and Figure 4.8 can be interpreted as the effect of changing flap immersion. Although some scatter is present, a reasonable curve can be drawn, confirming that wave slope depends on the depth of flap immersion. Experiment also showed that for a constant depth of flap immersion water speed did not directly influence the wave slope.

Steep waves, λ/h of 18, were generated, but a further increase in flap immersion produced a breaking first crest and greatly reduced the size of subsequent waves. It is considered possible that a curved flap rather than a flat one may allow steeper waves to be generated.

It is important to note that the relationship

$$c = \sqrt{\frac{g\lambda}{2\pi}} \quad \dots \quad 4.1$$

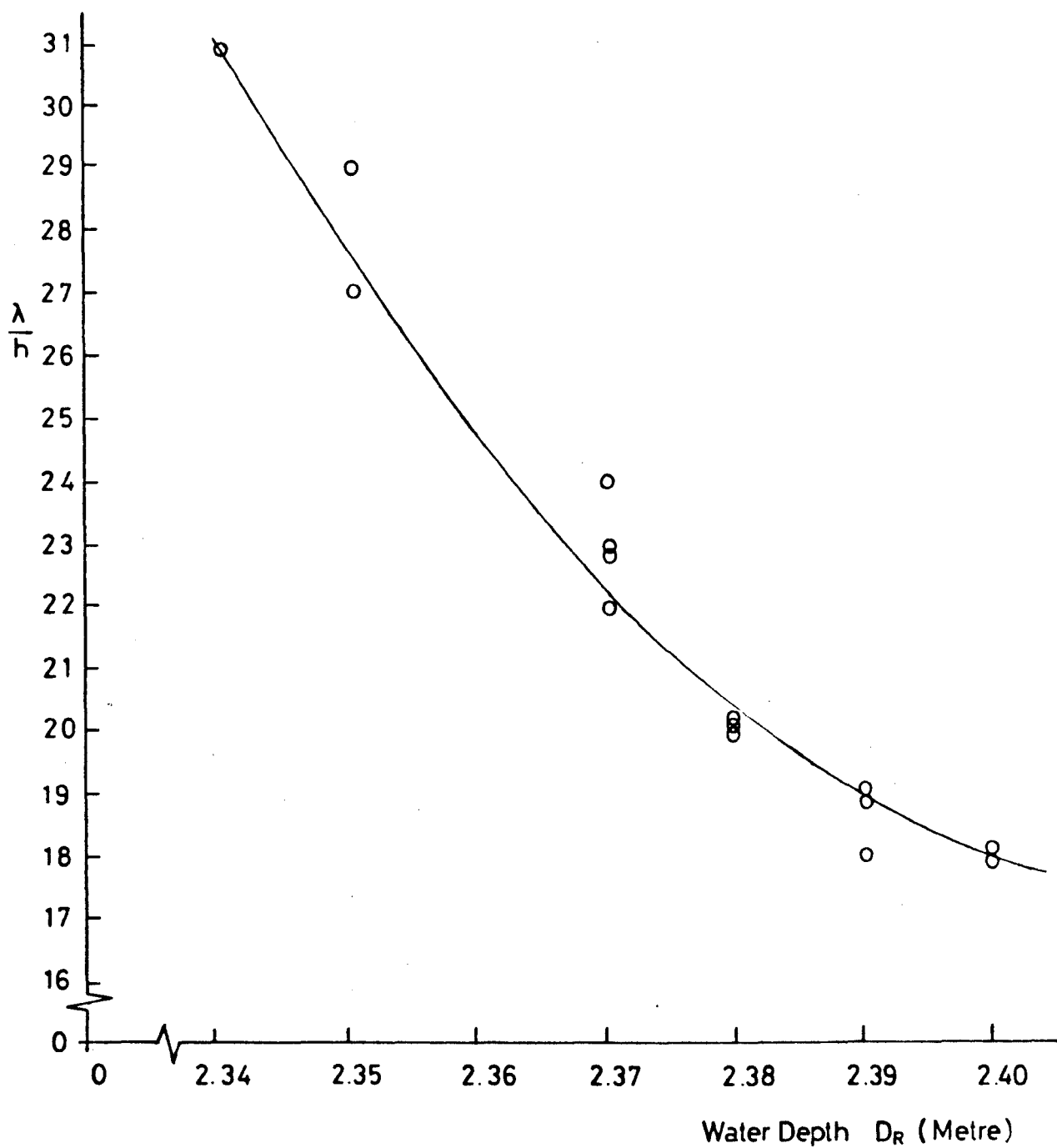


Figure 4.8 λ/h Against Running Water Depth

holds to within 1% for the conditions where the wavelength was measured and this discrepancy is easily explained by errors in speed and length measurement.

The generated waves appear stationary to an observer or to a ship model secured in the working section of the CWC, i.e. the ship model will have a zero frequency of encounter.

Planar Motion Mechanism Experiments

General:

The body plan of the model used in these experiments is given in Figure 4.9 and its principal dimensions are given in Table 4.2.

Three 1.1 KN modular force gauges were fitted into the model to measure the lateral and longitudinal forces. A general arrangement of the fully rigged model is given in Figure 4.10. A ten turn rotary potentiometer was fitted between the CWC carriage and the centre of the model so that the lateral position of the model could be constantly monitored.

A diagrammatic arrangement of the recording set-up is shown in Figure 4.11. The signals from the gauges and rotary potentiometer were fed through suitable amplifiers and filters to a Racal tape recorder with downstream monitoring being undertaken by a U/V recorder.

Prior to commencing the experiments the assertion made in Ref. 43 that blockage effect on transverse forces is negligible over the working range was checked and found valid.

Experiment Specification:

The water speed for the experiments in waves was 2.47 m/s which was as fast as practical in the CWC. This speed gave a wavelength of 3.9m ($\lambda/L = 1.07$). The Froude number for the model at this speed is 0.41. From the results of the free running model experiments conducted by Lloyd on the same fine form (see Chapter 1) it was estimated that the initial ship speed from which the acceleration must take place would be equivalent to a $F_n = 0.37$, which is a typical operating speed for this type of vessel and is equivalent to a CWC water speed of 2.22 m/s.

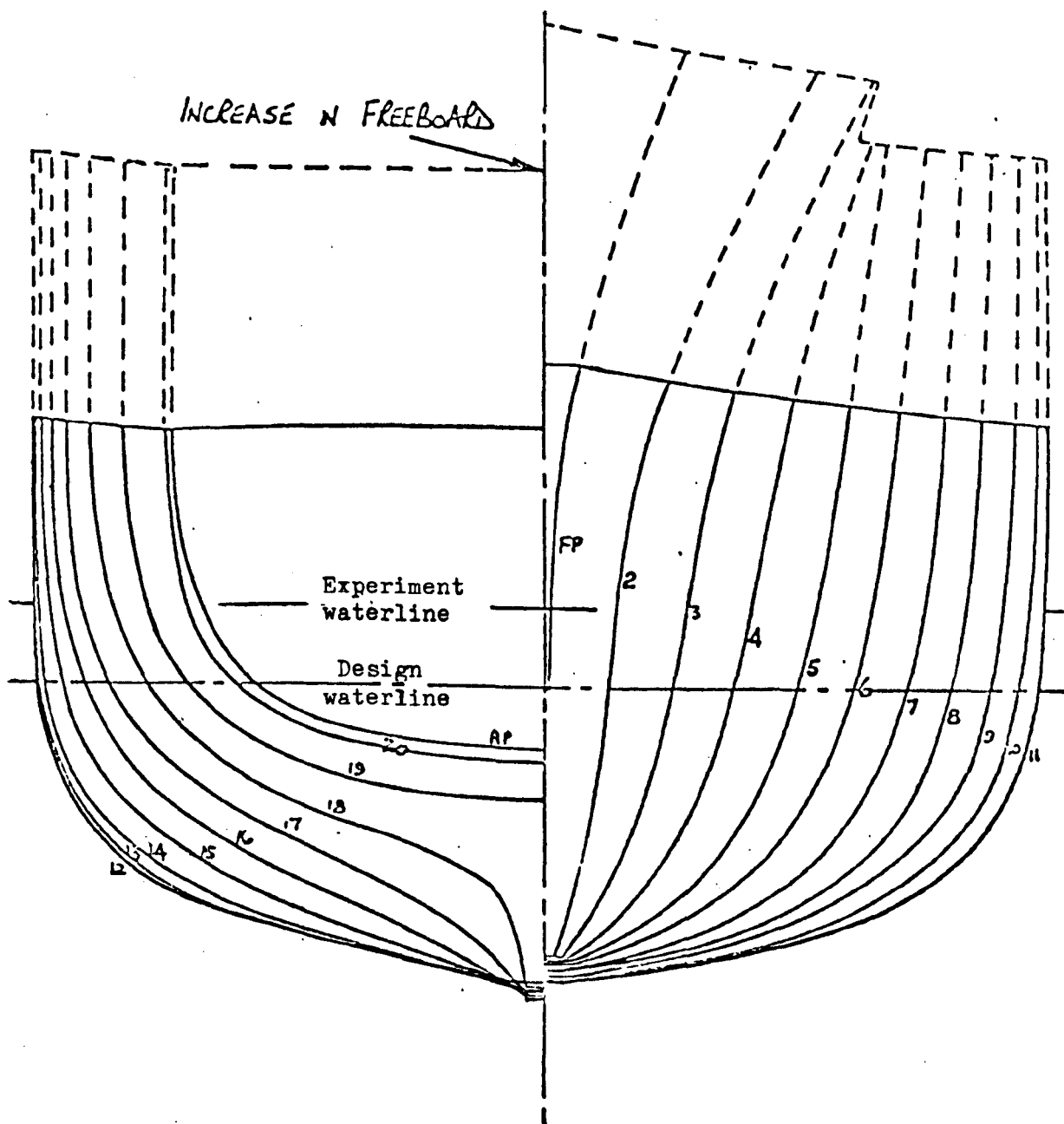


Figure 4.9 Body plan of fine form model.

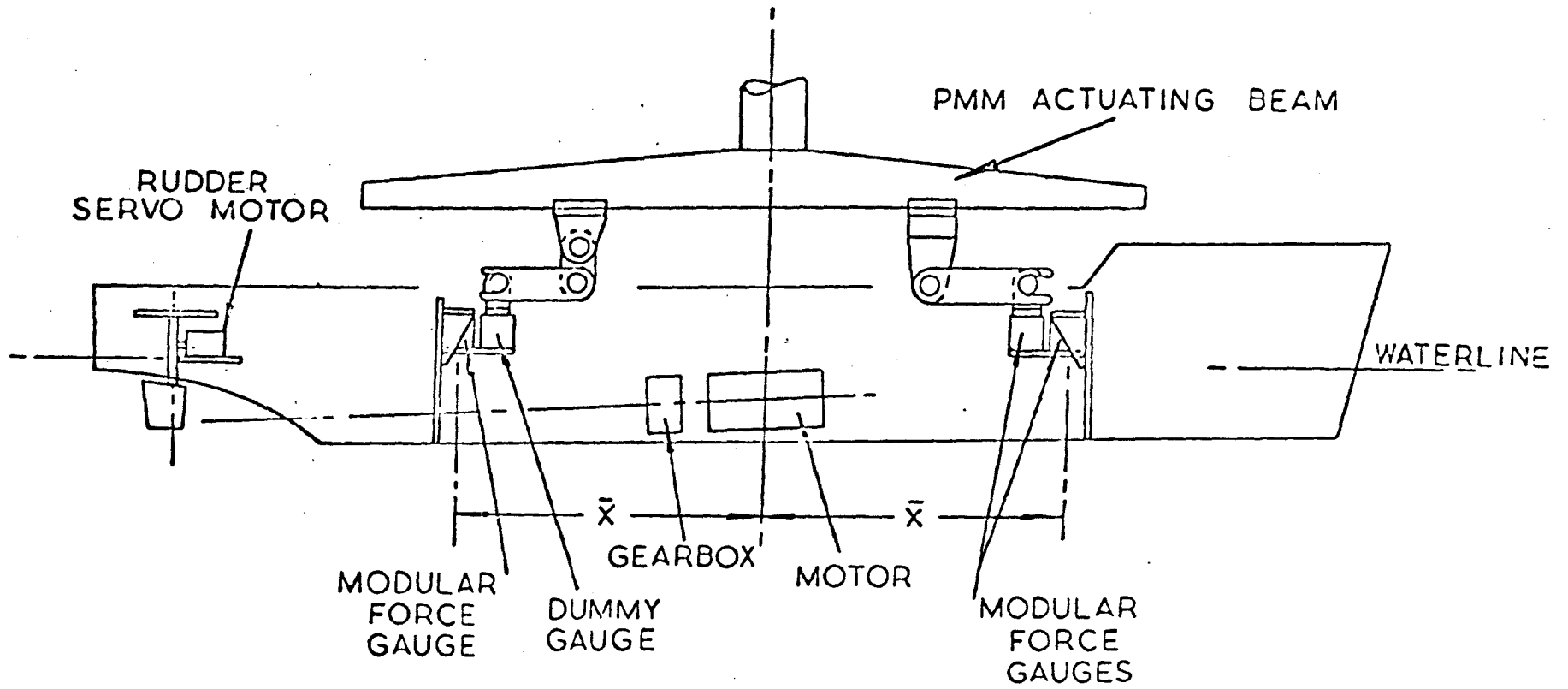


Figure 4.10 General arrangement of fine form model.

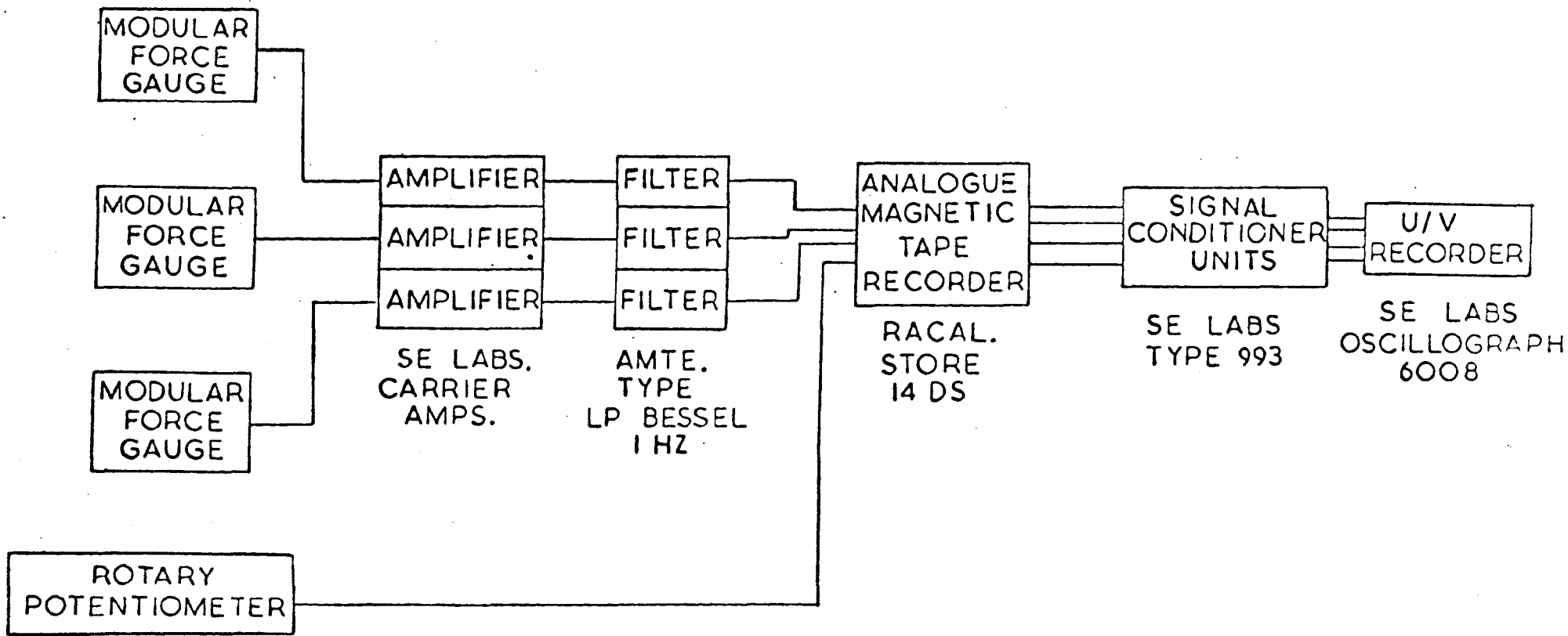


Figure 4.11 Diagrammatic arrangement of instrumentation

(a) Series I

With the CWC operating at 2.22 m/s (low speed) and without generating waves, the model self-propulsion revolutions ($SP_{2.22}$) was obtained. Conventional* PMM experiments were then conducted maintaining the propeller revolutions at $SP_{2.22}$.

(b) Series II

The water speed was increased to 2.47 m/s (high speed), calm water conditions being retained. The propeller revolutions were again set at the $SP_{2.22}$ value and the Series I experiment repeated.

(c) Series III

The initial depth of water (D_0) in the CWC was set to give a λ/h of 28 (steeper waves were found to swamp the model) and the water speed set at 2.47 m/s. The model was positioned with its transom on the third crest from the wavedozer and the Series I experiments repeated. The propeller revolutions were again set at the $SP_{2.22}$ value.

(d) Series IV - IX

The Series III experiments were repeated with the model sited at 6 further positions relative to the wave crest, the last position being a repeat of that in Series III, but one wave crest further downstream.

Many of the individual runs were repeated at later dates and, in general, there was good repeatability in the results. Some limited experiments were conducted in the next wave either side of that used for the majority of the experiments and, again, agreement was good.

Experiment Procedure:

Running conditions in the CWC were allowed to settle for at least ten minutes before any records were taken.

For the steady state runs, records were taken for a period of 10 - 15 seconds so that fluctuations in the measured forces could be averaged out.

* The conventional PMM experiments undertaken were as follows:

Steady state yaw angle; steady state rudder angle;
dynamic pure sway and dynamic pure yawing.

Two amplitudes of oscillation and a range of frequencies were used for all model/wave positions. For the dynamic sway runs they were:

Amplitudes y_0 0.40 and 0.60 metres
 Frequencies ω 0.1 → 1.0 radians/sec.

For the dynamic yawing runs three amplitudes were used with a different range of frequencies for each amplitude. This is because $\omega = U\alpha_0/y_0$ and reasonable forces had to be produced. The amplitudes and frequencies used were:

Amplitudes α_0 0.03 rad 0.09 rad 0.15 rad
 Frequencies ω 0.1 → 1.0 rad/sec 0.1 → 1.0 rad/sec 0.5 → 1.0 rad/sec.

Note: For both dynamic sway and dynamic yawing, the frequency was built-up slowly, 10 - 15 seconds being allowed at the running frequency before data recording commenced. At least ten cycles were recorded to enable any fluctuations due to wave disturbances to be averaged out.

Figure 4.12 shows the model in a wave. It will be seen that the freeboard had to be increased to reduce the possibility of swamping.

During the settling down period of one of the series it was noticed that the port rudder ventilated (despite being well immersed initially) as shown in Figure 4.13.

Analysis:

There were two sets of steady state experiments:

- (a) Varying heading angle, fixed rudder 0 degrees, and
- (b) Varying rudder angle, fixed heading 0 degrees.

In the calm water condition, heading angle (α) is equivalent to drift angle (β) and hence the drift derivatives (Y'_v and N'_v) can be obtained since $v = U\beta$ for small β . In the wave condition, however, the fact that the model is given a heading angle means that the wave derivatives (Y'_α, N'_α) account for part of the force. Thus, the measured force and moment correspond to

$$\begin{aligned} Y &= (Y'_v v + Y'_\alpha \alpha) \\ N &= (N'_v v + N'_\alpha \alpha) \end{aligned} \qquad \dots \qquad 4.2$$

where $v = -U\beta$ and $\beta \equiv \alpha$ in this case.

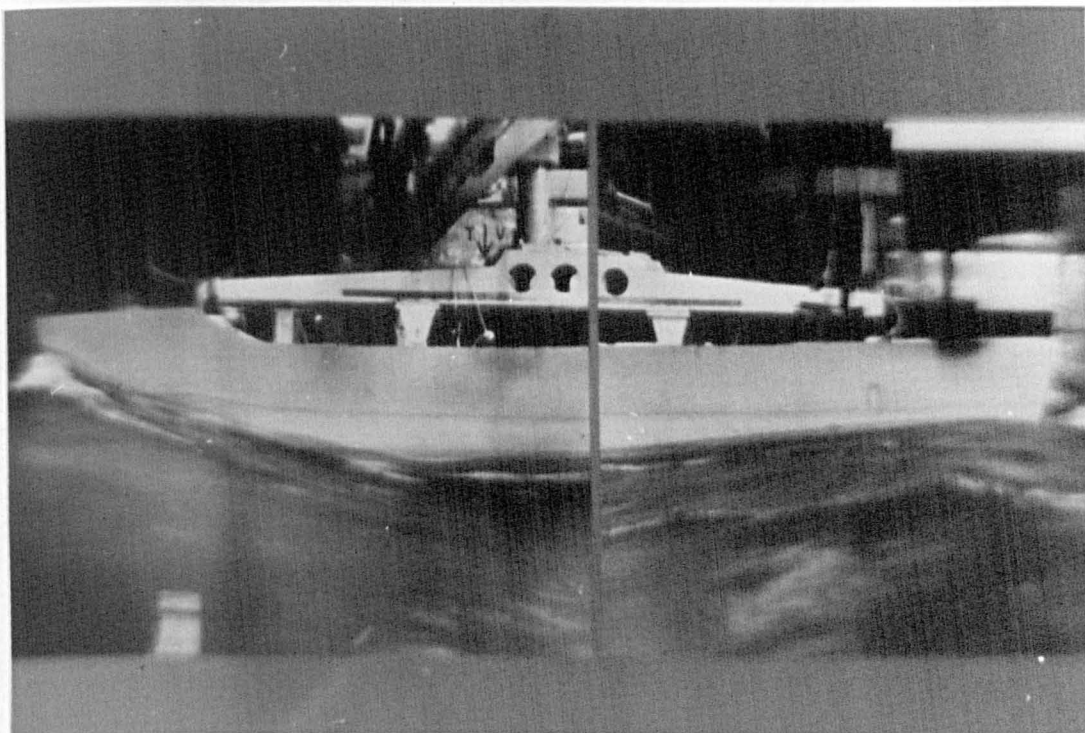


Figure 4.12 Model in a wave

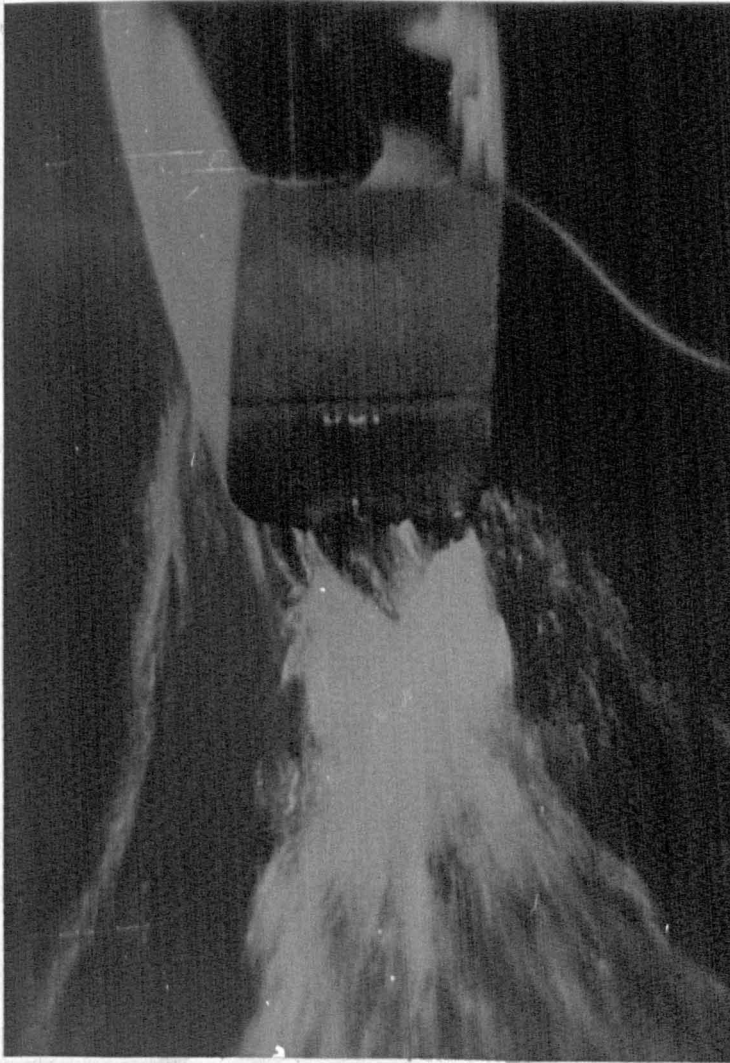


Figure 4.13 Rudder ventilation in a wave

Hence,

$$Y = \left(Y_v - \frac{Y_\alpha}{U} \right) v \quad \dots \quad 4.3$$

with a similar expression for the moment. Therefore, the derivatives Y_v and Y_α cannot be measured independently from the steady state results because they always appear in the form $(Y_v - Y_\alpha/U)$.

The rudder derivatives can be obtained using the same technique for the wave condition and the calm water condition, as the model has no heading or drift angle.

For both dynamic pure sway and dynamic pure yaw the model is given harmonic motion of the form $y = A \sin \omega t$. For pure sway the governing equations are

$$\begin{aligned} y &= y_0 \sin \omega t \\ v &= y_0 \omega \cos \omega t \\ \dot{v} &= -y_0 \omega^2 \sin \omega t \\ \alpha &= 0 = \delta \quad \beta_0 \neq 0 \end{aligned} \quad \dots \quad 4.4$$

and the sway force equation becomes

$$Y = Y_v y_0 \cos \omega t - (Y_{\dot{v}} - m) y_0 \omega^2 \sin \omega t \quad \dots \quad 4.5$$

This makes it possible to separate Y_v and $(Y_{\dot{v}} - m)$ from the force record using the in-phase and the out-of-phase components in the usual manner [29]. This approach, however, is complicated by the existence of frequency dependence and non-linearities as discussed in Appendix D. For this reason the technique outlined there was used for the analysis of all dynamic records.

The governing equations for pure yaw are

$$\begin{aligned} \alpha &= \alpha_0 \cos \omega t \\ r &= -\alpha_0 \omega \sin \omega t \\ \dot{r} &= -\alpha_0 \omega^2 \cos \omega t \\ \beta &= 0 = \delta \quad \alpha_0 \neq 0 \end{aligned} \quad \dots \quad 4.6$$

and the sway force equation becomes

$$Y = Y_\alpha \alpha_0 \cos \omega t - (Y_r - mU) \alpha_0 \omega \sin \omega t - (Y_{\dot{r}} - mX_G) \alpha_0 \omega^2 \cos \omega t \quad \dots \quad 4.7$$

From Eq. 4.7 it is not immediately possible to separate the derivatives Y_{α} and $(Y_{\dot{r}} - mx_G)$. The technique for doing this is similar to that for separating M_{θ} and $M_{\dot{q}}$ when testing submarine models with a vertical PMM. The combined coefficient, $[Y_{\alpha} \alpha_0 - (Y_{\dot{r}} - mx_G) \omega^2]$, is plotted against ω^2 for the range of frequencies tested and hence Y_{α} and $(Y_{\dot{r}} - mx_G)$ are obtained from the resulting straight line. This is discussed more fully for the submarine model in Ref. 29.

Results:

The results of the PMM experiments are all presented in the next chapter, where comparison is made with the results obtained from the theory developed in the previous chapter.

Table 4.1. SERIES 60 MODEL PARTICULARS

Length between perpendiculars	2.9m
Beam	0.399m
Draft	0.16m
Displacement	118 kg
GM	0.055m

Table 4.2. FINE FORM MODEL PARTICULARS

Length between perpendiculars	3.66m
Beam	0.417m
Draft	0.161m
LCB	0.0119m aft
Displacement	127.65 kg
I_z	81.3 kg m ²
Stern arrangements	Twin screw (outward turning) Twin rudder

Chapter 5

COMPARISON BETWEEN THEORETICAL AND EXPERIMENTAL
DETERMINATION OF THE COEFFICIENTS

The theoretical method developed in Chapter 3 was programmed in Fortran on the Department's PDP 11/40 digital computer. Each stage of every calculation was checked by hand to ensure that it was carried out correctly by the computer. Due to limitations in the size of the 11/40 it was not possible to carry out all the calculations in one large program and hence it was necessary to write three smaller programs, each requiring to be run separately (see Appendix C).

Once these programs were running and checked, the coefficients were calculated for the fine form in the same condition as used during the PMM experiments. The theoretical results are compared with the experimental ones in Figures 5.1 - 5.14.

Figure 5.1 shows the variation in trim over the ship's longitudinal position in the wave. Zero trim is taken to be that obtained when running at $F_n = 0.41$ in calm water. This shows that the assumption made early in Chapter 3 - that the position of the ship in the vertical plane can be calculated by assuming that the displacement must remain constant and that the longitudinal position of the LCB and the LCG must coincide - is reasonable, at least for determining the trim angle.

Figure 5.2 gives the longitudinal force as a function of ship position in the wave. The chain dotted line represents the experimentally obtained increase in resistance from initial speed to wave speed as discussed in Chapter 2. From this figure it can be seen that a free running model would probably spend most of its time between $\xi \approx 0.8$ and $\xi \approx 0.1$. Thus, lateral stability over this region would be most important. The agreement between experiment and theory is quite good considering the difficulties of calculating longitudinal forces on a slender body. The major discrepancy is between $\xi \approx 0.3$ and $\xi \approx 0.5$, which may not be too significant, as a free running model would not spend much time over this region anyway.

The wave-induced sway force and yaw moment derivatives are given in Figures 5.3 and 5.4 respectively. They can be obtained from the experimental records either using Eq. 4.3 or Eq. 4.7, and both results are given in the two figures. Considerable scatter is present in the experimental results, particularly for Y'_α , since the total measured force was quite small. It is thought that the method of Eq. 4.7 is more reliable (solid circles). Bearing in mind the experimental scatter, the correlation between theory and experiment is reasonable, particularly in the case of N'_α , which is more important for the prediction of broaching than Y'_α .

The rudder derivatives, as functions of longitudinal ship position in the wave, are given in Figures 5.5 and 5.6. Again, the Y' derivative is not predicted as well as the N' derivative, due to small total side force, but as it is not very significant in the prediction of broaching, this is not too important. The serious loss of rudder effectiveness often associated with a broach can be seen over the range $\xi \approx 0.55$ to 0.8 . However, this does not correspond to that in which Figure 5.2 implied the ship would spend most of its time. Thus, perhaps for a broach to occur a significant yawing motion must be set up in the short time that the ship passes through this region. A more thorough look at the effect the changing coefficients have on the ship motion is given in the next two chapters.

Figures 5.7 and 5.8 are plots of Y'_V and N'_V respectively against ξ . Y'_V is fairly large, so experimental scatter is not too great and correlation between theory and experiment is quite good. N'_V , on the other hand, is quite small and although the experimental points do not have a large scatter the correlation between them and the theory is poor.

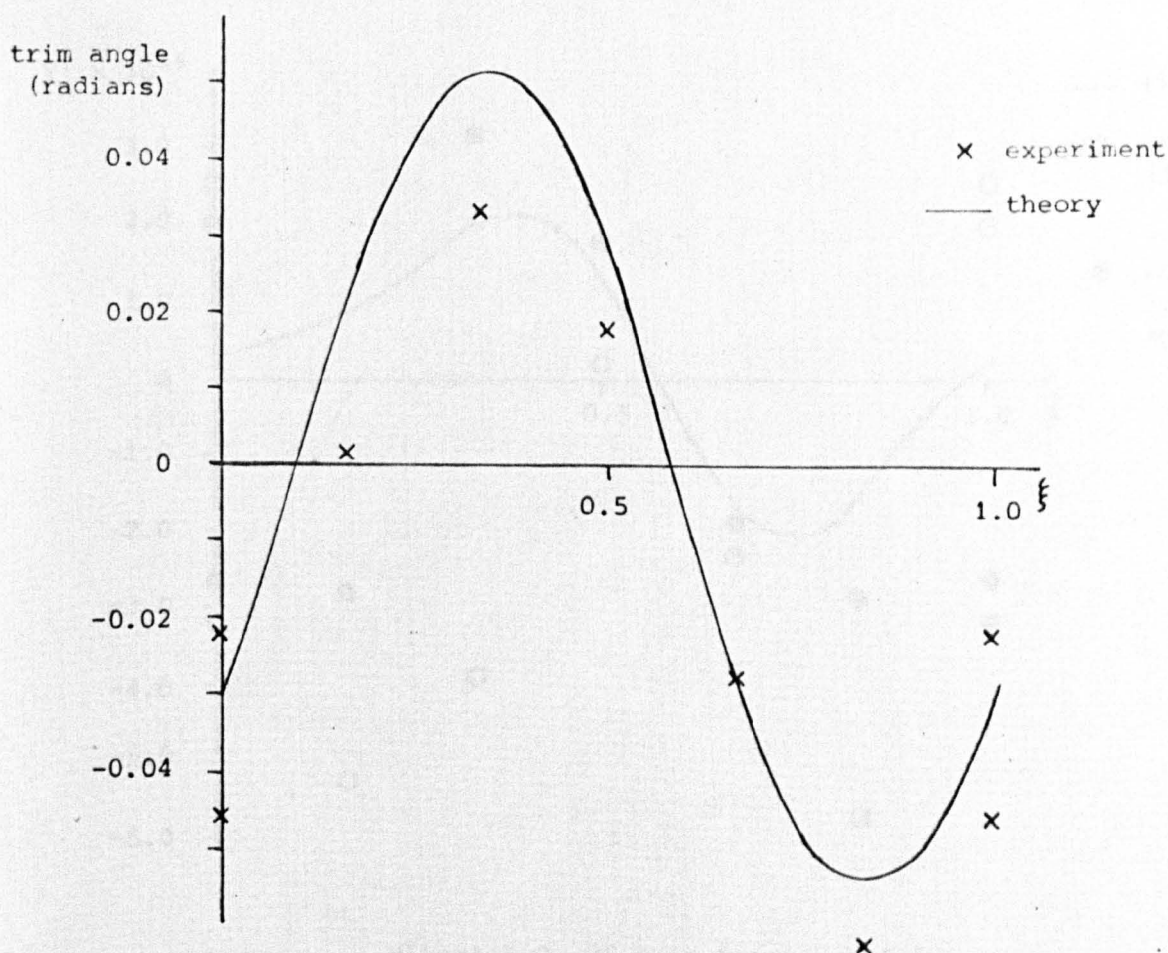
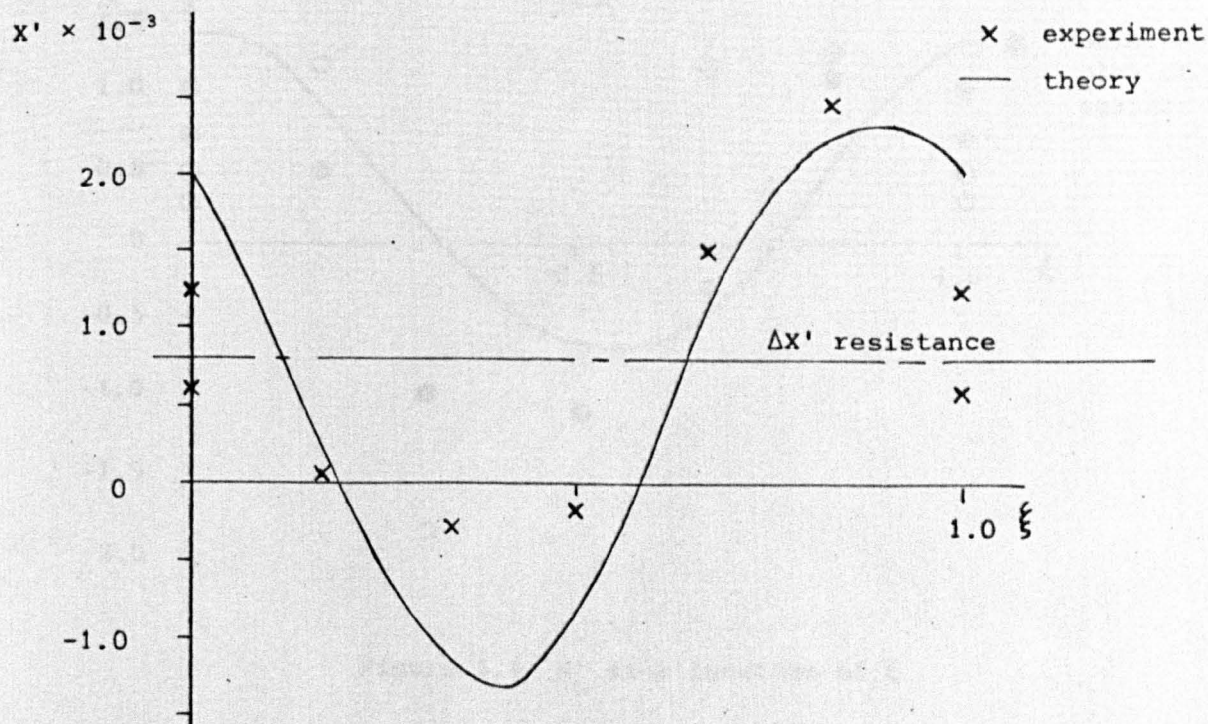
$(Y_r - m)'$ and $(N_r - mx_G)'$ are given as functions of ξ in Figures 5.9 and 5.10 respectively. Here $(Y_r - m)'$ is small and the experimental scatter is fairly large, with correlation between theory and experiment not being very good. This will not be too important as $(Y_r - m)'$ only has a second order effect in the prediction of yawing behaviour, since it is the coupling term between the yaw velocity (r) and the sway force (Y). $(N_r - mx_G)'$ has a direct influence on yaw

and not only is experimental scatter a lot less, but the correlation between theory and experiment is quite good.

The sway acceleration derivatives, $(Y_{\dot{v}} - m)'$ and $(N_{\dot{v}} - mx_G)'$ are given as functions of ξ in Figures 5.11 and 5.12. There is considerable scatter in both sets of experimental results and, although the correlation between theory and experiment is reasonable for $(Y_{\dot{v}} - m)'$, it is particularly bad for $(N_{\dot{v}} - mx_G)'$. Figures 5.13 and 5.14 show the rotary acceleration derivatives and again experimental scatter is quite high. Correlation between theory and experiment is reasonable and shows the considerable reduction in $(N_{\dot{r}} - I_z)'$ with the crest at amidships ($\xi = 0.5$), which may permit large yaw rates to be built-up rapidly when the ship is in this longitudinal position.

Conclusions

Although there is considerable scatter in a lot of the experimental results, and correlation between theory and experiment for some of the coefficients is poor, the more important ones (X' , N'_{α} , N'_{δ}) appear to be predicted quite well by the theory developed in Chapter 3 for the only wave condition tested. It is, therefore, proposed to use this theory to predict the values of the coefficients with other wave lengths in an attempt to determine theoretically the "broaching zones" discussed in the first chapter, although it is recognised that the theoretical results should really have been compared with the experimental ones for more than one wave condition. The next chapter discusses the effect the varying coefficients will have on the equations of motion, while Chapter 7 develops a complete analogue/digital hybrid simulation of ship motion based on simplified equations in order to predict the "broaching zones".

Figure 5.1 Trim as a function of ξ Figure 5.2 Non-dimensional X-force as a function of ξ

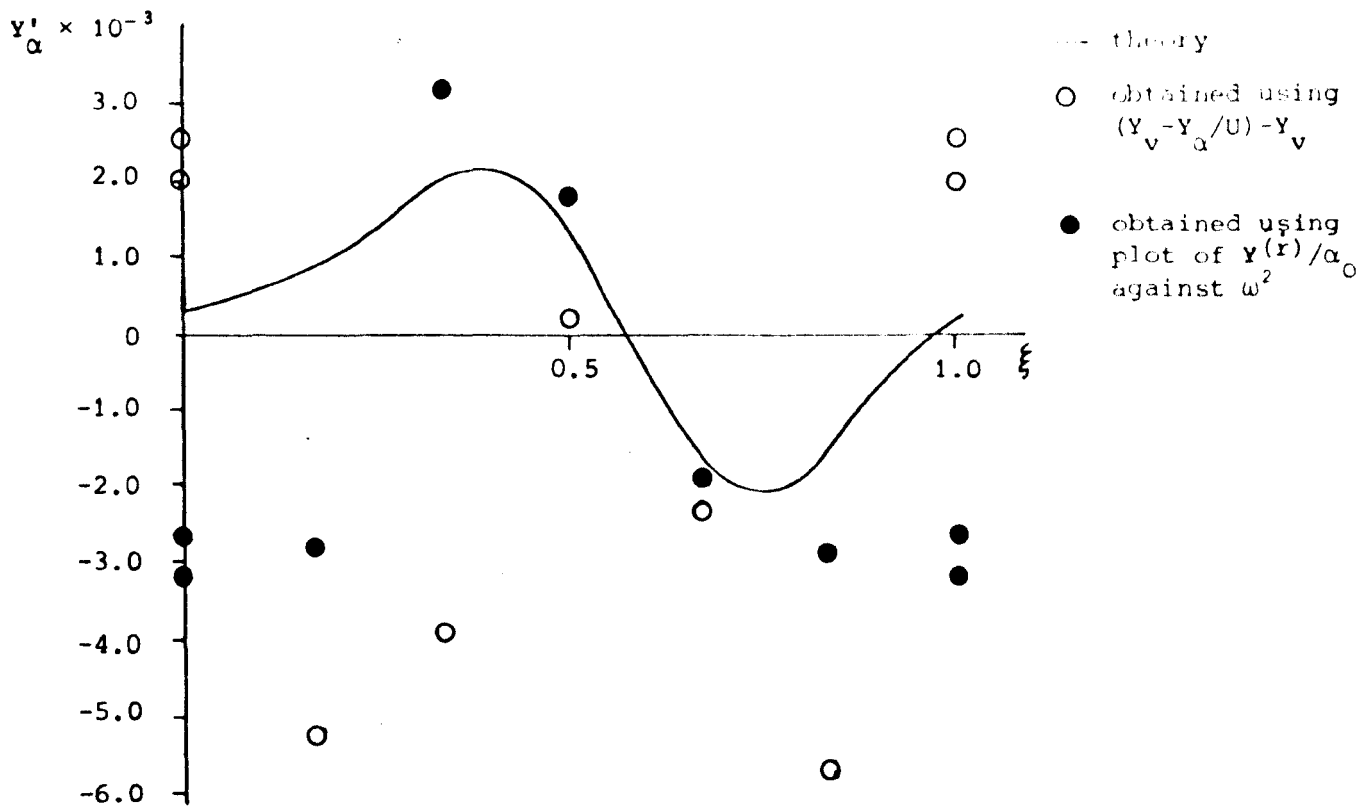


Figure 5.3 Y'_α as a function of ξ

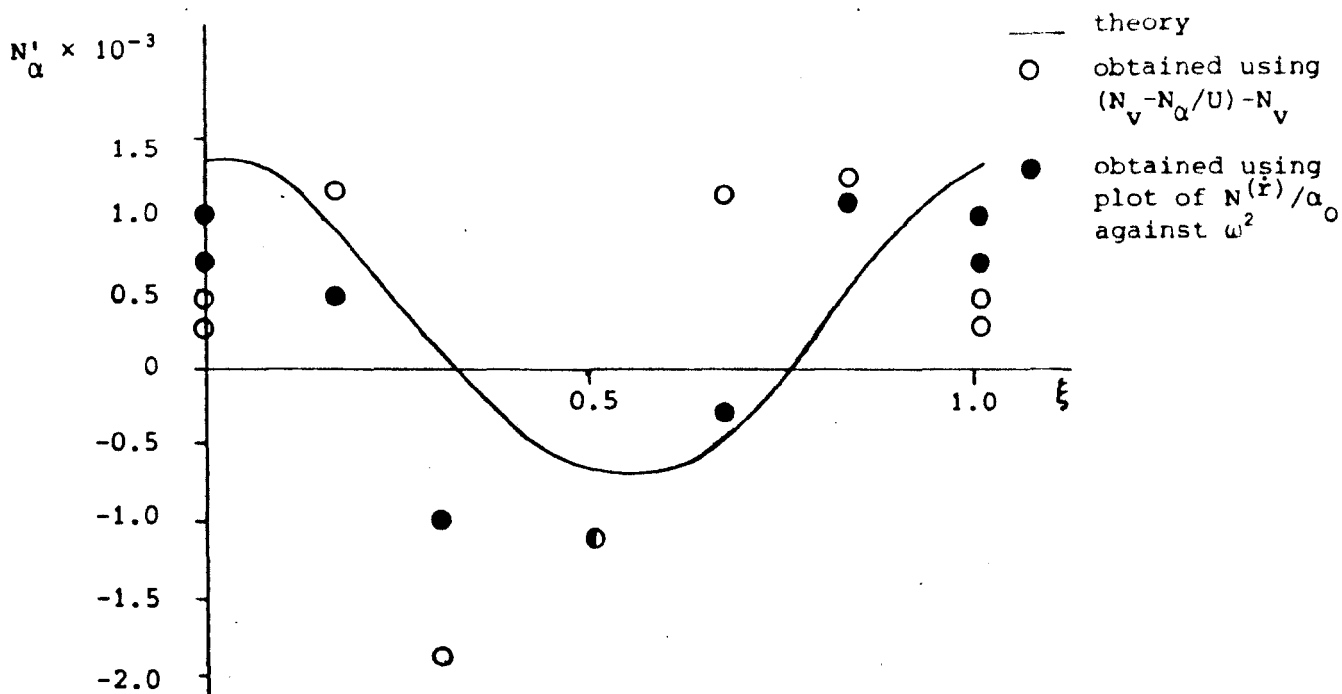
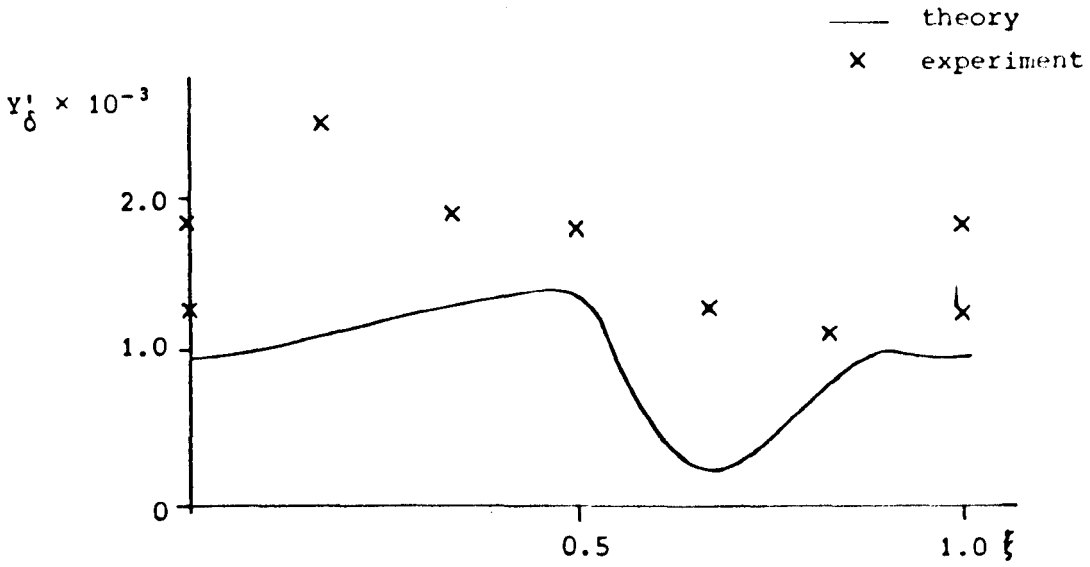
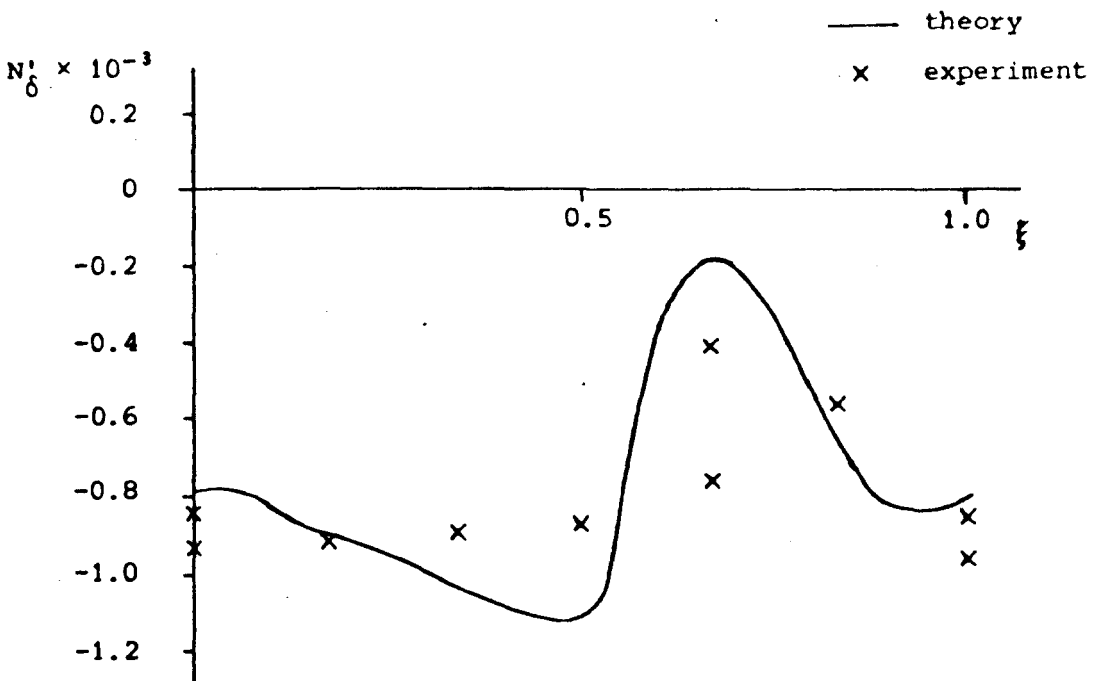
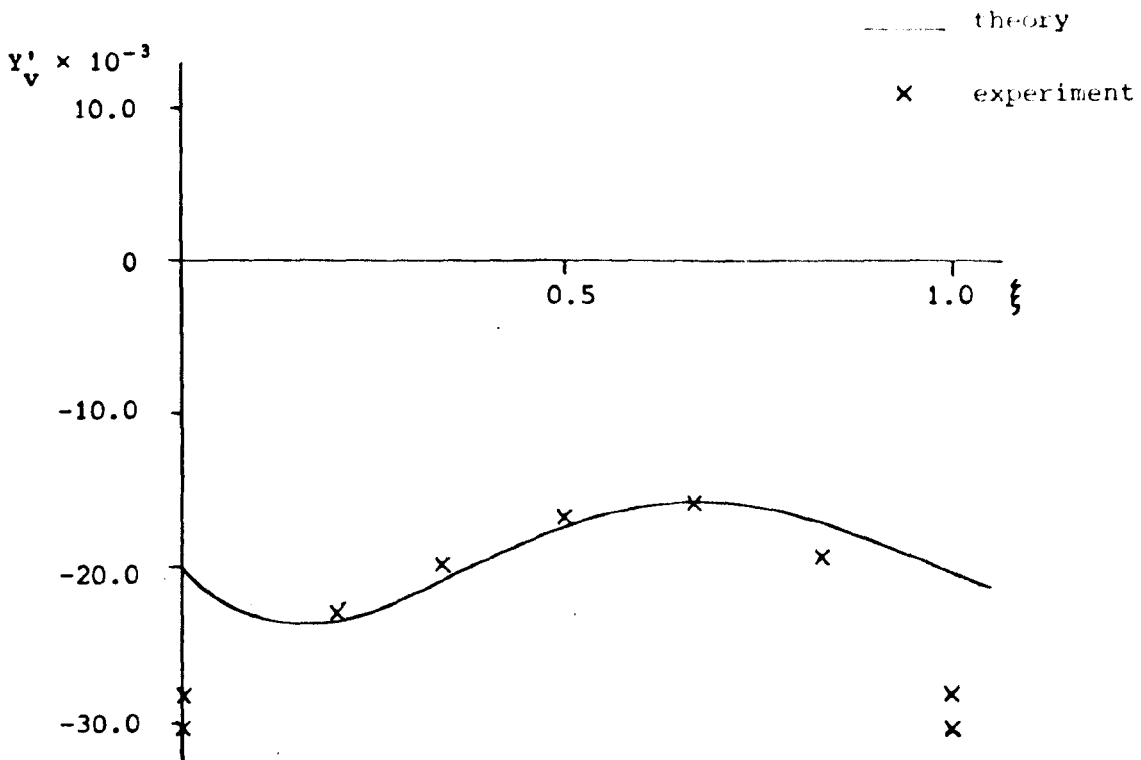
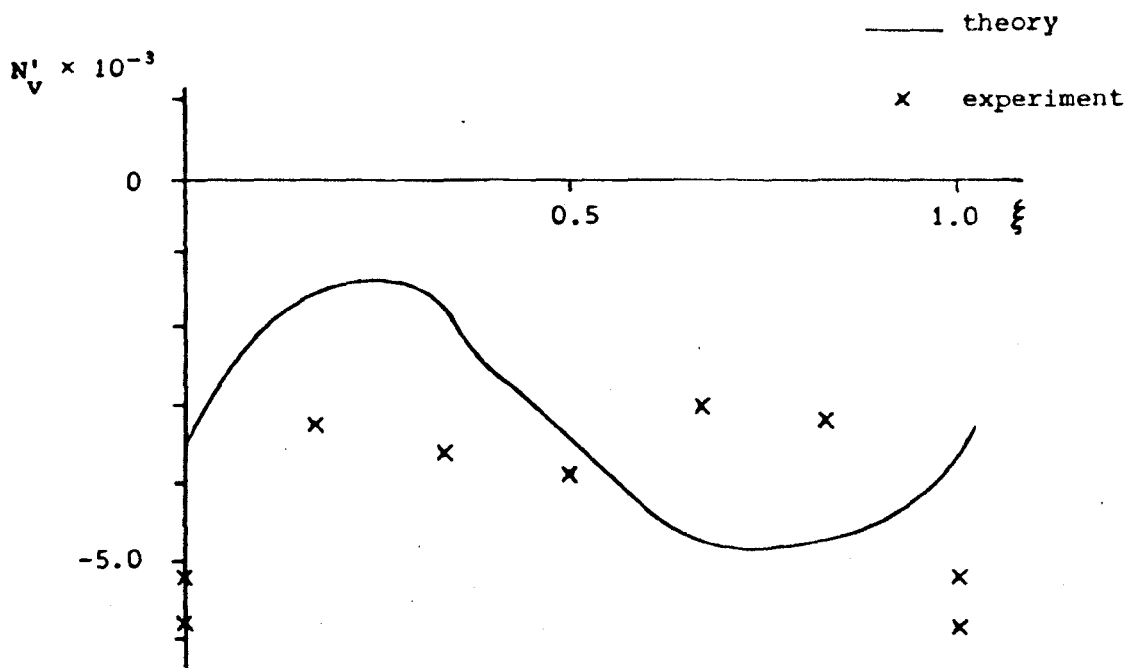
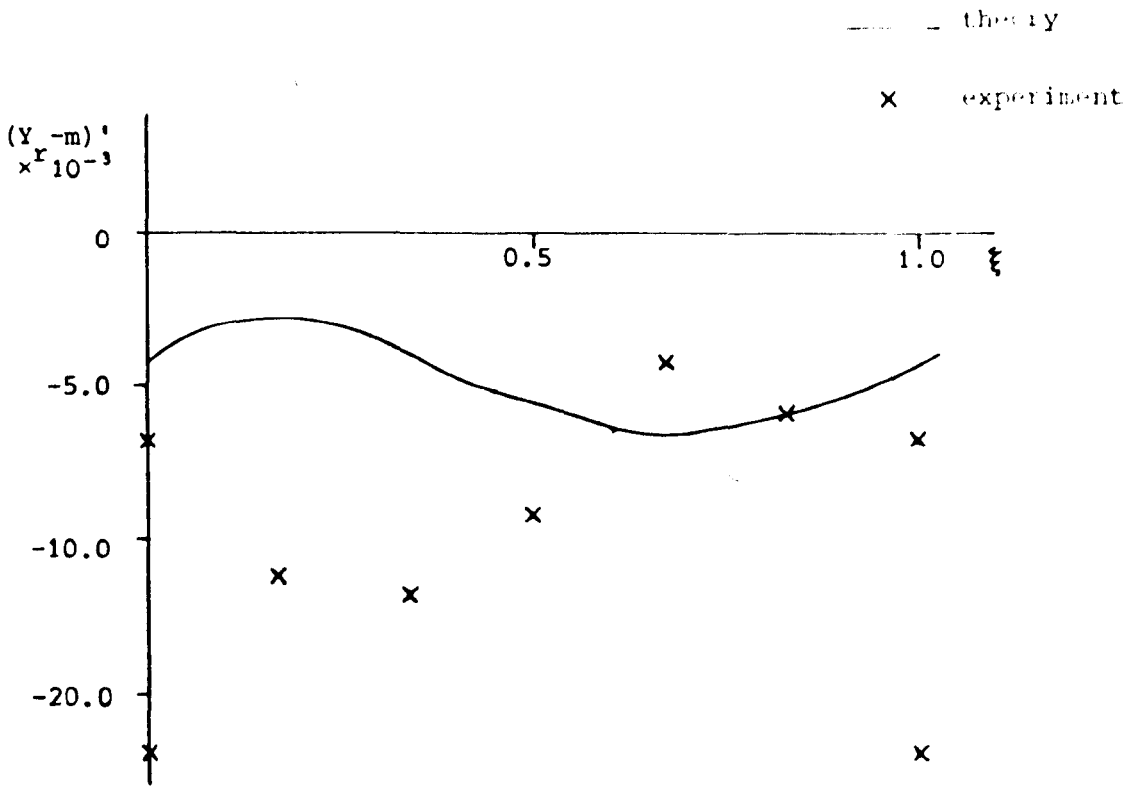
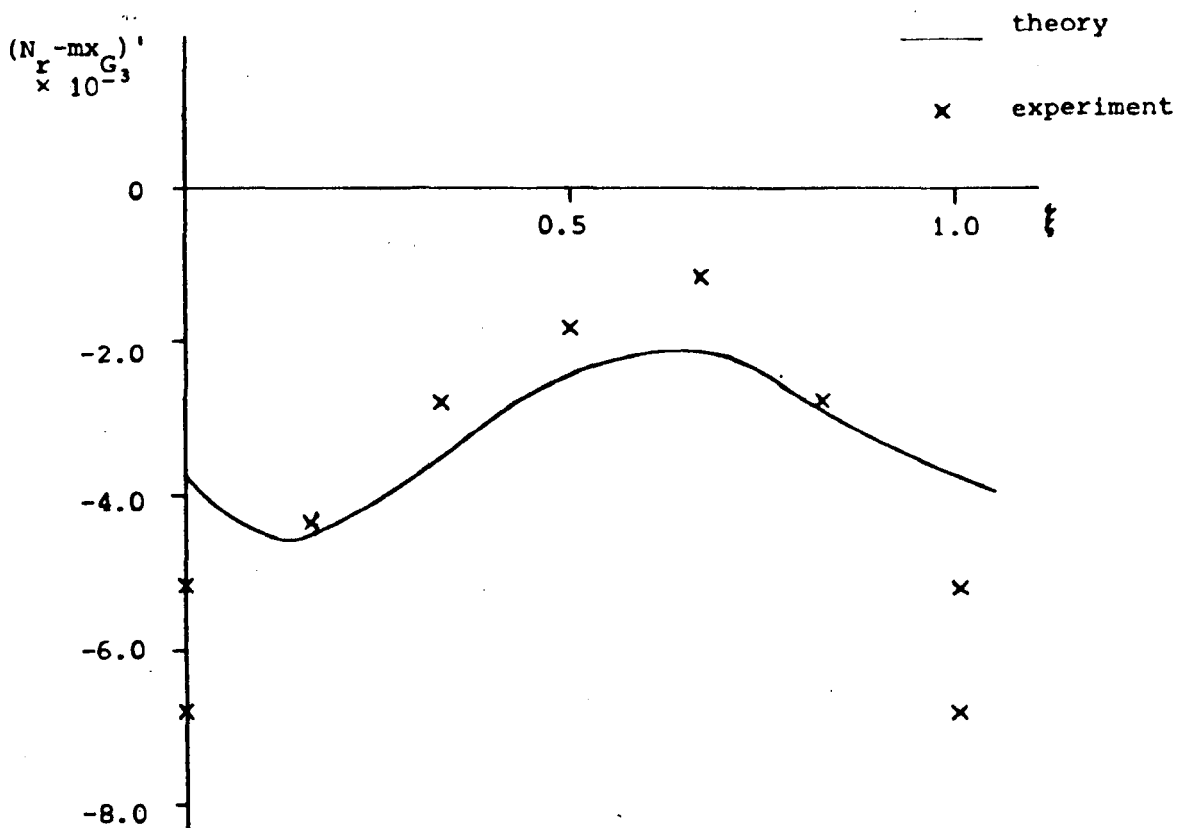


Figure 5.4 N'_α as a function of ξ

Figure 5.5 Y'_0 as a function of ξ Figure 5.6 N'_0 as a function of ξ

Figure 5.7 Y'_V as a function of ξ Figure 5.8 N'_V as a function of ξ

Figure 5.9 $(Y_r - m)'$ as a function of ξ Figure 5.10 $(N_r - mx_G)'$ as a function of ξ

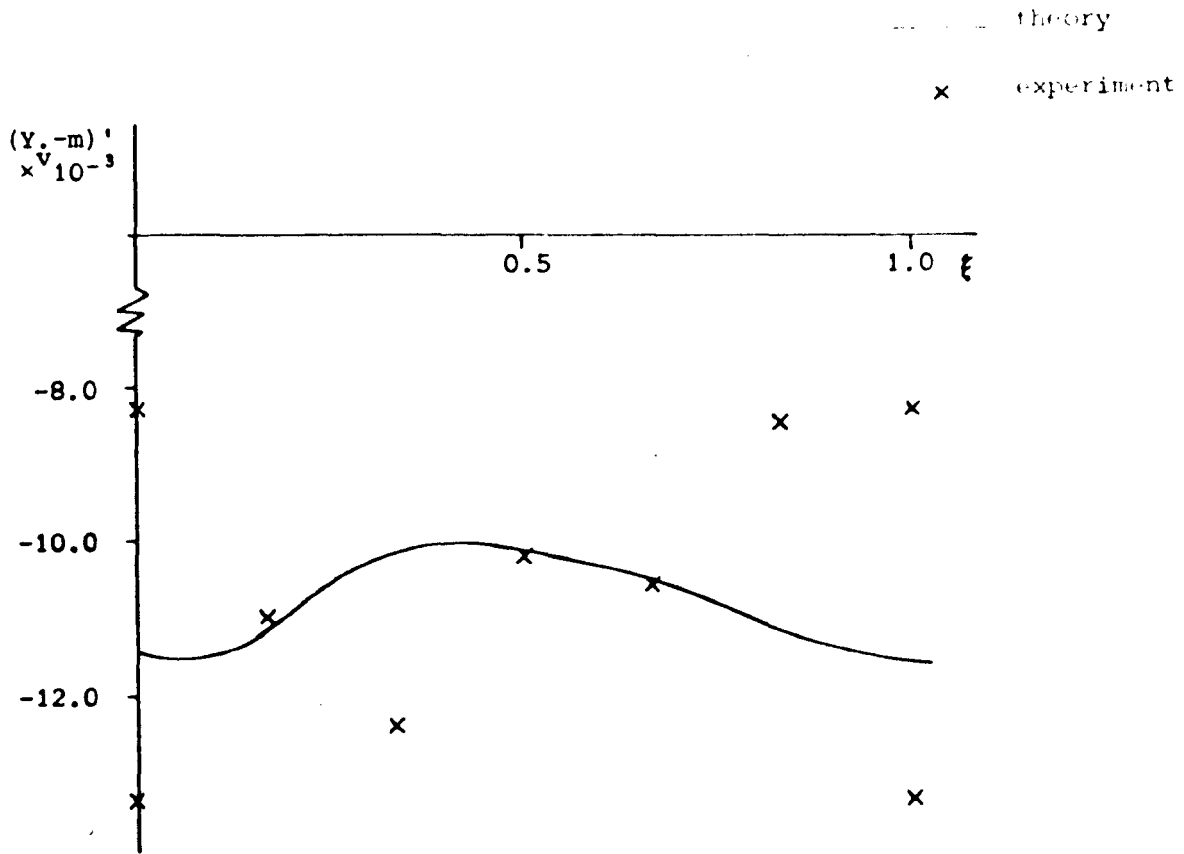


Figure 5.11 $(Y_v - m)'$ as a function of ξ

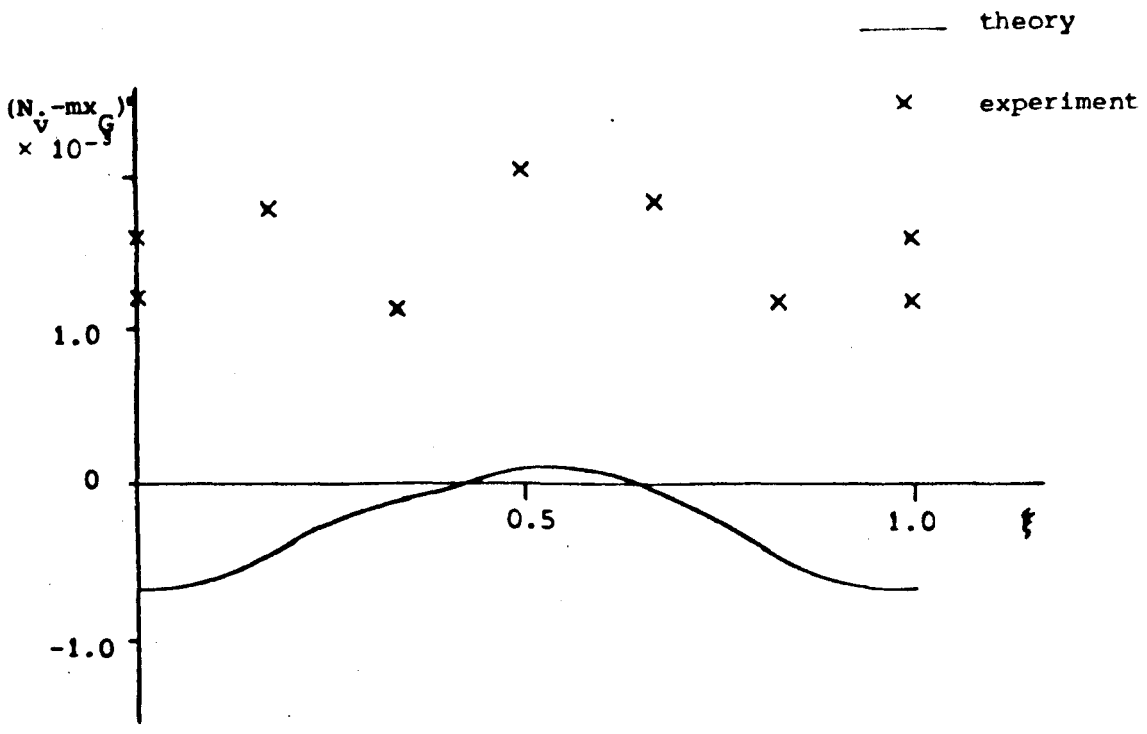


Figure 5.12 $(N_v - mx_G)'$ as a function of ξ

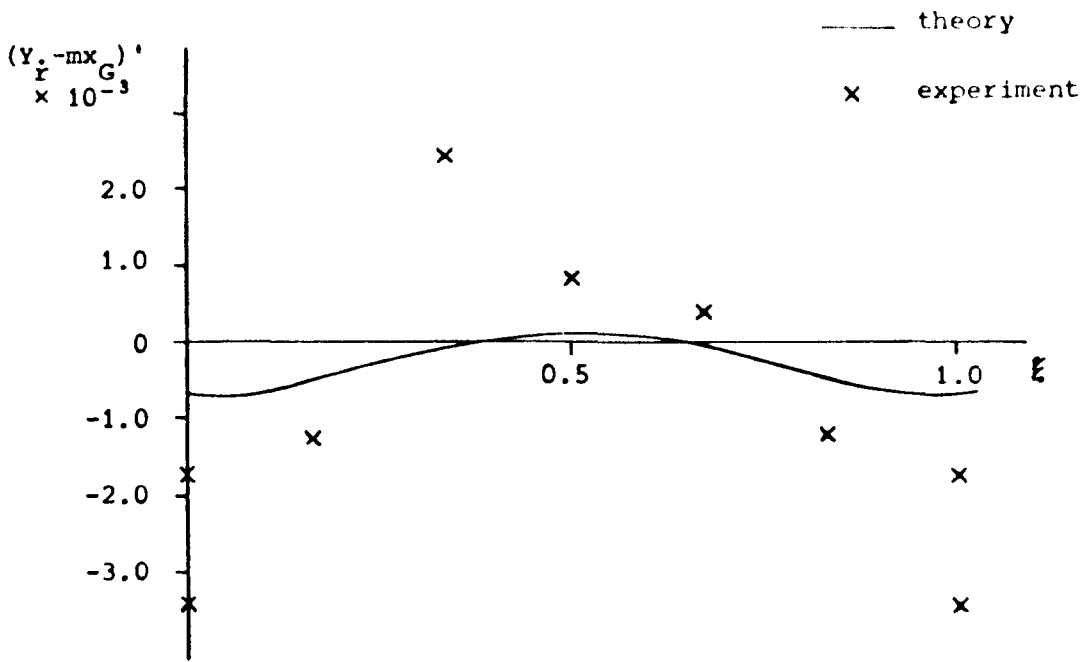


Figure 5.13 $(Y_r - mx_G)'$ as a function of ξ

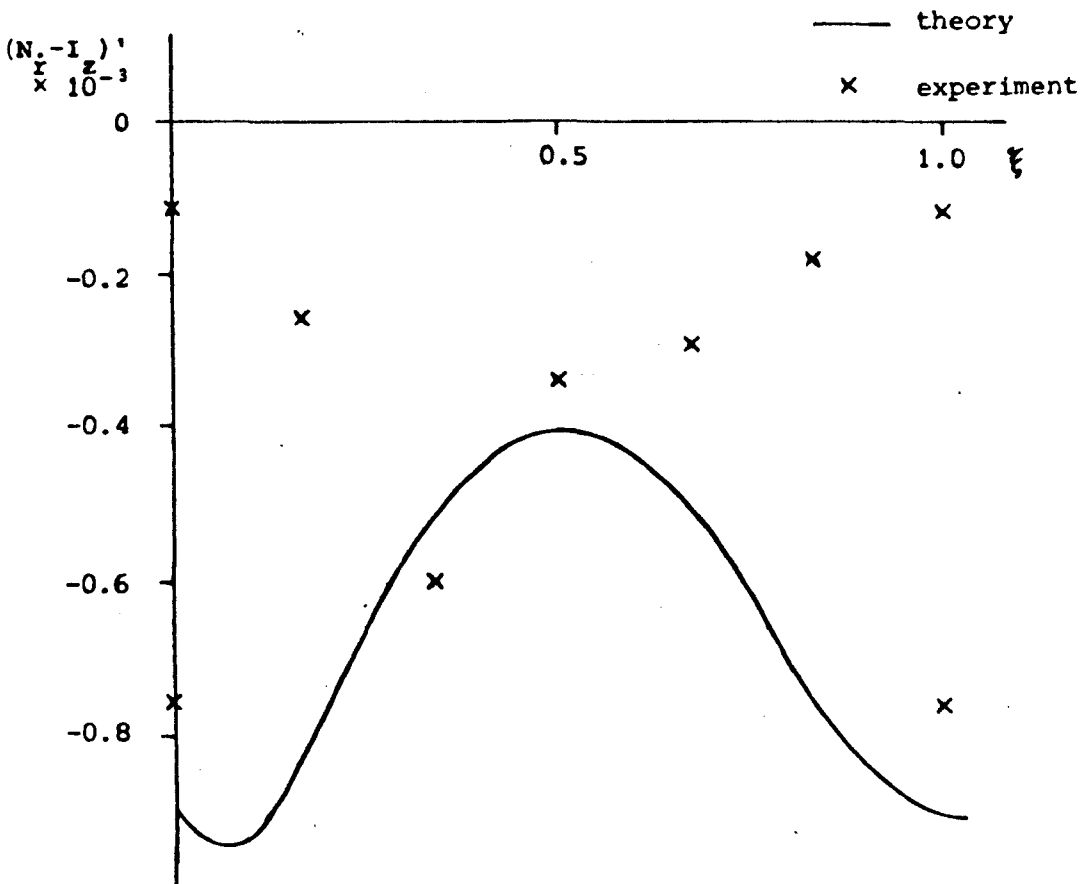


Figure 5.14 $(N_r - I_z)'$ as a function of ξ

Chapter 6

THE EFFECT OF THE VARIATION OF THE COEFFICIENTS
OF THE EQUATIONS OF MOTION

The theoretical method developed in Chapter 3 is used in this chapter to obtain the coefficients over a range of wave lengths. The effect these coefficients have on the equations of motion developed in Chapter 2 is discussed in an attempt to get an indication of which are the more important factors. Although it is not intended in this chapter to predict the "broaching zones" described in Chapter 1, it will be possible to make comparisons between different ships, etc., using the methods discussed here.

The Wave-Induced Longitudinal Force

The variation in non-dimensional wave force with ξ for various wave lengths is given in Figure 6.1. The peak positive value is fairly constant over the range, being only a little less at $\lambda/L = 0.9$ and 2.0. However, the main difference between λ/L values is the shift in ξ position. As discussed in Chapter 2, the longitudinal equilibrium positions are the intersections between the plot of X' against ξ and a horizontal straight line representing the non-dimensional increase in resistance from self-propulsion speed to wave speed. For a given self-propulsion speed the non-dimensional increase in resistance is larger for longer waves (since they travel faster), so there will be a particular wave length above which no equilibrium positions exist. This will give an upper bound for λ/L above which it is not possible for the ship to be forced to travel at wave speed with that value of self-propulsion speed. (When dynamic factors, increased resistance due to rudder action, etc., are taken into account, this maximum wave length will be reduced and will depend on other aspects, such as heading angle, etc.)

The important points to note from Figure 6.1 then, are that there will be an upper bound of λ/L for each self-propulsion speed above which no longitudinal equilibrium positions exist, and that the stable

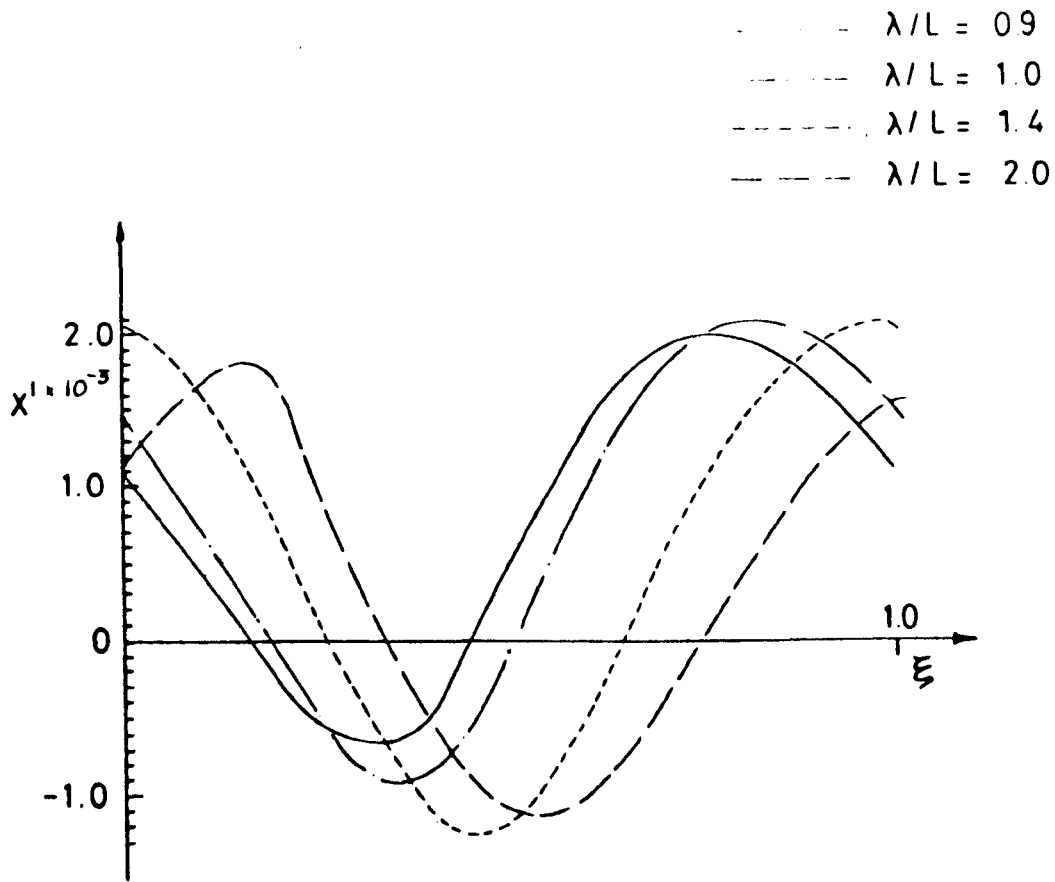


Figure 6.1 X' force as a function of ξ for various λ/L 's
 $D/L = 22.73$ $\lambda/h = 28$

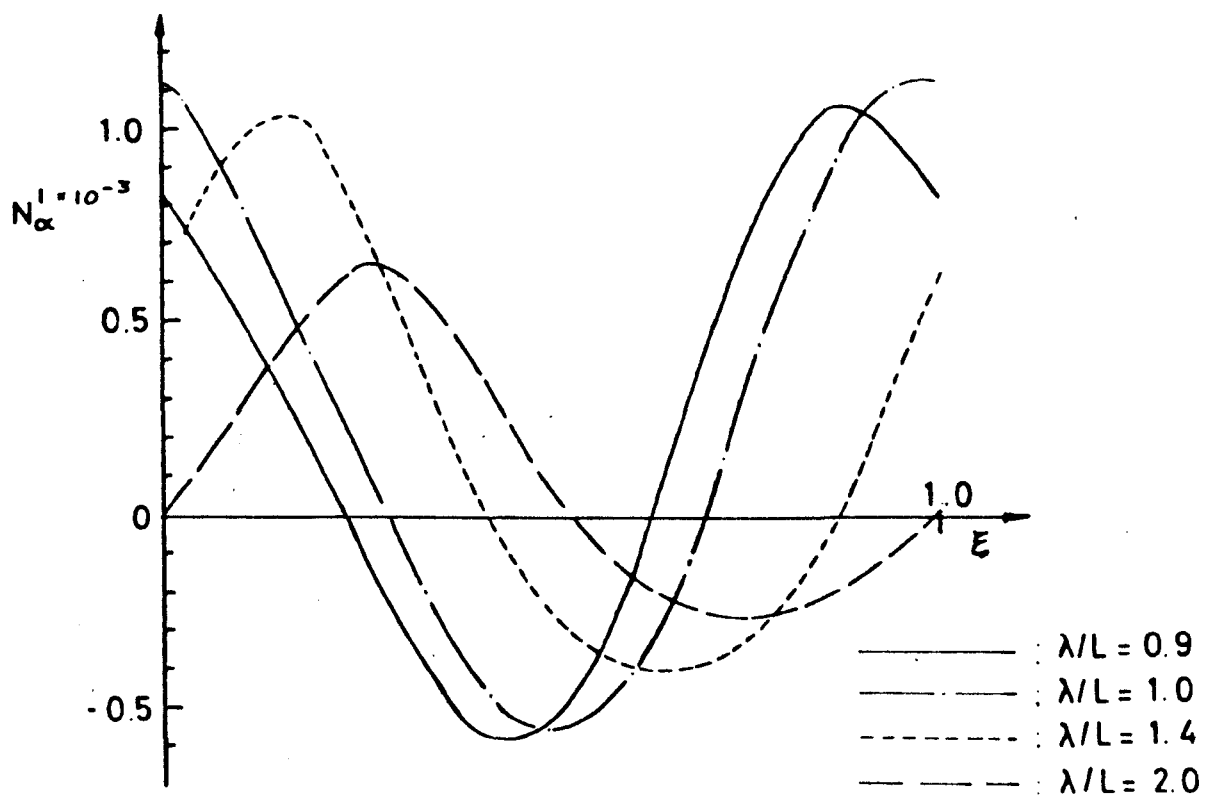


Figure 6.2 N'_α as a function of ξ for various λ/L 's
 $D/L = 22.73$ $\lambda/h = 28$

equilibrium position is between $\xi = 0.0$ and $\xi = 0.3$, depending on ship self-propulsion speed and λ/L , hence this is the region in which the ship will spend most time.

Wave-Induced Yaw Moment

A plot of the derivative, relating wave-induced yaw moment to heading angle N'_α , is given against ξ in Figure 6.2 for various λ/L values. As discussed in Chapter 2, N'_α is required to be positive to cause a broach, and it can be seen that this is the case over the region identified above as being the most important. There is a shift in ξ position with increase in λ/L in the same direction as for the plot of X' . However, the maximum value of the $\lambda/L = 2.0$ plot is much smaller than for the shorter wave lengths. This might imply that as λ/L increases there is a reduced tendency to broach, even when travelling at wave speed.

The Calm Water Stability Criteria

As discussed in Chapter 2, the calm water stability criteria is given by Eq. 2.4 where C must be positive for stability. A plot of C against ξ is given in Figure 6.3 as it was suggested that C becoming negative could be the cause of a broach. As can be seen, C is reduced considerably over the range $0.5 < \xi < 0.7$, but remains positive. In addition, this range corresponds to negative values of N'_α , whereas for a broach to occur, a positive value of N'_α is needed. It is, therefore, concluded that the change in the calm water stability criteria does not cause a broach and hence cannot be used directly as a measure of the liability to broach of a given ship.

Rudder Effectiveness

As was mentioned in the previous chapter, a loss of rudder effectiveness is often associated with a broach, and since the type and position of the rudders can be varied to a certain extent by the designer it is worth taking a closer look at this aspect. The effectiveness of the rudder can be easily judged by the derivative N'_δ and a plot of this against ξ for various λ/h ratios is shown in Figure 6.4.

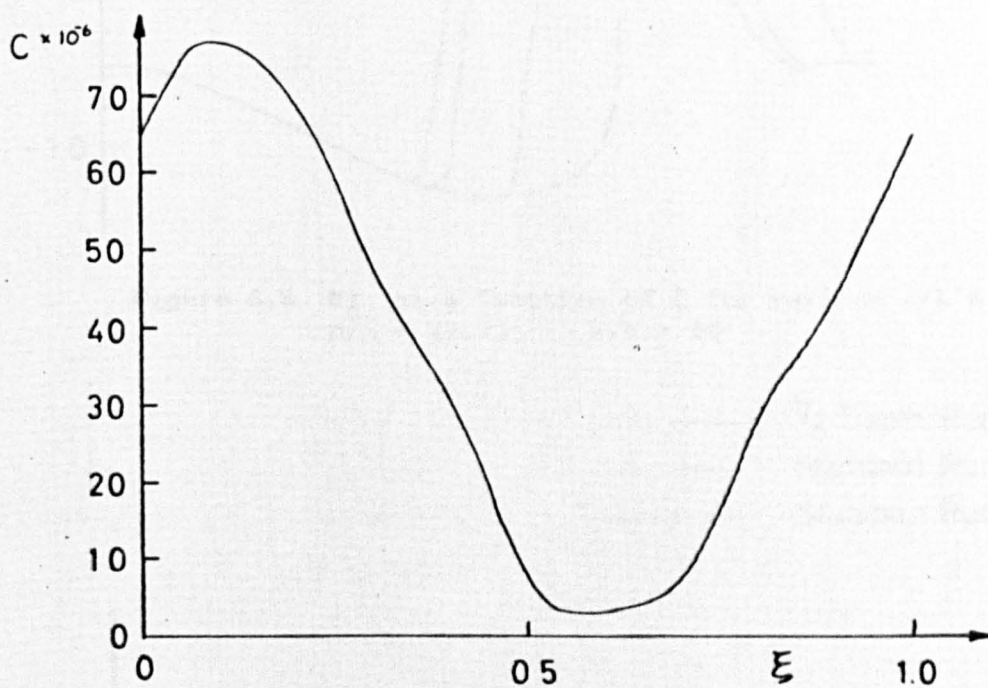


Figure 6.3 Calm water stability criteria, C , as a function of
 $\lambda/L = 1.0$ $\lambda/h = 28$

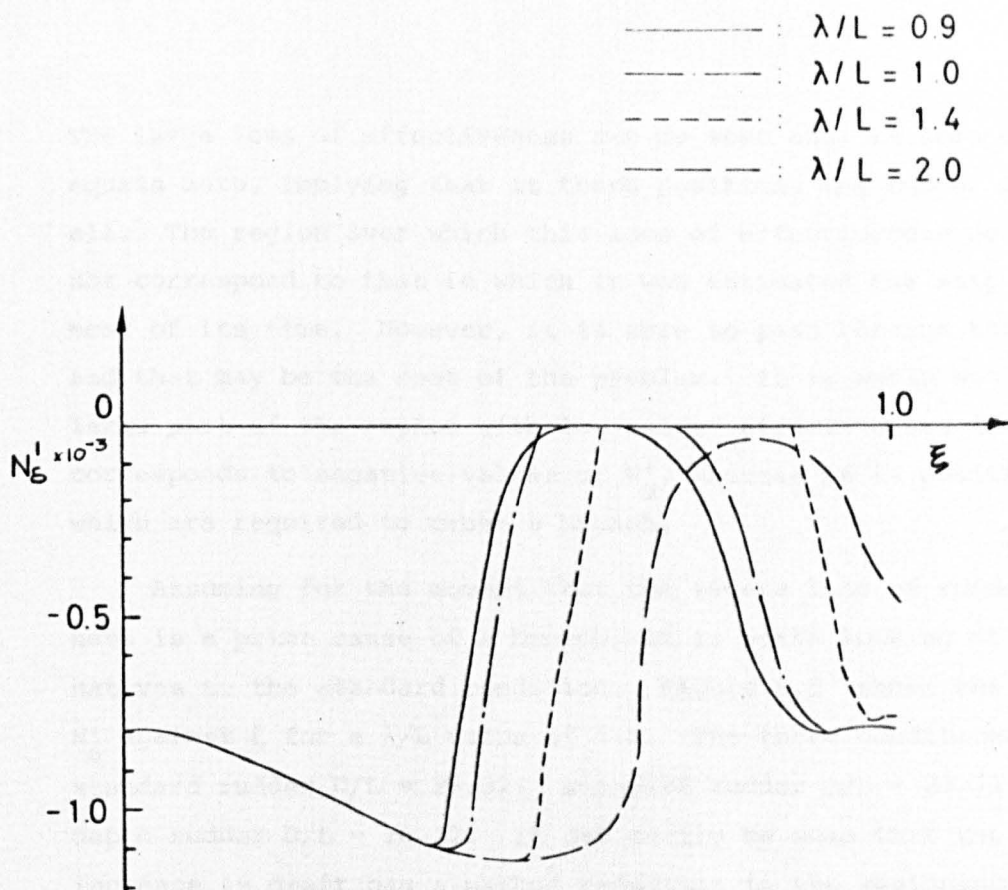


Figure 6.4 N_{δ}' as a function of ξ for various λ/L 's
 $D/L = 22.73$ $\lambda/h = 28$

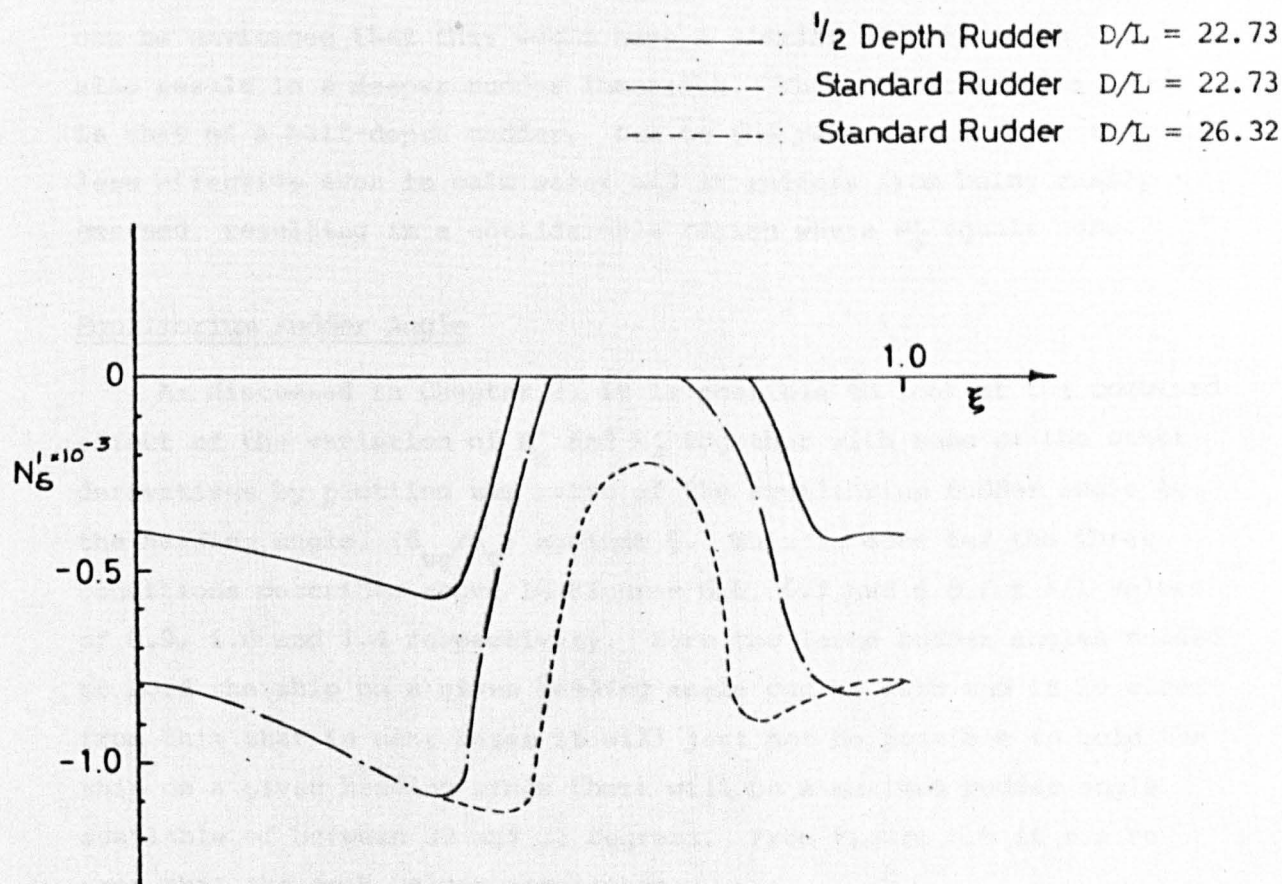


Figure 6.5 N_{δ}' as a function of ξ for various ship conditions
 $\lambda/L = 1.0$ $\lambda/h = 28$

The large loss of effectiveness can be seen and, in some cases, N'_δ equals zero, implying that at these positions the rudder is no use at all. The region over which this loss of effectiveness occurs does not correspond to that in which it was estimated the ship would spend most of its time. However, it is sure to pass through this region and that may be the root of the problem. It is worth noting that a large part of the region with low rudder effectiveness ($0.5 < \xi < 0.9$) corresponds to negative values of N'_α , whereas it is positive values which are required to cause a broach.

Assuming for the moment that the severe loss of rudder effectiveness is a prime cause of a broach, it is worth looking at two alternatives to the standard condition. Figure 6.5 shows the variation in N'_δ against ξ for a λ/L value of 1.0. The three conditions plotted are: standard rudder $D/L = 26.32$; standard rudder $D/L = 22.73$ and half-depth rudder $D/L = 26.32$. It can easily be seen that the slight increase in draft has a marked reduction in the seriousness of the loss of rudder effectiveness. This is due to obtaining a better immersion of the rudder, which is obviously very important. Although the condition with a marked trim by the stern was not investigated, it can be envisaged that this would have a similar effect, as it would also result in a deeper rudder immersion. The other condition shown is that of a half-depth rudder. Due to the reduction in size this is less effective even in calm water and it suffers from being easily emersed, resulting in a considerable region where N'_δ equals zero.

Equilibrium Rudder Angle

As discussed in Chapter 2, it is possible to look at the combined effect of the variation of N'_α and N'_δ together with some of the other derivatives by plotting the ratio of the equilibrium rudder angle to the heading angle, (δ_{eg}/α_o) against ξ . This is done for the three conditions described above in Figures 6.6, 6.7 and 6.8 for λ/L values of 0.9, 1.0 and 1.4 respectively. Here the large rudder angles needed to hold the ship on a given heading angle can be seen and it is clear from this that in many cases it will just not be possible to hold the ship on a given heading since there will be a maximum rudder angle available of between 30 and 35 degrees. From Figure 6.9 it can be seen that the peak values are higher

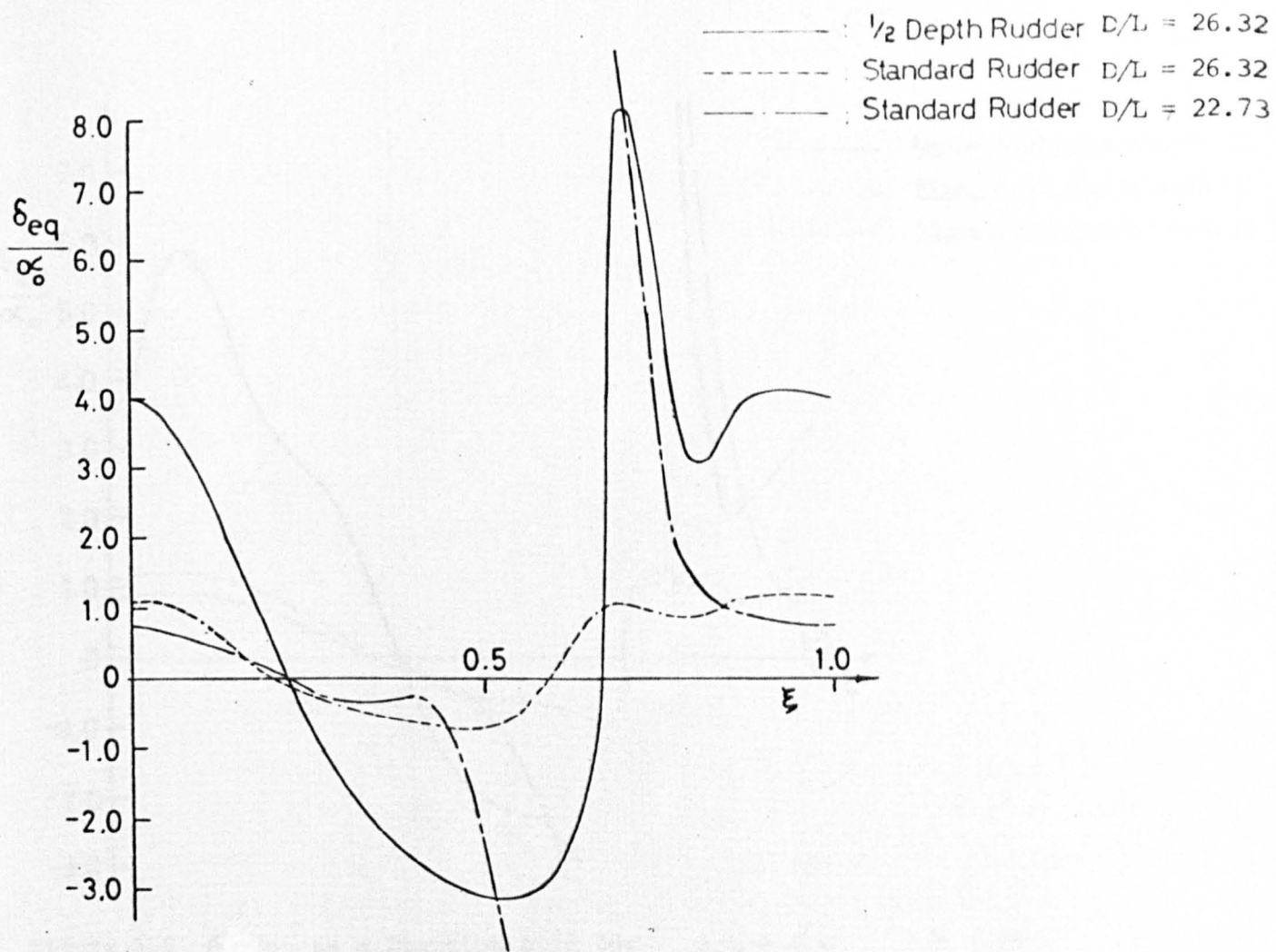


Figure 6.6 δ_{eq}/α_0 as a function of ξ for $\lambda/L = 0.9$ $\lambda/h = 28$

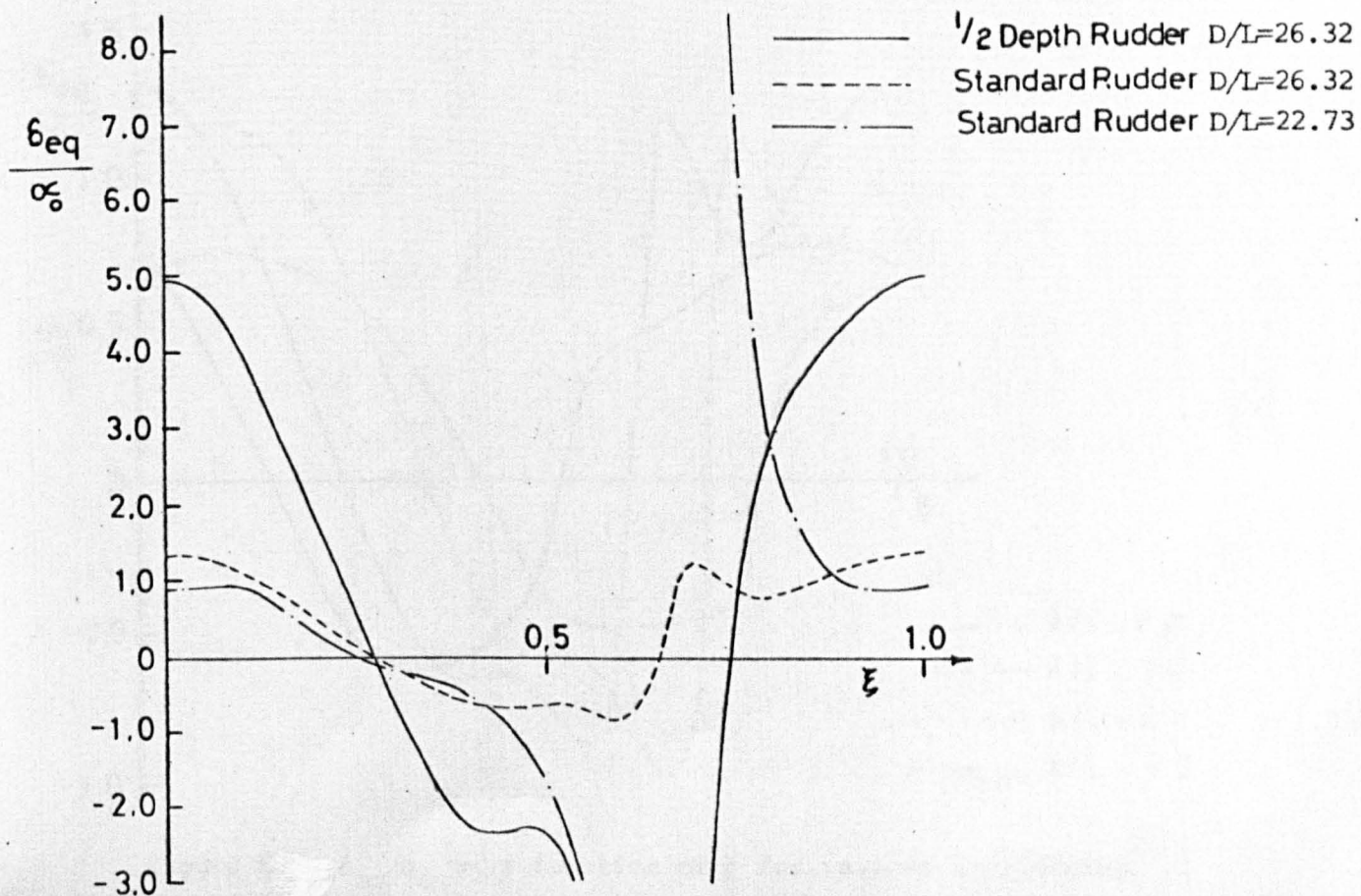


Figure 6.7 δ_{eq}/α_0 as a function of ξ for $\lambda/L = 1.0$ $\lambda/h = 28$

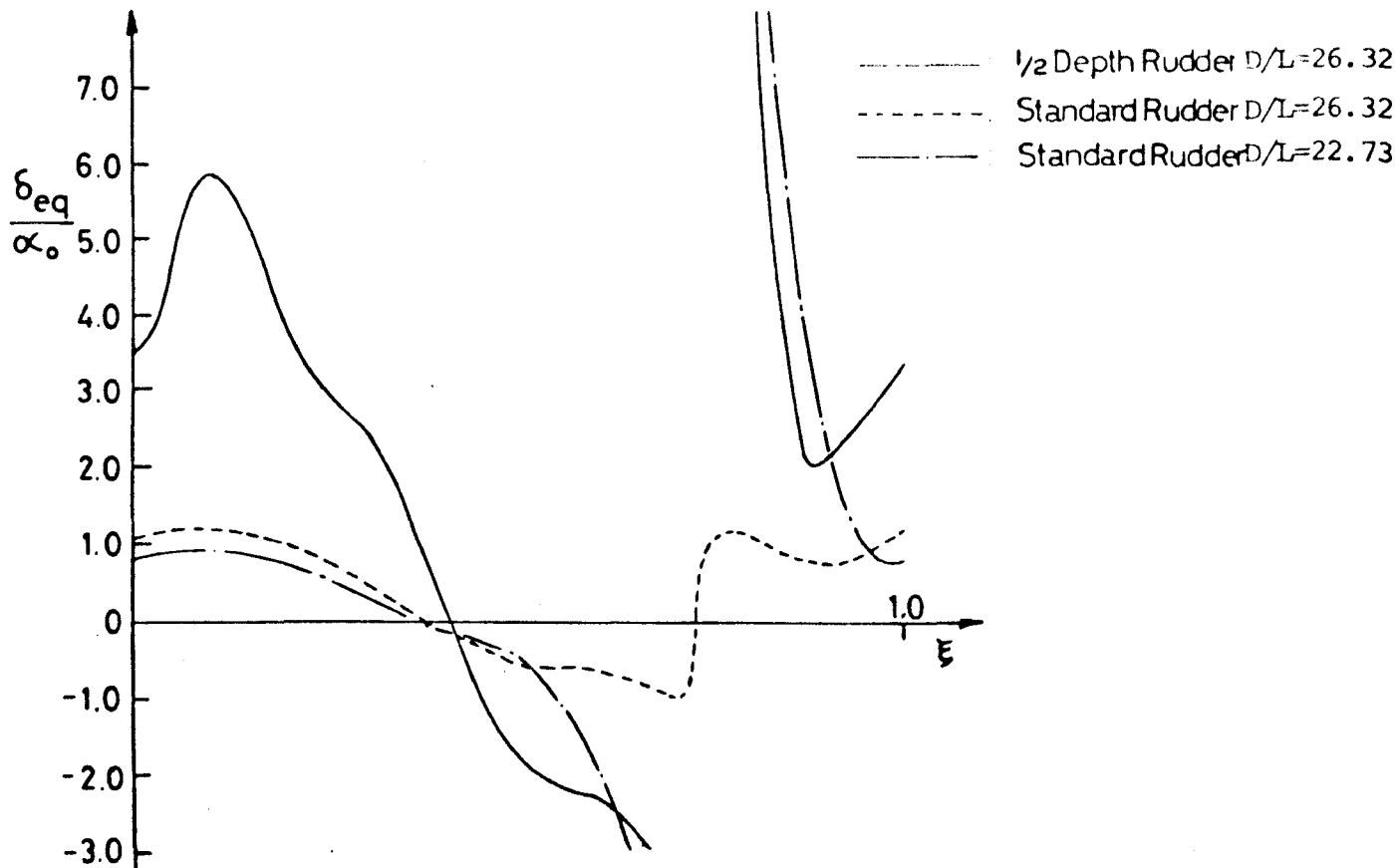


Figure 6.8 δ_{eq}/α_0 as a function of ξ for $\lambda/L = 1.4$ $\lambda/h = 28$

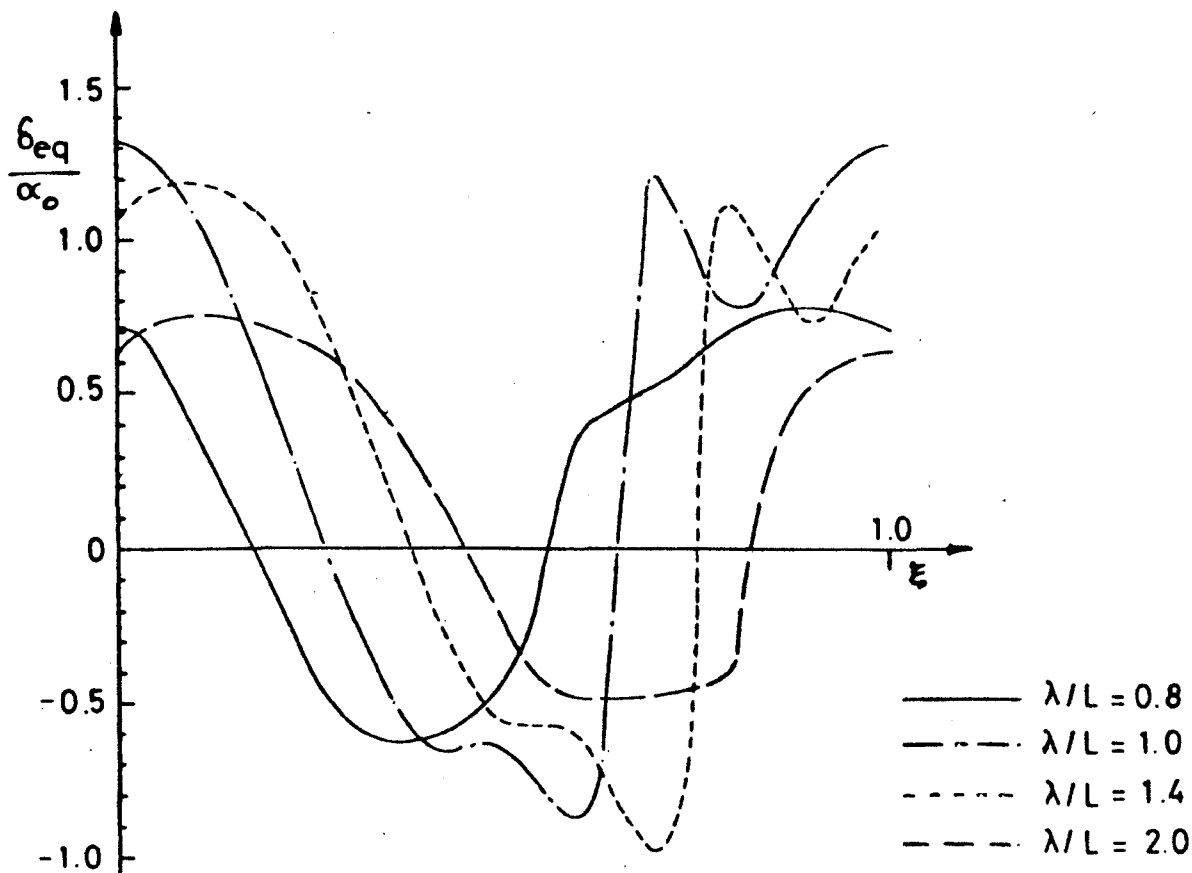


Figure 6.9 δ_{eq}/α_0 as a function of ξ for various wavelengths
Standard rudder $D/L = 26.32$ $\lambda/h = 28$

for λ/L of 1.0 and 1.4, implying that at λ/L of 0.8 and 2.0 a broach is less likely. The dangerous region for broaching is when δ_{eg}/α_o is large and positive and the stable longitudinal equilibrium position will be when X' is positive and $dX'/d\xi$ is negative, but since they do not appear to coincide, it is difficult to see why a broach occurs. The situation, however, will be dynamic, with the ship not settling down in its position immediately and so it may be that on passing through the dangerous region a large enough yaw acceleration is set up to initiate a broach. The only way to determine this is to set up a complete simulation of the broaching condition allowing all coefficients to vary as functions of ξ and this is what is done in the next chapter.

Solution of the Lateral Equations of Motion

As discussed in Chapter 2, the autopilot equation can be added to the lateral equations of motion and the resulting equations solved for each position along the wave length. This procedure can be repeated for different ships and different wave lengths to give an idea of the effect of certain parameters on the stability roots. In order to do this a computer program was written (see Appendix C) and some of the results are given in Figures 6.10 and 6.11.

Figure 6.10 shows the effect of varying the autopilot constants, while Figure 6.11 shows the effect of varying λ/L . The effect of the variation in autopilot constants over the range selected (typical ship values) is less than had been expected, although the addition of a small rate term (P_2) reduced the regions with complex roots significantly. However, this cannot be seen in Figure 6.10, which is only a plot of the real part of the principle root. When the root is positive the solution is unstable and it can be seen from Figure 6.11 that the unstable region is reduced markedly when $\lambda/L = 2.0$, again implying that a broach is less likely for longer waves.

Although solving the equations of motion does yield some useful results, particularly for comparative purposes, the simplifications, such as the assumption that the rudder will always be at the desired angle and the neglect of a maximum rudder angle, do impose limitations on this method.

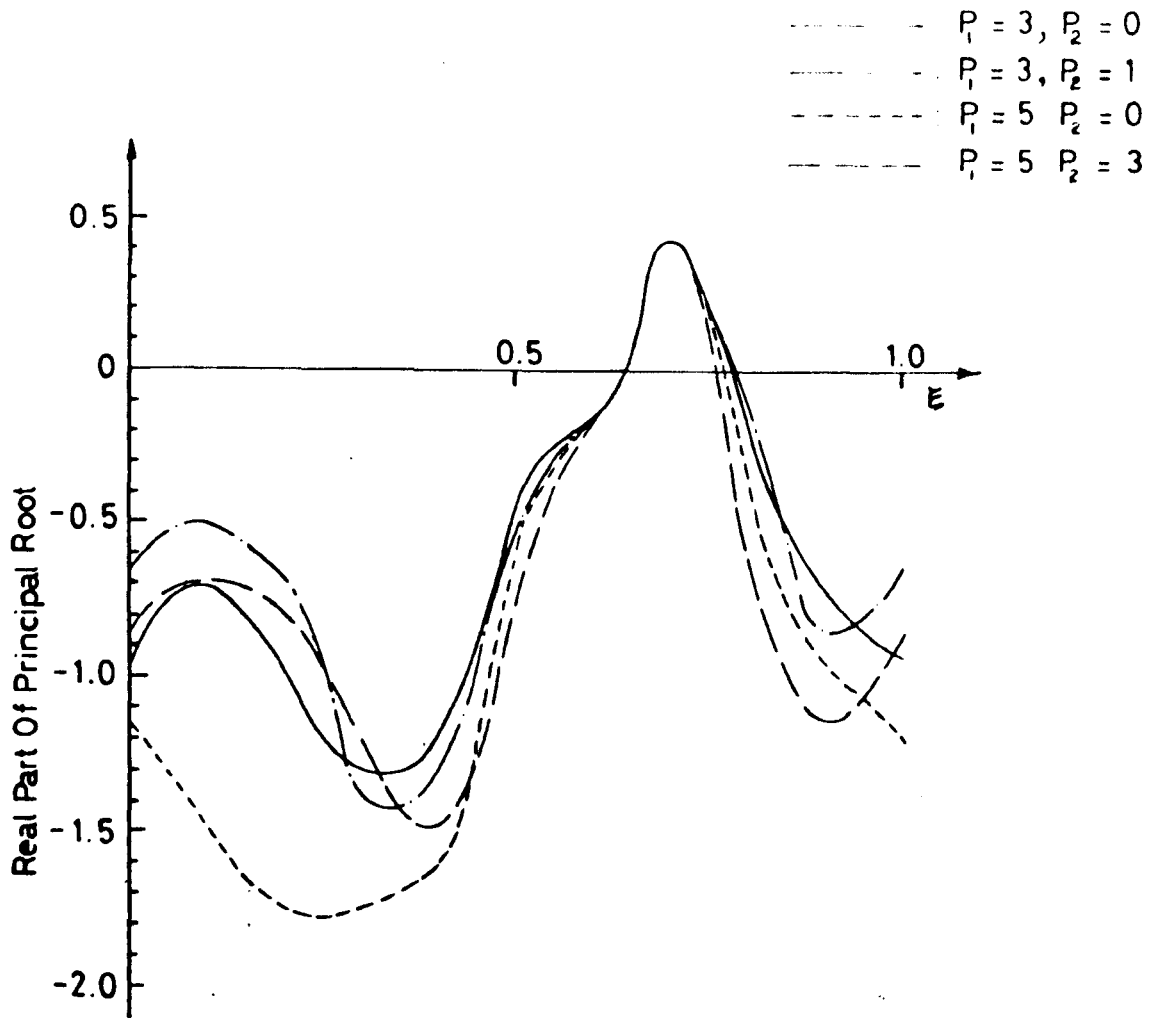


Figure 6.10 The real part of the principal root as a function of ξ
 Standard rudder $D/L = 22.73$ $\lambda/L = 1.0$ $\lambda/h = 28$

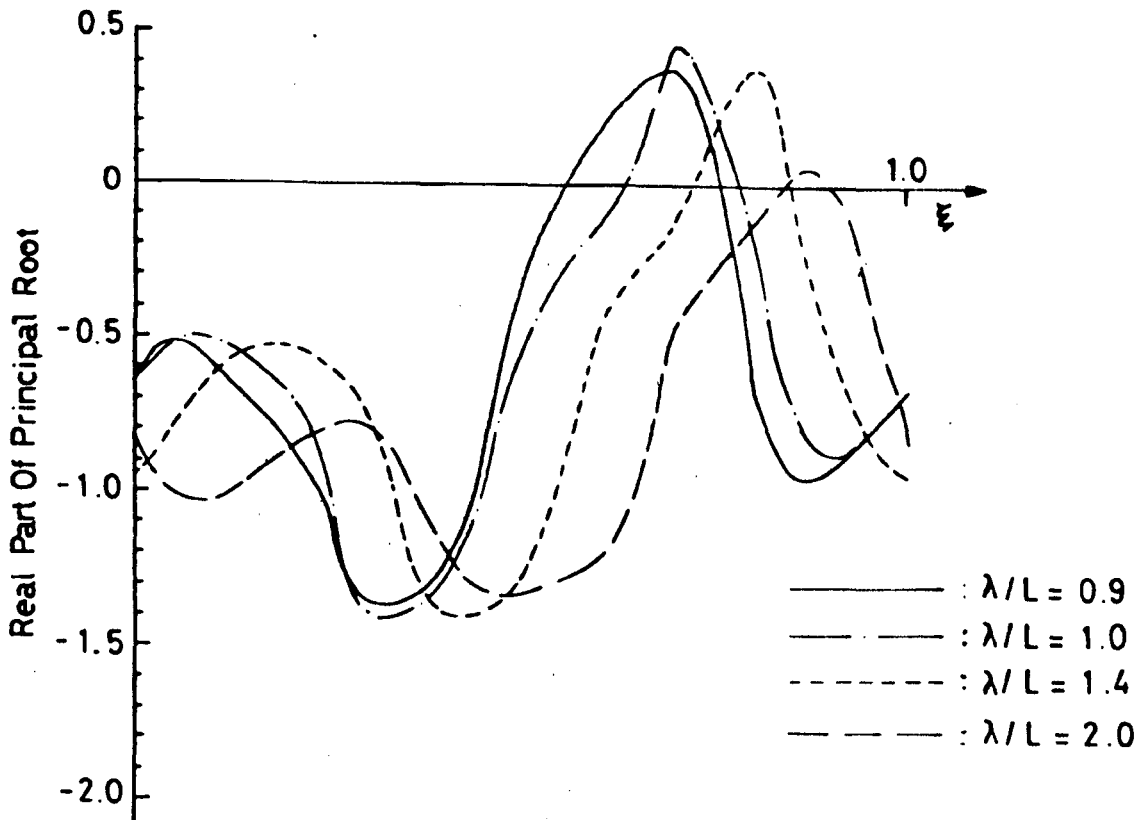


Figure 6.11 The real part of the principal root as a function of ξ
 Standard rudder $D/L = 22.73$ $P_1 = 3$ $P_2 = 1$ $\lambda/h = 28$

Conclusions

Two separate methods have been used in this chapter to investigate the cause of a broach. They have both remained independent of the longitudinal equation and, hence, have only been able to give comparative information which must be treated with a certain amount of caution. This is because the ship may well be able to suffer a severe instability over a region in which it spends little time.

From the plot of longitudinal force against ξ it is possible to estimate in which regions the ship will spend most time, and this information can be used, together with that obtained using the lateral equations only, to get a general impression of the factors involved. It is also possible from this plot to obtain a minimum self-propulsion speed for each λ/L , below which the ship cannot be accelerated to wave speed. (Or a maximum λ/L for each self-propulsion speed.) The region in which the ship will spend most of its time depends on λ/L , but will be from $\xi \approx 0.8$ through $\xi \approx 1.0$ to $\xi \approx 0.3$. This must be borne in mind when looking at lateral motions, but since the situation will be dynamic, with the ship not arriving in its equilibrium position immediately, other wave positions cannot be ignored.

The use of the equilibrium rudder angle approach is purely static, but allows different rudder configurations to be readily compared and it is fairly easy to interpret the resulting plot. This approach can also be used for comparing ships in different conditions of trim, draft, etc., and could be used to investigate the merits of transom versus round stern arrangements.

Solving the lateral equations permits the effect of the autopilot to be included and, although time lags are neglected in the analysis given here, they could be included in an approximate form by modifying the autopilot equation (see Ref. 30). This method could indicate an instability due to the build-up of oscillations which is not strictly a broach and has not been found to occur in either the full-scale or model cases. The fact that it does not appear to occur in practice could be due to non-linearities, the ship not remaining on that longitudinal position for long enough for the oscillations to become serious, or to the use of a better autopilot for the full-scale case

than that used in the present model. Since this type of instability does not appear in practice, results from this method must be treated with great caution.

From looking at the results of these two methods it appears that the most significant factor is probably the yaw moment caused by the wave and that due to the rudders. The fact that, over a region the rudders seriously lose their effectiveness, appears to be very significant and it seems that this may be able to be solved at the design stage by positioning the rudders deeper, thus reducing their tendency to emerge. A trim by the stern and an increase in draft also tend to submerge the rudders more, although in addition they have a slight effect on the wave-induced yaw moment. In the case of an increase in draft the change in yaw moment is insignificant and, although it has not been calculated, it is assumed to be small also for a trim angle. Thus, these are things which may be done at the operating stage to increase the rudder's ability to counter a broach.

The other comment which can be made from the results is that the tendency to broach appears to reduce as the wave length increases beyond λ/L of around 1.4 to 2.0. This is contrary to what is shown in Ref. 20, but is intuitively correct since, taken to the extreme, would imply that a very long wave ($\lambda/L > 10.0$) would not be able to cause a broach (for a ship travelling at wave speed), since the ship would see little change in pressure or acceleration along its length, resulting in a very small moment being set up. In addition, the water level would not change much along the ship length and so the rudders would be less likely to emerge.

The next stage is to couple the lateral equations to the surge equations and study the resulting lateral stability. This is done in the following chapter in the form of an analogue/digital hybrid simulation which also takes into account time lags and maximum rudder rate.

Chapter 7

SIMULATION

In order to predict whether the ship will broach in certain conditions it is necessary to couple the lateral equations to the surge equation for the reasons given in the previous chapter. It is also desirable to model the maximum rudder velocity, maximum rudder angle and any time delays which may occur in the autopilot system. It was, therefore, decided to set up a simulation based on a simplified form of the equations developed in Chapter 2 using the theoretical technique for predicting the coefficients developed in Chapter 3.

Before looking at the complete simulation, the longitudinal and lateral equations were set up independently. Once the separate simulations were checked and found to be working correctly they were combined to form the complete simulation.

Surging

When separated from the lateral and roll equations in 2.2 the longitudinal equation becomes

$$0 = X'_u u' + (X'_u - m) \dot{u}' + X'_\xi \xi \quad \dots \quad 7.1$$

This equation is in non-dimensional form based on a reference velocity U_0 . In order to run the simulation at real time for any model or ship and to get a "feel" for the factors involved, it is convenient to dimensionalise Eq. 7.1 and to introduce a squared relationship between resistance and velocity. Thus, the longitudinal equation becomes

$$0 = X_{u^2} U^2 + (X_{\dot{u}} - m) \dot{u} + X_\xi \xi + X_{prop} \quad \dots \quad 7.2$$

where U is the total forward velocity (i.e. $U = U_0 + u$) and X_{prop} is the thrust from the propeller that balances $X_{u^2} U_0^2$ which is the resistance at self-propulsion speed in calm water. In Eq. 7.2 X_ξ is dependent on ξ but all the other coefficients are assumed to be constant.

ξ is given by

$$\xi = \frac{1}{\lambda} \int_0^t [U - C] dt \quad \dots \quad 7.3$$

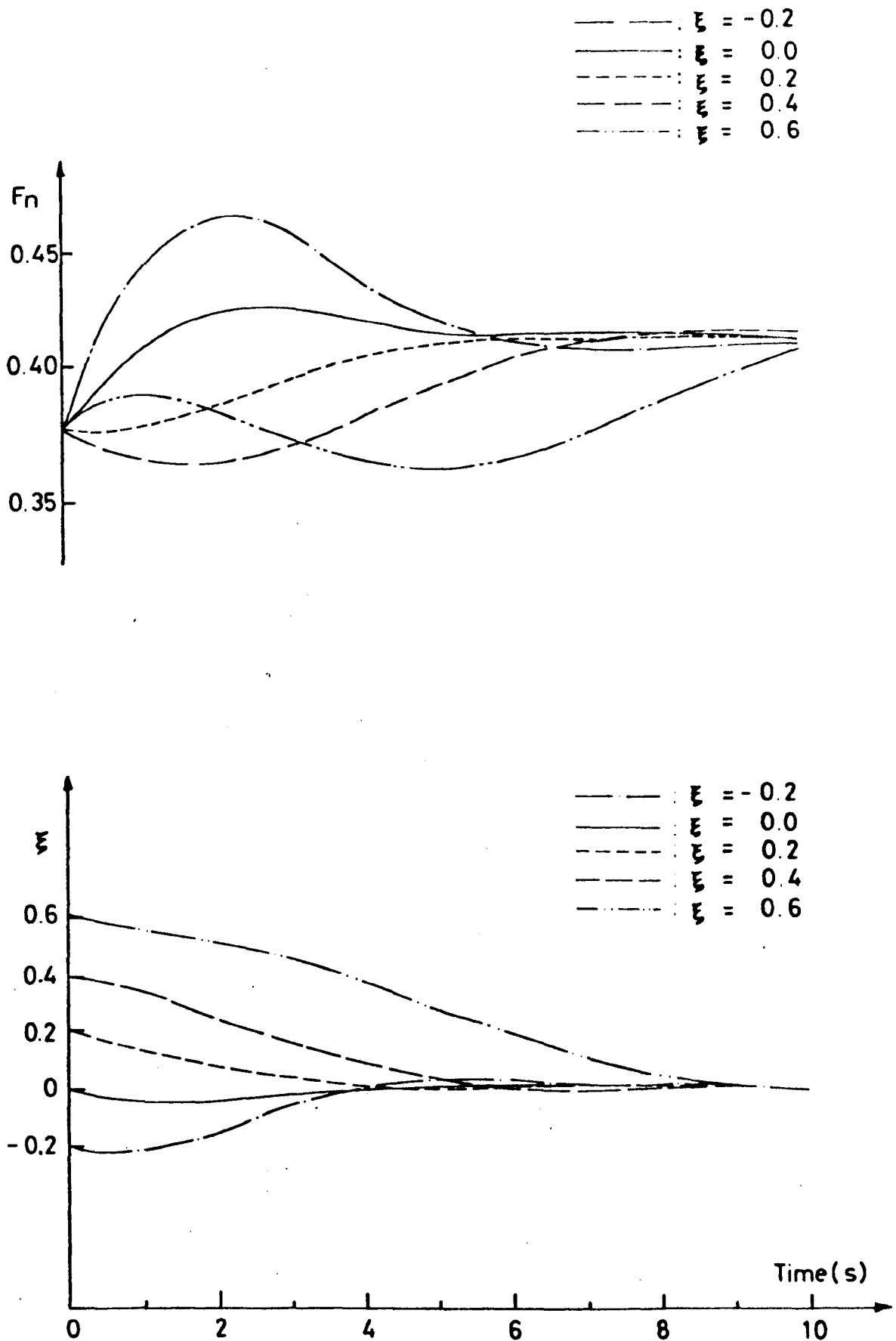


Figure 7.1 Digital simulation of surging; varying ξ_0
 $\lambda/L = 1.07$ $\lambda/h = 28$ $F_{no} = 0.37$

A digital simulation based on Eqs. 7.2 and 7.3 was set up on the Department's PDP 11/40 digital computer (see Appendix C) and an example of the results obtained is given in Figure 7.1. This simulation was repeated for a number of different conditions. However, it was very slow and used a lot of computer space. Because of the time involved for each run and because the problem was going to be made significantly more complex by the addition of the lateral equations, an analogue simulation was set up on the Faculty's EAI 2000 analogue computer. A comparison between the analogue and the digital simulation is given in Figure 7.2. Here it can be seen that there is good agreement and since by using the analogue method the problem could be run at very high speeds resulting in a considerable saving in time, it was decided to abandon the digital approach. The simulation can be run at real time on the analogue computer and this gives an additional advantage to this method as it is possible to get a "feel" for what is happening.

Lateral Simulation

After dimensionalising and separating the lateral equations from Eqs. 2.2 they become

$$\begin{aligned}
 0 &= Y_v \dot{v} + (Y_{\dot{v}} - m) \ddot{v} + Y_\alpha \alpha + (Y_r - mU) \dot{\alpha} + (Y_{\ddot{r}} - mx_G) \ddot{\alpha} + Y_\delta \delta \\
 0 &= N_v \dot{v} + (N_{\dot{v}} - mx_G) \ddot{v} + N_\alpha \alpha + (N_r - mx_G U) \dot{\alpha} + (N_{\ddot{r}} - I_z) \ddot{\alpha} + N_\delta \delta \\
 & \dots \dots \dots \quad 7.4
 \end{aligned}$$

The desired rudder angle is given by

$$\delta_d = P_1 \psi + P_2 \dot{\psi} \quad \dots \dots \quad 7.5$$

However, the actual rudder angle is the integral of the actual rudder angular velocity which is limited by the power of the steering gear. There is also a limit to the maximum rudder angle available due to the design of the steering gear.

Thus

$$\begin{aligned}
 \delta_a &= \int_0^t \dot{\delta}_a dt \\
 -C_s &< \dot{\delta}_a < C_s \quad \dots \dots \quad 7.6 \\
 -\delta_{a_m} &< \delta_a < \delta_{a_m}
 \end{aligned}$$

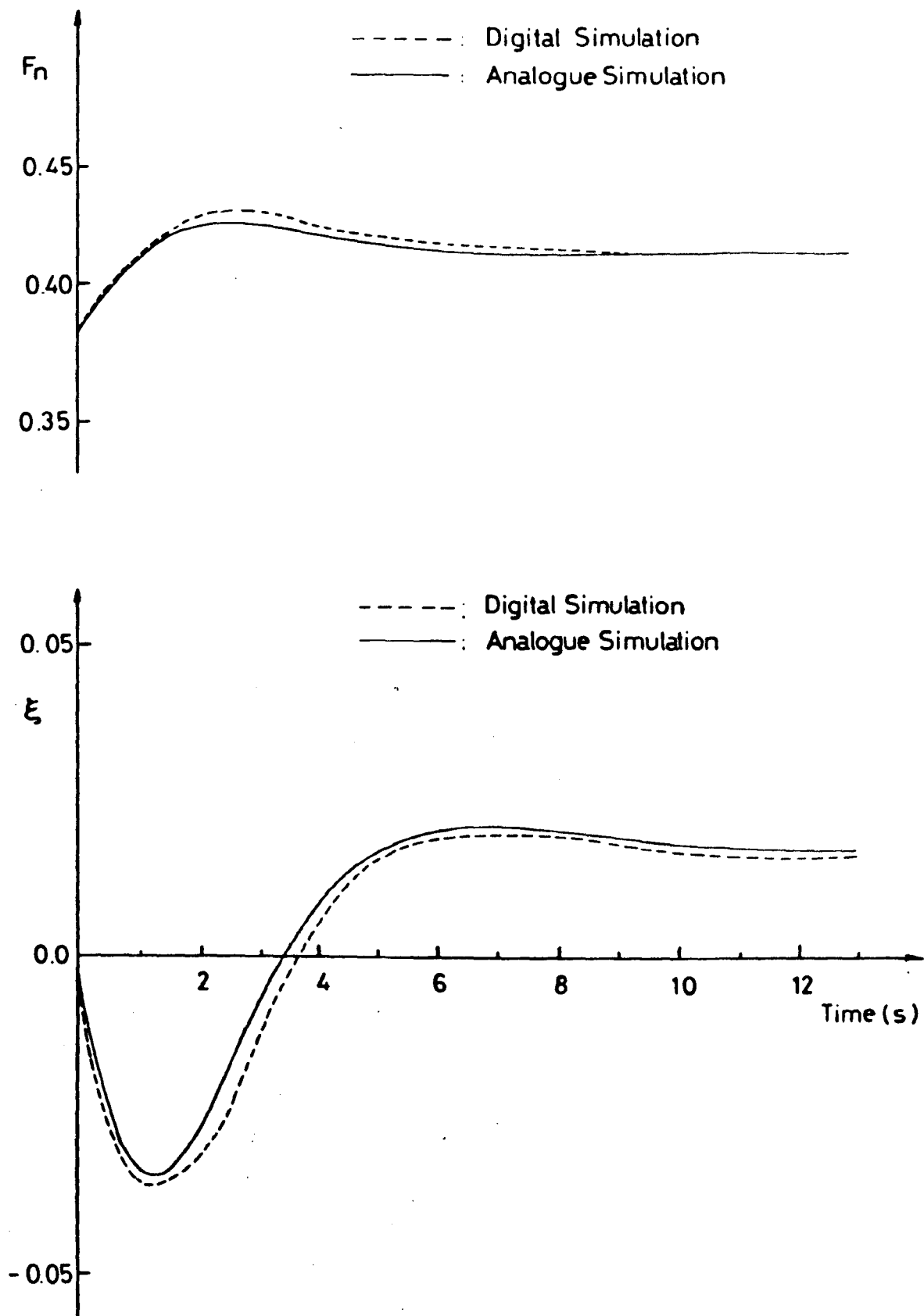


Figure 7.2 Comparison of digital and analogue simulation of surging
 $\lambda/L = 1.07$ $\lambda/h = 28$ $F_{no} = 0.37$

where δ_{am} will be about 35° and C_3 will vary depending on the power of the steering gear. A value of C_3 greater than $2\frac{1}{2}^\circ/\text{sec}$ is required by law for certain types of ships^[26] and a typical modern frigate will have a value of around $5^\circ/\text{sec}$.

Looking at the lateral stability alone, it is possible to identify regions along the ξ axis which are unstable due to oscillatory motion and regions which are unstable due to a broach-like motion with a single swing in the direction of the initial heading angle. It is possible to vary the values of P_1 , P_2 , δ_{am} and C_3 , and observe the effect they have on the resultant motion. Figure 7.3 shows the effect of varying P_1 over the complete range of ξ . The system is given an initial heading angle and the resulting motion observed. If it is stable the initial heading angle is increased and the test repeated until the minimum value of initial heading angle required to induce instability is found. This is plotted against ξ for the various conditions to be compared, and it can be seen that there are two distinct regions of instability. The region between about $\xi = 0.3$ and $\xi = 0.65$ is unstable due to the build-up of oscillations and can be reduced by addition of the P_2 term in the autopilot equation. However, the other region is unstable due to a broach-like motion as discussed in the previous chapter and is, therefore, the significant region.

Although the lateral simulation alone can be used to investigate the effects of varying certain parameters, as discussed in the previous chapter, it is necessary to couple the lateral and longitudinal equations together to predict what will actually happen in the physical condition. Now that both the longitudinal and lateral simulations have been shown to be working, they can be combined to form the complete simulation.

Simulation of Longitudinal and Lateral Motions Combined

When dimensionalised and simplified the equations become

$$\begin{aligned}
 0 &= Y_v \dot{v} + (Y_{\dot{v}} - m) \ddot{v} + Y_\alpha \dot{\alpha} + (Y_r - mU) \dot{\alpha} + Y_\delta \dot{\delta} \\
 0 &= N_v \dot{v} + N_\alpha \dot{\alpha} + (N_r - m x_G U) \dot{\alpha} + (N_{\ddot{r}} - I_z) \ddot{\alpha} + N_\delta \dot{\delta} \quad \dots \quad 7.7 \\
 0 &= X_{u^2} U^2 + (X_{\dot{u}} - m) \dot{u} + X_\xi + X_{\text{prop}} + X_\delta |\dot{\delta}|
 \end{aligned}$$

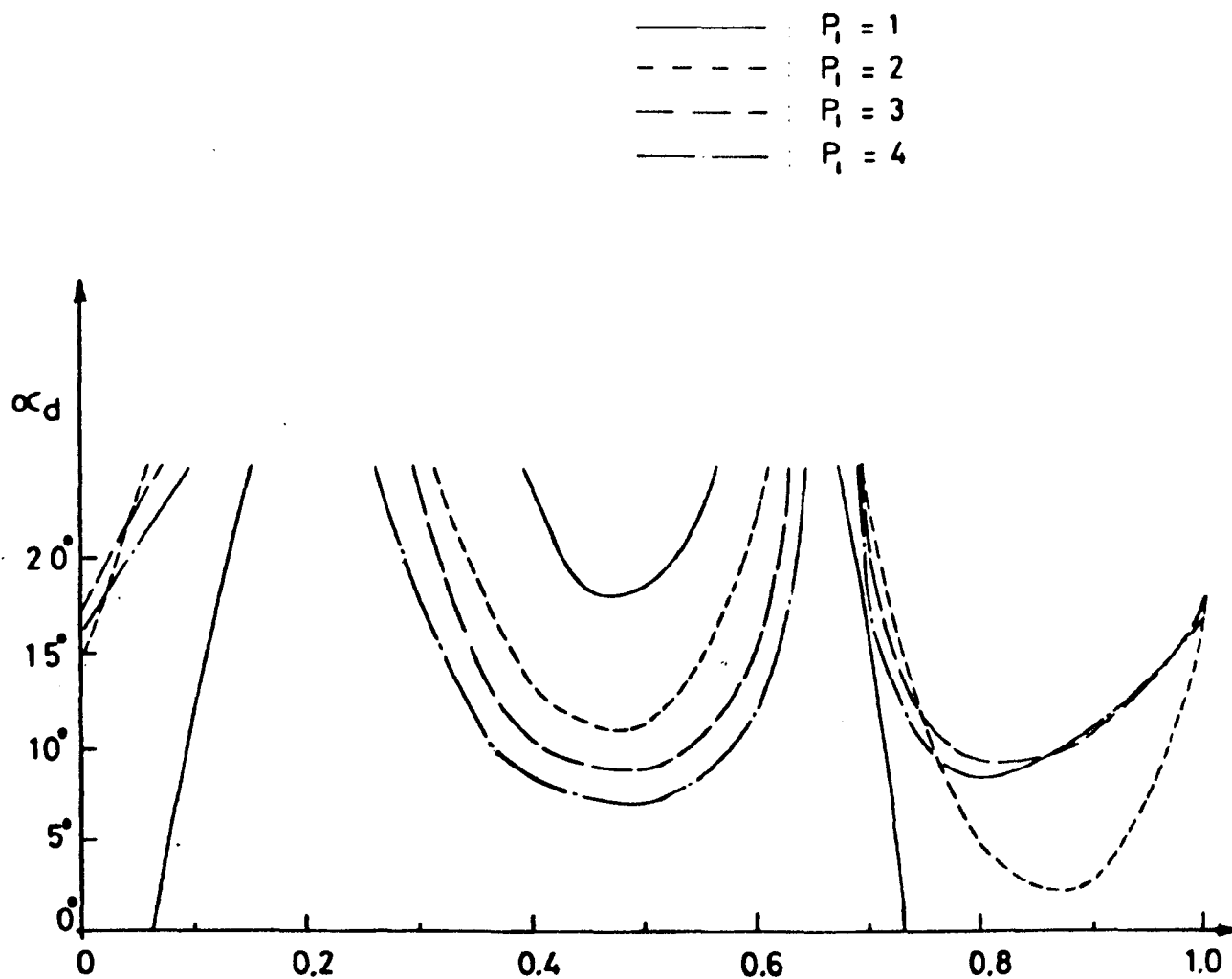


Figure 7.3 Stability in lateral plane only; varying P_1
 $\delta_d = P_1$ ($P_2 = 0$) $\lambda/L = 1.07$ $\lambda/h = 28$

$$\xi = \frac{1}{\lambda} \int_0^t [U - C - v\alpha] dt$$

$$\delta_d = P_1 \psi + P_2 \dot{\psi}$$

$$\delta_a = \int_0^t \dot{\delta}_a dt \quad \dots \quad 7.7$$

$$-C_3 < \dot{\delta}_a < C_3$$

$$-\delta_{a_m} < \delta_a < \delta_{a_m}$$

where $\cos \alpha$ is assumed to be equal to 1 and $\sin \alpha$ to be equal to α . The cross coupling acceleration terms and the coupling between v and r and X have been ignored since they are small and there was a shortage of coefficient units. The resulting patch diagram is given in Figure 7.4. In addition to Eqs. 7.7 a first order Padé circuit has been incorporated between the demand for the rudder and the start of the rudder movement in order to provide an approximation to a time delay [44]. The main problem with the total simulation on the analogue computer was that many of the coefficients of the equations were dependent on ξ . A digital set function generator (DSFG) was used to provide the dependence of X_ξ on ξ , but as there was only one of those available, an alternative method had to be used for the remaining coefficients. The technique involved using the PDP 11/45 digital computer which is connected to the EAI 2000 through serial and parallel ports. At first the serial port connections were used to alter coefficient values, but this proved too slow, so the parallel port connection was adopted. The procedure was as follows. The digital computer set up the initial conditions as normal using the serial port, and the counter on the logic part of the analogue computer was set to a pre-determined value. The '2000 was then put into the operate mode by the '11 and the counter started counting down to zero. The simulation continued with X_ξ being varied by the DSFG, but with all other coefficients remaining constant. When the counter reached zero (this took 0.05 of a second) the '2000 was put into the hold mode using the patch panel control. The digital computer then sampled the output from A61 (ξ) through an analogue to digital converter and calculated the values of the variable coefficients using interpolation from previously fed data. The appropriate coefficient values were then set at the 6 digital to analogue converter's and the

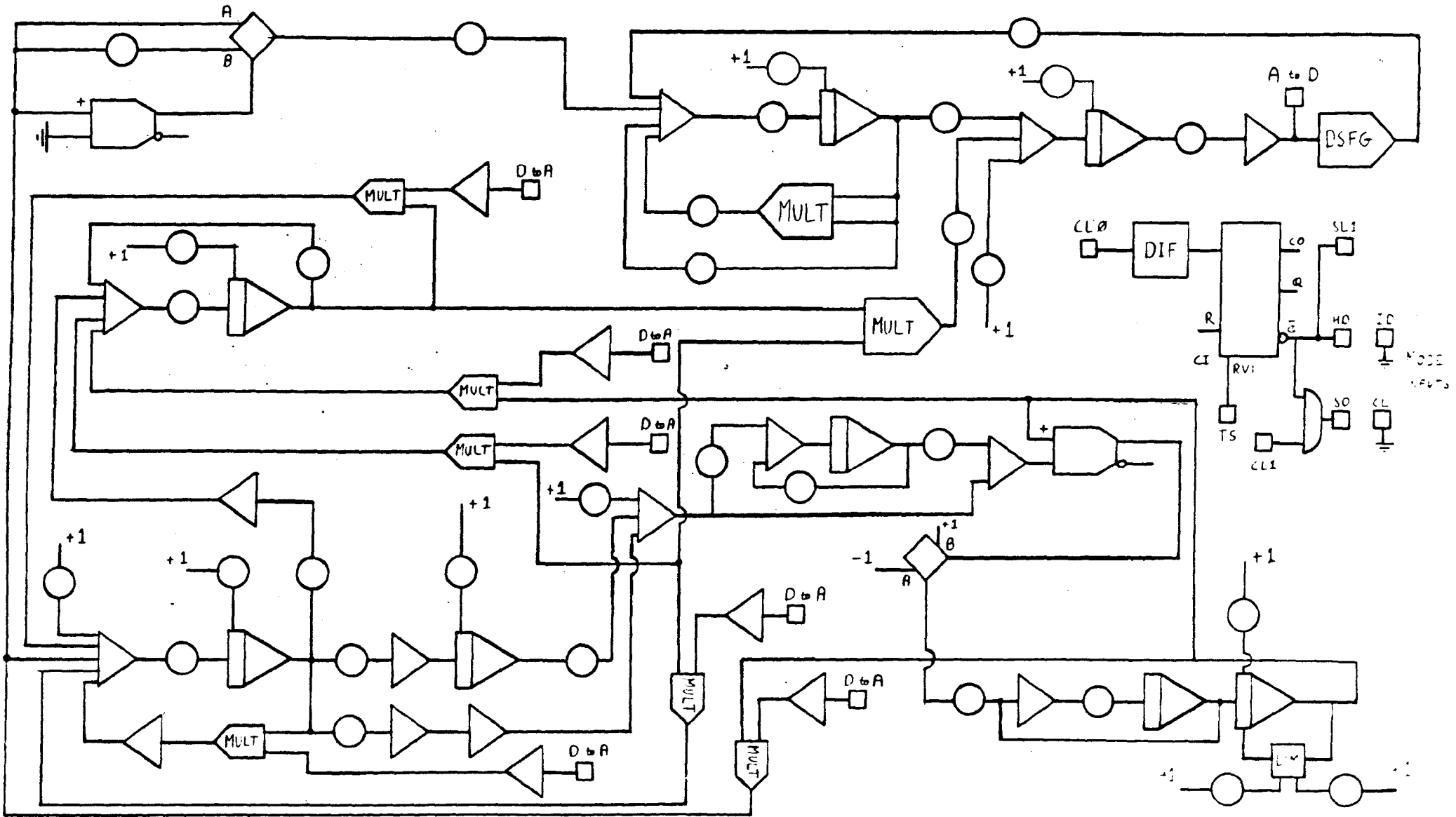


Figure 7.4 Patch diagram for complete hybrid simulation.

'2000 put back into the operate mode. This continued until (a) the ship was overtaken by three waves, (b) it was broached, or, (c) the time limit elapsed. The time spent in the hold mode depended on how heavily the PDP 11/45 was being used by other users, but was generally negligible and, by watching the simulation, it was difficult to tell that it was stopping every 0.05s.

Unfortunately, there were only 6 digital to analogue converter's available and 8 required. This was solved by assuming $[Y_v / (Y_v - m)]$ and $[(Y_r - mU) / (Y_v - m)]$ remained constant at their calm water value, and the effect of this on the yaw motion is thought to be negligible.

Comparison of Simulation with Free Running Model Experiments

Since the relationship between motion and force was assumed to be linear, prediction of the model's path during a broach was not attempted. Instead, the simulation was used to predict the broaching zones discussed in the first chapter. Although the hydrodynamic coefficients can be calculated using the method developed in Chapter 3, the coefficients governing the rudder motion have not yet been discussed. The maximum rudder angle possible on the model was $\pm 35^\circ$ and the maximum rudder rate was scaled from the ship which had a value of $3^\circ/\text{sec}$. The radio-controlled model was steered by a helmsman who stood at the side of the manoeuvring basin directly behind the model. He relayed the desired rudder angle via a walkie-talkie to the controller who selected the angle from a series of buttons. This then operated the servo motor on the model via radio control. As can be seen, it is not very easy to model this system using an autopilot equation. Values of P_1 and P_2 were chosen to be 3 and 1 respectively. It was assumed that once the rudder started to move it would reach maximum speed almost immediately. However, the time delay from the moment the rudder was required to when it started moving was estimated to be 3 seconds model scale. The standard rudder and half-depth rudder conditions were both investigated in waves of $\lambda/h = 28$, which corresponded to the free running experiments discussed in the first chapter. Comparison between the broaching zones obtained using the simulation and the experimental results are given in Figures 7.5 and 7.6. The desired heading angle was 20° since the limited experimental records available showed that this was what

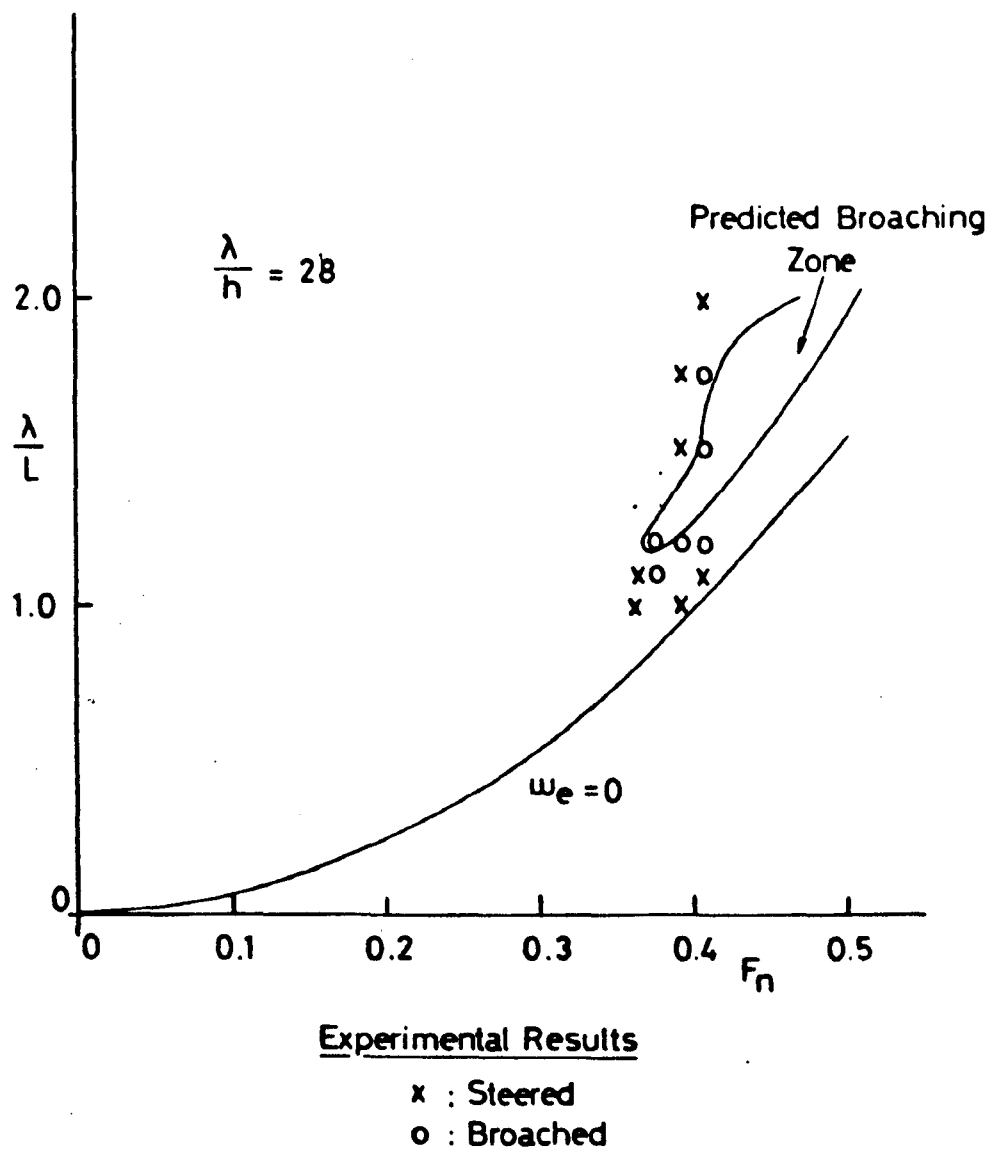


Figure 7.5 Comparison between predicted and experimental results for standard rudder

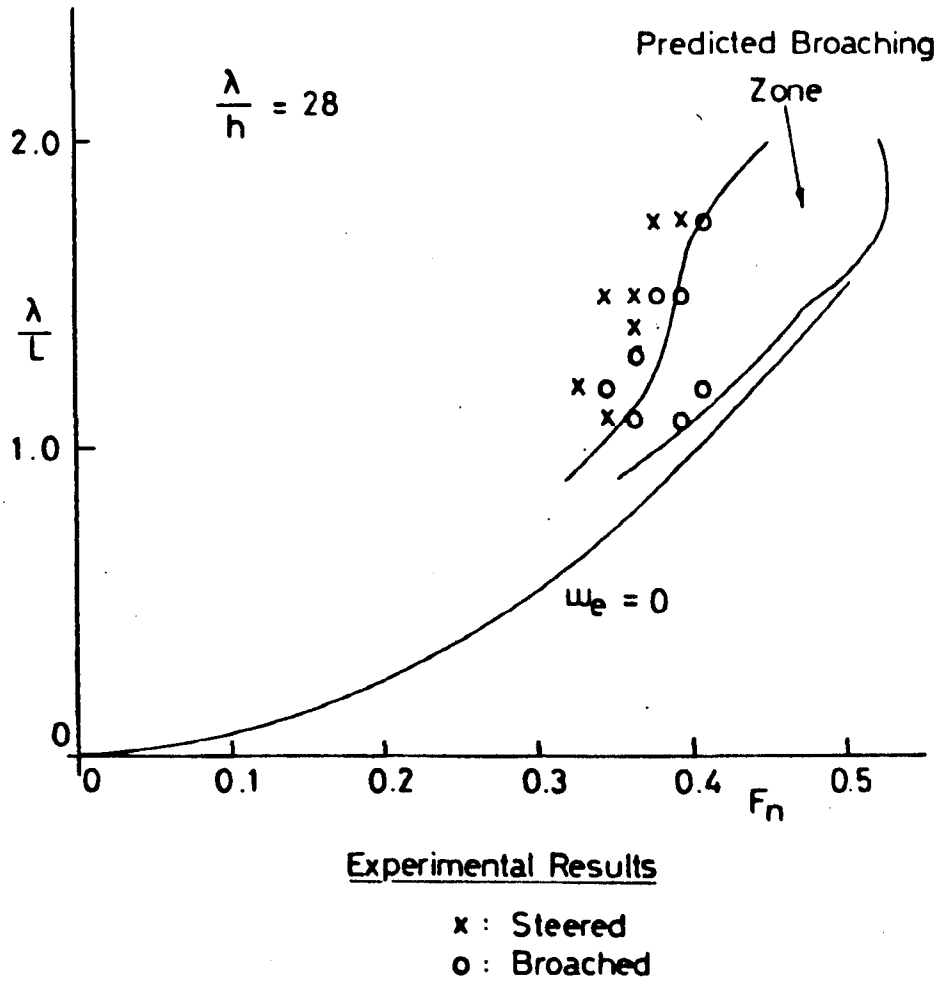


Figure 7.6 Comparison between predicted and experimental results for $\frac{1}{4}$ depth rudder

was used in the experiments. A broach was considered to have occurred if either there was an overload* or the heading angle exceeded 40° . If the model was overtaken by three waves without broaching then the run was assumed to be steered, although it was possible in some of these cases that, if the initial value of ship speed was greater than self-propulsion speed (i.e. $u > 0$), a broach would have occurred. The other way in which a steered run could be obtained was if the model was carried along by the wave at a constant heading angle. This generally happened if the self-propulsion speed was nearer to wave speed as the model settled into its longitudinal equilibrium position almost immediately.

Looking at Figures 7.5 and 7.6, the comparison between the predicted zones and the experimental results is quite good. This is especially so considering that there are a large number of imponderables, such as, calculation of coefficients, neglect of heel angle, simplification of equations and, not least, the modelling of the rudder.

Discussion

Assuming for now that the reasonable correlation between theory and experiment shown in the previous section indicates that the simulation gives a good model of a broach, it is now possible to look closer at what is happening in an attempt to see why a ship broaches. As mentioned in the previous chapter, the longitudinal equilibrium position does not correspond to the region which requires the highest equilibrium rudder angles. Thus, it is presumably a combination of the lateral and longitudinal motion which is causing a broach. Looking at Figure 7.7 it can be seen that the build-up of heading angle starts before the ship has settled down into its longitudinal equilibrium position. In fact, it seems to be the longitudinal oscillations which are causing the broach. From Figure 6.6, the region with the large equilibrium rudder angle is around $\xi = 0.7$, with fairly large angles required from $\xi = 0.7$ to 1.0. From the lower graph in Figure 7.7 it can be seen that the ship passes through this region fairly rapidly at time $t = 0.5s$

* On an analogue computer all variables must be within the range -1 to +1 and the equations are scaled using expected maximum values before being patched up. If the value of a variable goes outside these limits during a simulation an overload is said to occur implying that the value has exceeded the expected maximum.

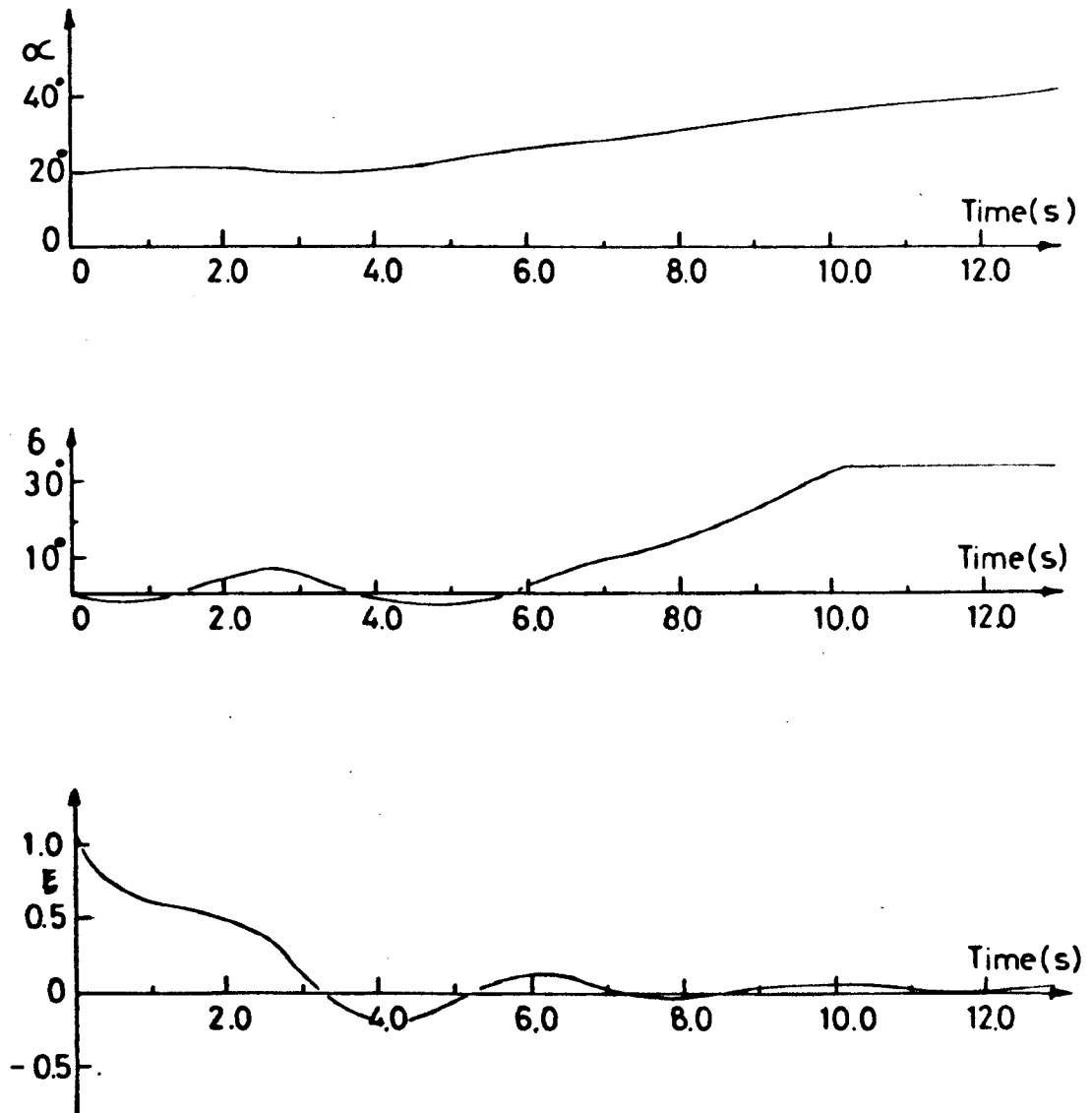


Figure 7.7 Record from simulation for: $\lambda/L = 0.9$, $F_{no} = 0.33$
 $\frac{1}{4}$ depth rudder, $C_s = 3^\circ/\text{sec. full-scale}$, no
time delay = 3 secs model scale

with only a slight yawing motion (upper graph). The ship then continues to be overtaken by the wave. However, the relative speed begins to reduce beyond $\xi = 0.0$ until $\xi = -0.2$ ($t = 4.1s$) when $U = C$. At this point large equilibrium rudder angles are required as $\xi = -0.2$ corresponds to $\xi = 0.8$ for the next wave. The ship then moves forward with respect to the wave system (still in the region with a reasonably high equilibrium rudder angle) and by now a large yaw rate has been built-up due to the large amount of time spent in the critical region. The rudder cannot cope and the ship continues to yaw, resulting in a broach. Very similar behaviour can be seen for $\lambda/L = 1.6$ in Figure 7.8.

Thus, the principle cause of a broach is that the ship is being overtaken by the waves and will be accelerated, but before reaching wave speed will overshoot the longitudinal equilibrium position and enter the region which has a high required equilibrium rudder angle. There will now be a low relative velocity between the waves and the ship which will reduce to zero and then the ship will slowly move forward with respect to the wave system, passing through the critical region again. It is all this time spent in the critical region which will initiate the broach. If the self-propulsion speed is higher the ship will not overshoot its longitudinal equilibrium position by so much, and hence will not spend so much time in the critical region, thereby permitting it to be steered. On the other hand, if the ship self-propulsion speed is lower, it will pass through the critical zone with reasonably high relative velocity - spending a much shorter time there, again permitting it to be steered.

The critical factor then is the amount of time spent in the part of the wave which requires high equilibrium rudder angles and this is influenced by the relative velocity between the ship and the wave as this region is entered. Although this is governed in the regular wave condition by the ship self-propulsion speed, in the jumble of an irregular sea it will depend to a certain extent on the previous wave and, hence, predicting a broach in these conditions will be far more difficult.

Increasing the maximum rudder rate seems to have little effect on the motion, as can be seen by comparing Figure 7.7 with Figure 7.9.

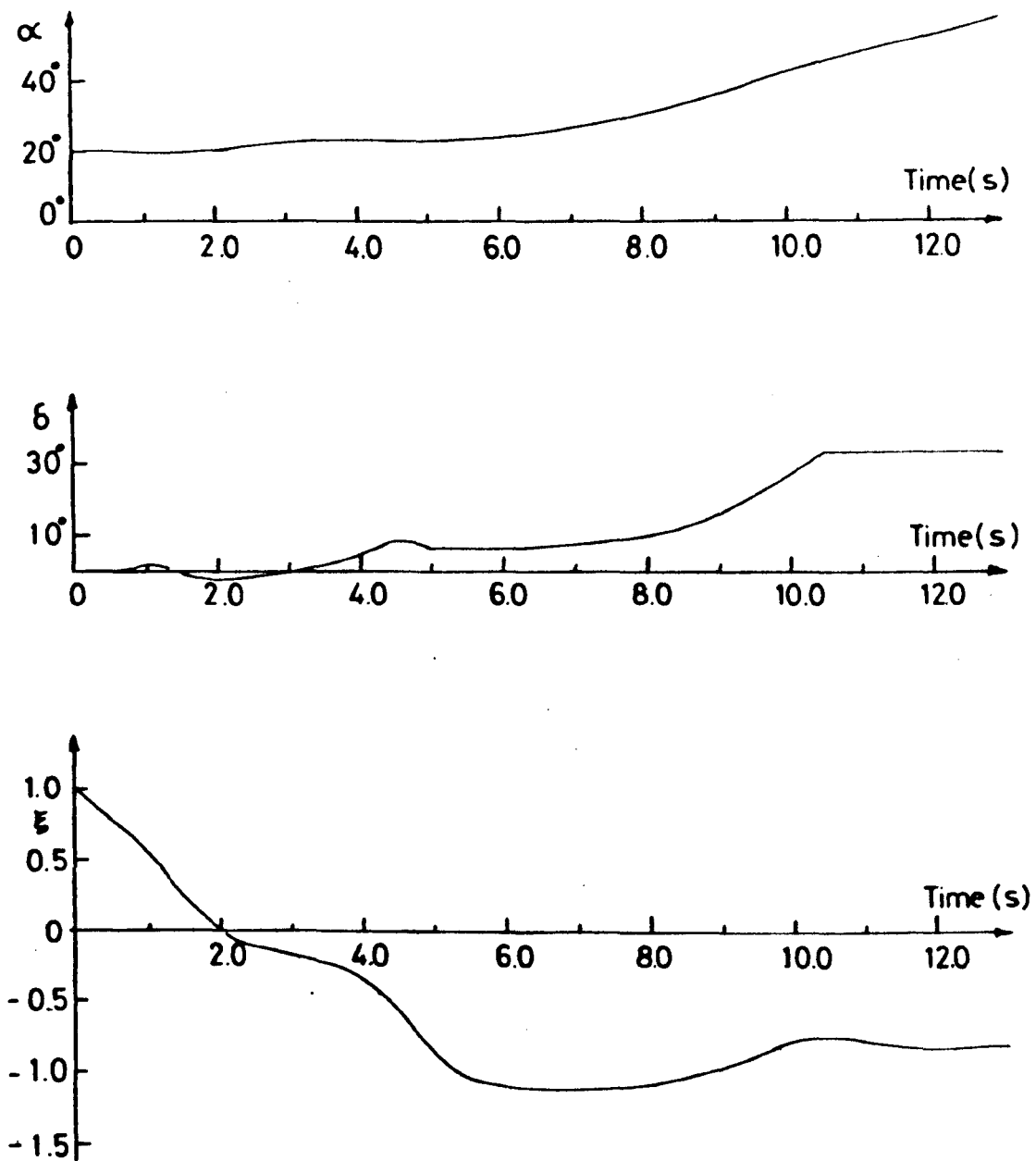


Figure 7.8 Record from simulation for: $\lambda/L = 1.6$, $F_{no} = 0.43$
 $\frac{1}{4}$ depth rudder, $C_s = 3^\circ/\text{sec}$. full-scale, no
time delay = 3 secs model scale

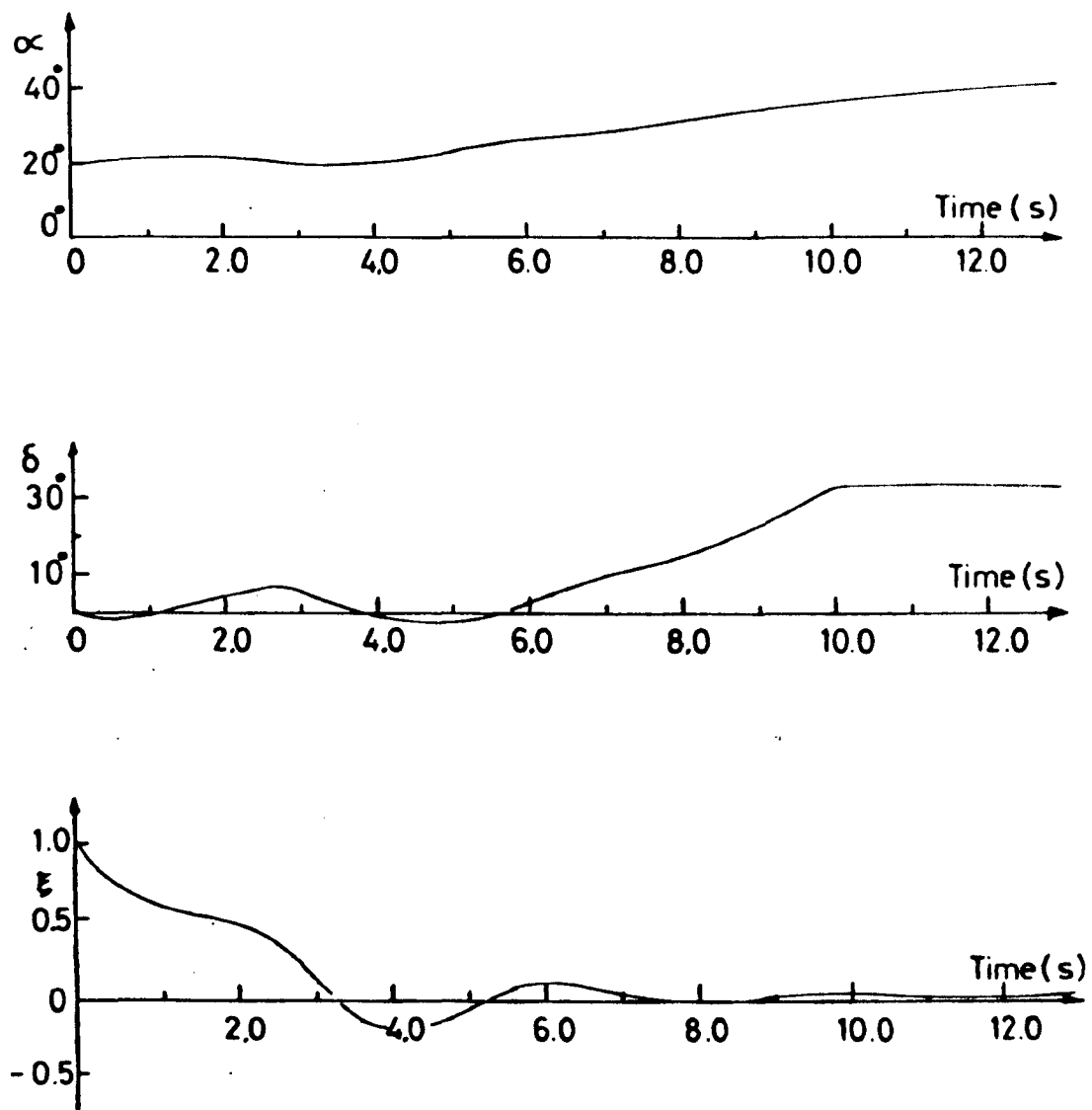


Figure 7.9 Record from simulation for: $\lambda/L = 0.9$, $F_{no} = 0.33$
 $\frac{1}{2}$ depth rudder, $C_r = 6^\circ/\text{sec}$. full-scale, no
time delay = 3 secs model scale

This is because the rudder never reaches maximum rate due to the low rate of change of desired rudder angle. Over the complete range of λ/L 's there is only a marginal reduction in the size of the broaching region when increasing the maximum rudder rate. This is contrary to the findings of Crago who stated in his discussion to Ref. 1 that "if model rudders can be moved at an unrepresentatively high rate, then even a bad hull form can be easily controlled in a severe following sea". This contradiction could be due to two things: (1) Using manual control it may be possible to anticipate a broach and order full rudder which, if applied immediately, may save an otherwise broached situation. This would depend to a certain extent on the ability of the helmsman and is not modelled by the simple autopilot equation used in the simulation. (2) The model tested in Ref. 1 represents a considerably smaller ship with a rudder rate of $3\frac{1}{2}^\circ/\text{sec}$. Since rudder rate scales with $1/\sqrt{L}$ this represents a rate for a 5m long model of $9\frac{1}{2}^\circ/\text{sec}$ compared to that used in the experiments of AMTE(H) of $14^\circ/\text{sec}$. This much lower rate could be below the desired rate which would then mean that an improvement could be made by increasing the actual permitted rate.

The effect of reducing the time lag can be seen by comparing Figures 7.8 and 7.10. Here it can be seen that there is a slight improvement, although a broach still occurs. This is typical of the complete λ/L range where, although in each case a broach does not happen so quickly with the reduced time lag, the actual boundaries of the broaching zones are little changed. Thus, it can be concluded that, although reducing the time lag does help to a certain extent, it is not nearly as good as increasing the size and depth of the rudders.

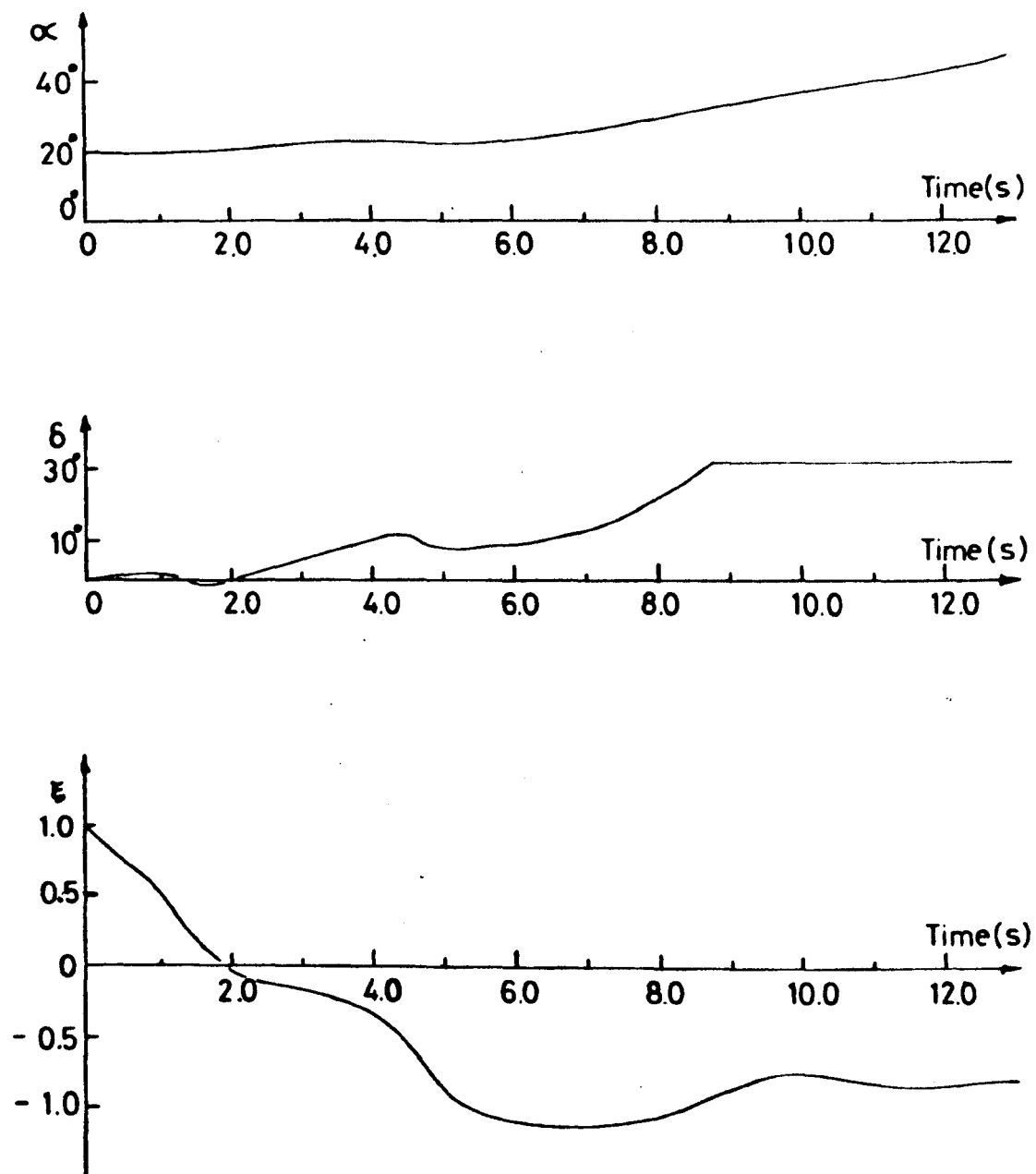


Figure 7.10 Record from simulation for: $\lambda/L = 1.6$, $F_{no} = 0.43$
 $\frac{1}{4}$ depth rudder, $C_s = 3^\circ/\text{sec}$. full-scale, time delay = 1 sec model scale

Chapter 8

DISCUSSION AND CONCLUSIONS

As discussed in the introduction, there were essentially two objectives to this work. (1) To develop a technique for theoretically predicting the broaching zones, and (2) to identify the principle factors affecting the liability of a ship to broach.

Simulation

The method of achieving the first objective was to develop a digital/analogue hybrid simulation using simplified equations. The broaching zones obtained using this method agreed reasonably well with those obtained experimentally, despite the many simplifications and approximations. The most important thing to note, however, is that the simulation predicts the change from standard to half-depth rudder quite well and could, therefore, be used for obtaining minimum rudder size requirements for future designs as proposed in the first chapter. The problems with using this technique are that a digital/analogue hybrid facility is required and that the calm water manoeuvring coefficients must be known. Comparison between two similar proposed designs or rudder configurations, etc., can be made using the techniques developed in Chapter 6, although the limitations here must be borne in mind.

Possible Improvements to the Mathematical Model:

As mentioned above, there are considerable simplifications involved in the simulation method. Probably the most important of these is the neglect of the roll equation, and any improvements should include this. In addition, the equations governing the rudder movement with the first order Padé circuit could be improved. Since the simulation can be run at real time the autopilot equation could be replaced by a human helmsman. This may correspond better to the free running model experiments. However, considerable thought would have to be given as to how to display the course and heading error data to simulate the information available during the experiments. The inclus-

ion of the coupling terms ignored in the present work would be reasonably straightforward. However, it would probably have little effect on the prediction of the broaching zones. Including all the non-linear terms would be a formidable task, requiring a much larger analogue computer and would be unlikely to improve the results since accuracy is limited by the theoretical method of predicting the coefficients.

Possible Improvements to the Coefficient Prediction Method:

Obviously the best way to obtain the coefficients is to run model experiments for each wave condition, self-propulsion speed and ship condition required. This is, however, prohibitively time-consuming and costly, so the theoretical method was developed. The comparison between theoretical and experimental results is made in Chapter 5, where it can be seen that there are substantial differences for some of the coefficients. It is not possible accurately to obtain the coefficients theoretically for the low speed calm water condition using the state-of-the-art knowledge, so it is unlikely that accurate coefficients can be obtained for the wave conditions - even using the calm water experimental results as a basis. Future developments in the calm water manoeuvring field can be applied here if required and these may follow the methods of Chapman [45,46,47] or others [48,49].

Despite the inaccuracies involved with some of the coefficients, the more important ones (N'_α , N'_δ and X'_ξ) are predicted reasonably well and hence it is thought that the present prediction method is adequate for the existing mathematical model. However, if the roll equation were to be included, considerable thought would have to be given to obtaining the additional coefficients, particularly N'_ϕ and K'_α .

Conclusions:

It can be concluded that the simulation method developed here can be used to predict the broaching zone, and the way in which it changes with rudder size, quite well. It is, therefore, adequate to use this to predict whether a proposed design will meet the standard criteria discussed in the introduction and, if not, to determine the increase in rudder size required.

Inclusion of the heel equation and a better modelling of the rudder movement could improve the simulation should this prove necessary. The principle drawback to the method is the need for the calm water manoeuvring derivatives which, at present, can only be obtained by model experiment.

Factors Affecting a Broach

From studying the simulation results it is possible to determine the principle factors involved. One of the most important points is the surging of the ship to wave speed. As described in Chapter 6, if the ship self-propulsion speed is high enough there will be a longitudinal stable equilibrium position. There will also be a region where there is a high positive wave-induced yawing moment and a reduced rudder effectiveness (the critical region). These two regions do not coincide, so if the ship settles into its longitudinal steady state position immediately, the rudder should be able to prevent a broach. (This could happen in regular waves if ship self-propulsion speed is near wave speed.) On the other hand, if it spends a long time in the critical region, a high yaw rate may be set up which cannot be countered by the rudder - resulting in a broach. The length of time spent in the critical region depends on the relative velocity between the ship and the wave and, in regular waves, this will depend on ship self-propulsion speed. However, in irregular waves it will depend to a certain extent on the previous wave.

The assumption that broaching is caused by the ship becoming unstable as measured by the calm water directional stability criteria, has been shown in Chapter 6 to be incorrect.

Since the cause of a broach is principally the imbalance between the high wave-induced yawing moment and the low counteracting moment from the rudder, with reduced effectiveness, a simple way of comparing different conditions is to plot the ratio of required equilibrium rudder angle to heading angle over the non-dimensional wave position.

Using the results from the simulation, together with those from Chapter 6, it is possible to formulate some provisional guidelines for operators and designers in order to reduce the likelihood of broaching.

The limitations of the simulation must be borne in mind - particularly the neglect of the roll equation and the restriction to regular waves. However, it is thought that the guidelines can be applied fairly well to the full-scale condition.

Guidelines for Reducing the Liability to Broach
at the Operating Stage:

The first step is to recognise when the sea is severe enough to cause a broach. The predominant wave length must be of the order of the ship length or greater, with the wave amplitude the order of the ship draft or greater. In these conditions broaching may occur if running in following seas and the safest advice is to avoid that heading. If the ship is not able to avoid being in a following sea (due to operational requirements) there are one or two actions which can be taken in order to reduce its susceptibility to broaching.

The most obvious factor, next to heading angle, which is under the control of the captain, is the ship speed. The situation to try and avoid is being accelerated to wave speed by a steep wave as long as, or longer than, ship length. Thus, if the ship takes on a low frequency surging motion with the maximum speed near to wave speed, then it is time to slow down - before encountering a slightly steeper wave which might just carry the ship along for long enough to be broached. The speed ought to be reduced till the surging motion becomes less noticeable and the waves are overtaking the ship with a reasonably high frequency.

As can be seen from Figures 1.3 and 1.4 no broaching occurs when ship self-propulsion speed is close to wave speed (i.e. faster than the broaching zone) and it may be presumed from this that an alternative to slowing down might be to speed up. Unfortunately, it is unlikely that this would work in a real irregular sea since there is always the possibility of encountering a longer wave resulting in acceleration to this wave's speed and hence broaching. As was noticed in Chapter 6, however, the liability to broach appears to reduce with very long waves so increasing speed may reduce the liability to broach for speeds above about $F_n = 0.6$. This is outwith the scope of the present investigation and is unattainable for conventional high-speed displacement craft.

As discussed in Chapter 6, loss in rudder effectiveness due to emersion is an important factor which can be reduced by submerging the rudders as much as possible. This can be done by either increasing draft or increasing trim by the stern, or both, and could reduce considerably the liability to broach. This is particularly important if the rudders are near the surface in the calm water condition - such as with short spade rudders.

Guidelines for Reducing the Liability to Broach
at the Design Stage:

When a ship is being designed which may have to travel at high Froude numbers (greater than about 0.25) in rough seas, it is necessary to give considerable attention to its susceptibility to broaching. Since the critical wave lengths are dependent on the ship length, shorter ships will encounter more severe conditions and, hence, are more likely to broach. In addition, because time scales with the inverse square root of ship length, a broach will occur more rapidly on shorter craft, resulting in the need for higher rudder rates and shorter time lags.

By far the most important variable at the design stage is the rudder and it has been shown how the loss in rudder effectiveness caused by emersion has an important influence on broaching. The spade rudders common to twin screw ships are prone to emersion in waves, since they are near the calm water line and tend to be short to reduce the bending moment on the stock. Increasing their depth can result in a marked reduction in the liability to broach. However, this may make the ship difficult to dry dock. The method developed in this thesis can be used to determine how big the rudders need to be in order to meet a desired criteria. The single deep skeg-mounted rudder favoured by American destroyers is less likely to emerge and may prove to be better at preventing broaching, although more work will have to be done in this direction.

A reduction in beam over the stern region may decrease the amount by which the stern is lifted by the waves permitting the rudders to emerge. The reduction would have to be continued forward for a short distance and would also have to include a reduction in flare over the

stern region. This could tend to imply that the wider transom-sterned ships may be more vulnerable, particularly if associated with considerable flare to increase deck area aft. The techniques developed in Chapter 6 can be used to compare two similar ships in this respect quite easily.

During a broach the bow is well immersed, while the stern emerges, so the use of a bow rudder may reduce the liability to broach. This has not been studied here and more work is needed before its effects can be quantified.

Increasing the rudder rate can have a slight effect on a ship's susceptibility to broaching. However, when it exceeds the rate of change of desired rudder angle it will not have any effect at all. The optimum rate will depend on ship length, being faster for shorter ships. Reducing the time lag can also have a slight effect on broaching and, again, this is more critical for shorter ships.

Closure

It is thought that this work represents a step forward in isolating the predominant factors contributing to broaching and in quantifying the forces and moments involved. Although considerable work still has to be done, particularly on the inclusion of the roll equation, the simulation method developed here can be used to determine whether a new design will meet a given criteria and to carry out parametric studies in order to reduce its liability to broach.

APPENDIX (A) - CO-ORDINATE SYSTEMS

Since the ship and the wave are both moving independently with respect to the earth, three co-ordinate systems are used. They are: earth fixed, wave fixed and body fixed and are denoted by (x^+, y^+, z^+) , (x^*, y^*, z^*) and (x, y, z) respectively. All three co-ordinate systems are right-handed and all velocity components, force components, etc., are positive in the positive direction of the axis concerned. All rotations, angular velocity components, moment components, etc., are positive in the clockwise sense looking along the positive direction of the axis concerned from the origin, with the angles measured in radians unless otherwise stated.

The wave fixed axis system has its origin on the calm water surface at a crest position with the positive x^* -axis being in the direction of wave travel, as shown in Figure A1. The positive z^* -axis is vertically downwards.

The earth fixed system is chosen such that it coincides with (x^*, y^*, z^*) at $t = 0$, therefore

$$\begin{aligned}x^* &= Ct + x^+ \\y^* &= y^+ \\z^* &= z^+\end{aligned}$$

The body fixed axis has its origin on the centreline amidships at a depth corresponding to the calm water level when the ship is in calm water. The positive x -axis is forward and parallel to the load waterline, while the positive y -axis is to starboard (Figure A2).

Thus,

$$\begin{aligned}x^* &= x \cos \alpha \cos \tau - y \sin \alpha \cos \tau + x^* \\y^* &= y \cos \alpha + x \sin \alpha \\z^* &= z \cos \tau\end{aligned}$$

The heading angle (α) is defined as the angle between the projection of x vertically onto the horizontal plane and x^* as shown in Figure A3. α_d is the desired heading angle and the heading error (ψ) is defined as

$$\psi = \alpha - \alpha_d$$

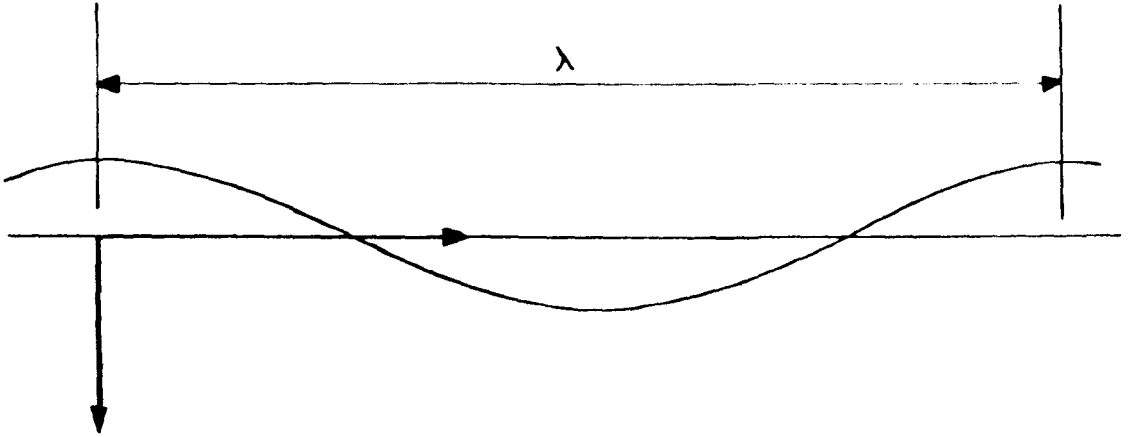


Figure A1 Wave fixed co-ordinate system

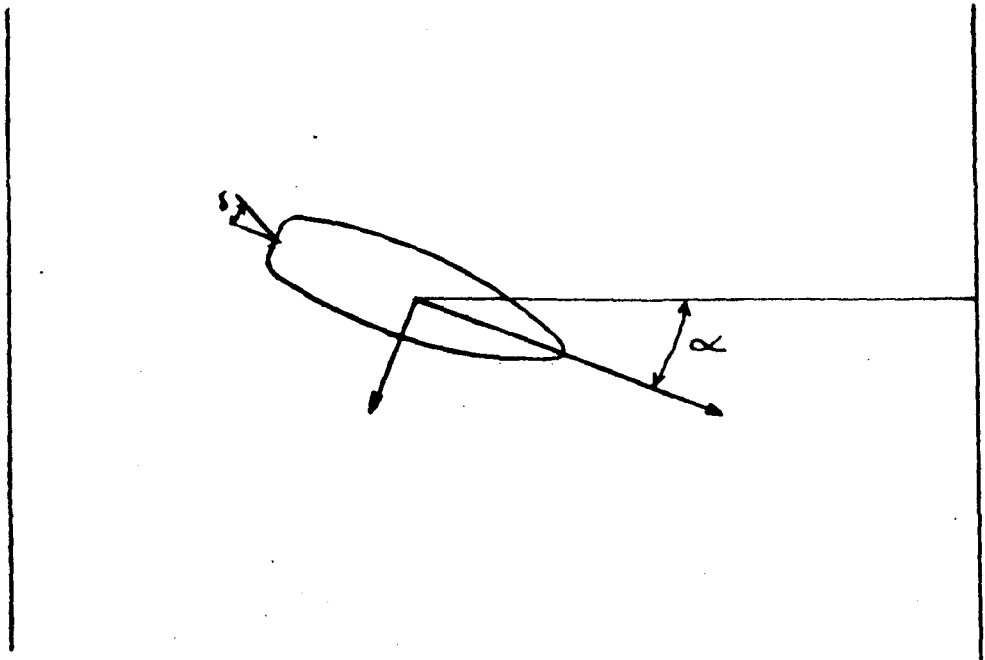


Figure A2 Body fixed co-ordinate system

APPENDIX (B) - NOTATION

A	Wave amplitude
AP	After perpendicular
AR	Effective aspect ratio
AR _C	Effective aspect ratio in the calm condition
AR _w	Effective aspect ratio in the wave condition
B ₁	Local half breadth
b	Half breadth
C	Calm water stability criteria
C	Wave speed
Cal	Added mass coefficient of half a rhombus calculated using the Schwarz-Christofel transformation
C _{Dc}	Cross flow drag coefficient
C _H	Local transverse added mass coefficient
C _L	Lift coefficient
C _r	Maximum rudder rate
D	Draft
D ₀	Initial depth of water in CWC
D _R	Running depth of water in CWC
D _{Rw}	Draft at rudder in wave condition
D _T	z* displacement of bottom of strip
D _{wc}	Draft of strip in wave condition
d _c	Depth of rudder in calm condition
d _w	Depth of rudder in wave condition
F	Force, generally
Fn	Froude number
FP	Forward perpendicular
GM	Transverse metacentric height
g	Acceleration due to gravity
h	Wave height
I _x	Moment of inertia about the x-axis
I _z	Moment of inertia about the z-axis
K	Wave number (= 2π/λ)
K	Component of moment about x-axis
K _p	Roll moment derivative with respect to roll velocity
K _{ṗ}	Roll moment derivative with respect to roll acceleration

$K_{\dot{r}}$	Roll moment derivative with respect to angular velocity
$K_{\ddot{r}}$	Roll moment derivative with respect to angular acceleration
K_v	Roll moment derivative with respect to sway velocity
$K_{\dot{v}}$	Roll moment derivative with respect to sway acceleration
K_{α}	Roll moment derivative with respect to heading angle
K_{δ}	Roll moment derivative with respect to rudder angle
L	Ship length
L	Lift on rudder
l_R	x co-ordinate of rudder
m	Ship mass
$N_{\dot{r}}$	Yaw moment derivative with respect to angular velocity
$N_{\ddot{r}}$	Yaw moment derivative with respect to angular acceleration
N_v	Yaw moment derivative with respect to sway velocity
$N_{\dot{v}}$	Yaw moment derivative with respect to sway acceleration
N_{α}	Yaw moment derivative with respect to heading angle
N_{δ}	Yaw moment derivative with respect to rudder angle
N_{δ_C}	Value of N_{δ} in the calm condition
N_{δ_E}	Calm water value of N_{δ} obtained experimentally
N_{δ_W}	Value of N_{δ} in the wave condition
N_{ϕ}	Yaw moment derivative with respect to roll angle
N^P	Total yawing moment due to pressure
P	Pressure
P_1	Autopilot proportional control constant
P_2	Autopilot rate control constant
p	Roll velocity
\dot{p}	Roll acceleration
r	Angular velocity
\dot{r}	Angular acceleration
S_p	Wetted surface on port side of strip
S_R	Rudder area
S_{R_C}	Rudder area in calm condition
S_{R_W}	Rudder area in wave condition
S_S	Wetted surface on starboard side of strip
T	Draft
U	Ship speed
U_0	Self-propulsion speed
u	Surge velocity
\dot{u}	Surge acceleration

V_R	Relative velocity of water past the rudder
V_S	Ship speed
v	Sway velocity
\dot{v}	Sway acceleration
v_0	Orbital velocity at centre of area of rudder
X	Component of force along x-axis
X_r	Surge force derivative with respect to angular velocity
X_u	Surge force derivative with respect to surge velocity
$X_{\dot{u}}$	Surge force derivative with respect to surge acceleration
X_v	Surge force derivative with respect to sway velocity
X_{δ}	Surge force derivative with respect to rudder angle
X_{ξ}	Wave induced surge force
X_{PROP}	Thrust from the propeller
X^a	Total force in x direction due to acceleration
X_{POINT}^a	Acceleration force in x direction on a point
X_{STRIP}^a	Acceleration force in x direction on a transverse strip
$X_{TRANSOM}^a$	Acceleration force in x direction on the transom
X^P	Total force in x direction due to pressure
X_{STRIP}^P	Pressure force in x direction on a transverse strip
$X_{TRANSOM}^P$	Pressure force in x direction on the transom
x_G	x co-ordinate of the centre of gravity
x_{ws}	x^* co-ordinate of the stern
x_C^*	x^* co-ordinate to centre of strip
x_P^*	x^* co-ordinate to port side of strip
x_{pf}^*	value of x_P^* on free surface
x_S^*	x^* co-ordinate to starboard side of strip
x_{sf}^*	value of x_S^* on free surface
x_T^*	x^* co-ordinate of the stern
Y	Component of force along y-axis
Y_r	Sway force derivative with respect to angular velocity
$Y_{\dot{r}}$	Sway force derivative with respect to angular acceleration
Y_v	Sway force derivative with respect to sway velocity
$Y_{\dot{v}}$	Sway force derivative with respect to sway acceleration
Y_{α}	Sway force derivative with respect to heading angle
Y_{δ}	Sway force derivative with respect to rudder angle
$Y_{\delta C}$	Value of Y_{δ} in the calm condition
$Y_{\delta E}$	Calm water value of Y_{δ} obtained experimentally

Y_{δ_w}	Value of Y_{δ} in the wave condition
Y_{ϕ}	Sway force derivative with respect to roll angle
Y_{in}	In phase component of measured sway force from PMM experiments
Y_{out}	Out of phase component of measured sway force from PMM experiments
Y^a	Total force in y direction due to acceleration
Y_{STRIP}^a	Acceleration force in y direction on a transverse strip
Y^P	Total force in y direction due to pressure
Y_{STRIP}^P	Pressure force in y direction on a transverse strip
$Y(\dot{v})$	Measured sway force due to all sway velocity terms
$Y(\ddot{v})$	Measured sway force due to all sway acceleration terms
Y_0	Sway amplitude of PMM oscillation
z_G	z displacement of centre of gravity

α	Heading angle
α_0	Desired heading angle
α_0	Yaw amplitude of PMM oscillation
$\dot{\alpha}$	Angular velocity
$\ddot{\alpha}$	Angular acceleration
β	Drift angle
γ	Rudder chord
Δ	Displacement
δ	Rudder angle
δ_a	Actual rudder angle
δ_{a_m}	Maximum rudder angle
$\dot{\delta}_a$	Actual rudder rate
δ_d	Desired rudder angle
$\dot{\delta}_d$	Desired rudder rate
δ_{eq}	Equilibrium rudder angle
ϵ	Phase shift
ζ	z co-ordinate of centre of area of rudder
η	Ratio of relative velocity of water past the rudder to the ship velocity
η	Wave elevation
θ	Angle between tangent to the waterline and the centreline measured in such a way that it is negative towards the bow and positive towards the stern
λ	Wavelength

μ_c	Aspect ratio factor for rudder caused by its proximity to the hull in the calm water condition
μ_w	Aspect ratio factor for rudder caused by its proximity to the hull in the wave condition
ξ	Non-dimensional x^* co-ordinate of the stern
ρ	Mass density of water
σ	Clearance between the baseline and the bottom of the rudder
τ	Pitch angle
ϕ	Roll Angle
ψ	Heading error ($= \alpha - \alpha_d$)
$\dot{\psi}$	Heading error rate
ω	Frequency
ω_e	Encounter frequency

Superscript ' indicates that the quantity has been non-dimensionalised as follows:

Non-dimensional mass	$= m' = m / \frac{1}{2} \rho L^3$
Non-dimensional force	$= X' = X / \frac{1}{2} \rho L^2 U^2$
Non-dimensional velocity component	$= v' = v / U$
Non-dimensional angular velocity component	$= r' = r L / U$
Non-dimensional acceleration component	$= \dot{v}' = \dot{v} L / U^2$
Non-dimensional angular acceleration component	$= \dot{r}' = \dot{r} L^2 / U^2$
Etc.	

APPENDIX (C) - SUMMARY OF COMPUTER PROGRAMS

<u>Main Program</u>	<u>Subroutines</u>	<u>Description</u>
FRANK2		Calculates transverse AVM for each station. Input file = Offset data; Output file = AVM data.
	INDAT	Reads in data file
	SHAPE2	Calculates geometric quantities for each segment.
	FIND2	Calculates normal derivatives of logarithmic singularities.
	MATINV	Called by FIND2, inverts matrix by pivot method (Library routine)
DERIV1		Calculates manoeuvring derivations in wave condition. Input files = Offset data, AVM data.
	SUB1	Reads in data and balances ship on wave.
	VAVE	Called by SUB1, calculates hydrostatics.
	BLK1)	These short subroutines are involved with the numerical integration.
	BLK6)	
	BLK8)	
	SUB3	Calculates rudder derivatives.
FORCE3		Calculates Y'_α , N'_α and X'_ξ
		Input files = Offset data, AVM data.
	SUB1	Reads in data and balances ship on wave.
	VAVE	Called by SUB1, calculates hydrostatics.
	BLK1, BLK2,)	These short subroutines are involved with the numerical integration.
	BLK3, BLK4,)	
	BLK5, BLK6,)	
	BLK7, BLK8,)	
	BLK9)	
	BLK10	Calculates longitudinal force
ROOTS1		Calculates roots of differential equations.

<u>Main Program</u>	<u>Subroutines</u>	<u>Description</u>
	CO2AEF	Library routine which calculates the roots of polynomials using the method of Grant and Hitchen.
READ		Reads digitised data from disc, plots records and calculates required values.
	PLT DEV	
	MARGIN	
	PACK IN	
	JBAXES	Library routines which organise plotting of records.
	TITLE	
	JOIN PT	
	ENDPLT	
WAVE5		Digital simulation of surging.
	SUB1	Reads in data and balances ship on wave.
	VAVE	Called by SUB1, calculates hydrostatics.
	SUB2	Calculates transverse AVM.
	SUB3	Calculates rudder derivatives
SAMPLE		Digital program which controls EAI2000 analogue computer for broaching simulation.
		Input files = constant settings; variable settings.
	SETCK	Library routine which initialises EAI2000
	BSIM2	Reads in variable coefficients and organises them in arrays.
	COEFF1	Reads A to D values and uses straight line interpolation to reset D to A's.

+ EAI Hybrid Library routines for altering priority, changing mode of EAI2000 and setting and reading component values.

APPENDIX (D) - PLANAR MOTION MECHANISM ANALYSIS

This appendix deals with the PMM analysis technique used to obtain the results presented in Chapter 5. The data handling procedure is described and this is followed by a brief outline of conventional PMM analysis and its problems. The method used here is then explained, together with examples of some of the results.

Data Handling:

The results were recorded in analogue form at NMI using a Racal 14-channel magnetic tape recorder recording at 1.875 inches per second. They were then digitised and stored on disc by replaying at real time through the A to D converters of the PDP 11/40 at Glasgow University. The sample rate was 8 samples/sec and the data was stored in blocks of 1024 samples. Each run was then checked by plotting on the Tektronix digital plotter to obtain records similar to those shown in Figures D1 to D4. For the lower frequency runs more than one block of 1024 samples was required to cover the whole run.

A computer program was written to analyse the results, but many of the runs were checked manually using both the original U/V records and the plots of the digitised results. Agreement with the computer results was very good.

Conventional PMM Analysis:

Considering the sway force only in the dynamic pure sway condition, the equations of motion are*

$$y = y_0 \sin \omega t$$

$$v = y_0 \omega \cos \omega t \quad \dots \quad D1$$

$$\dot{v} = -y_0 \omega^2 \sin \omega t$$

and the force equation is

$$Y = Y_v v + (Y_{\dot{v}} - m) \dot{v} \quad \dots \quad D2$$

* The method for the sway force in the pure sway experiment is described, but the technique is similar for the other coefficients.

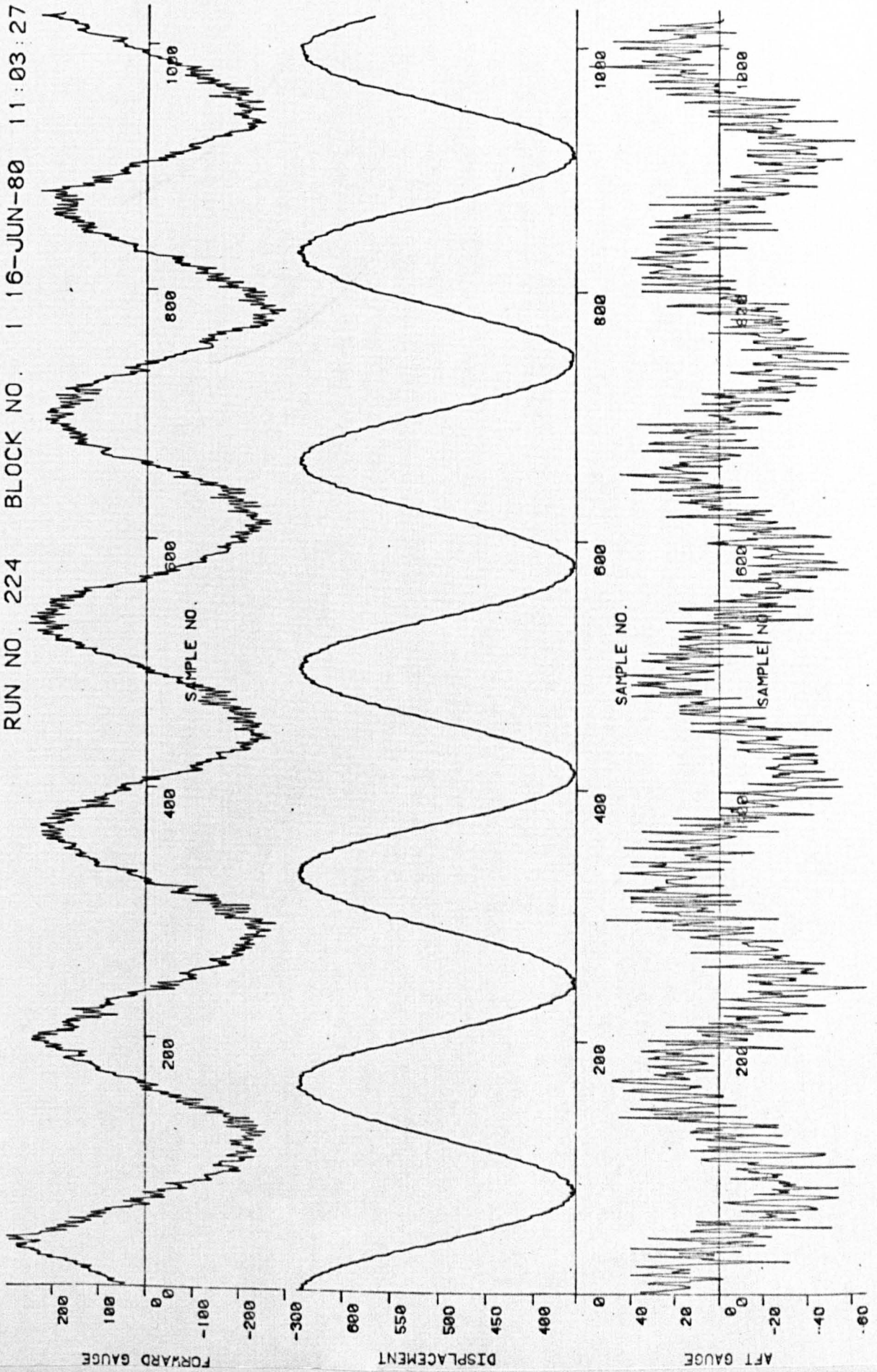


Figure D1 Pure Sway In Calm Water $U_0 = 2.22$ m/s, $\omega = 0.3$ rads/sec, $y_0 = 0.6$ m.

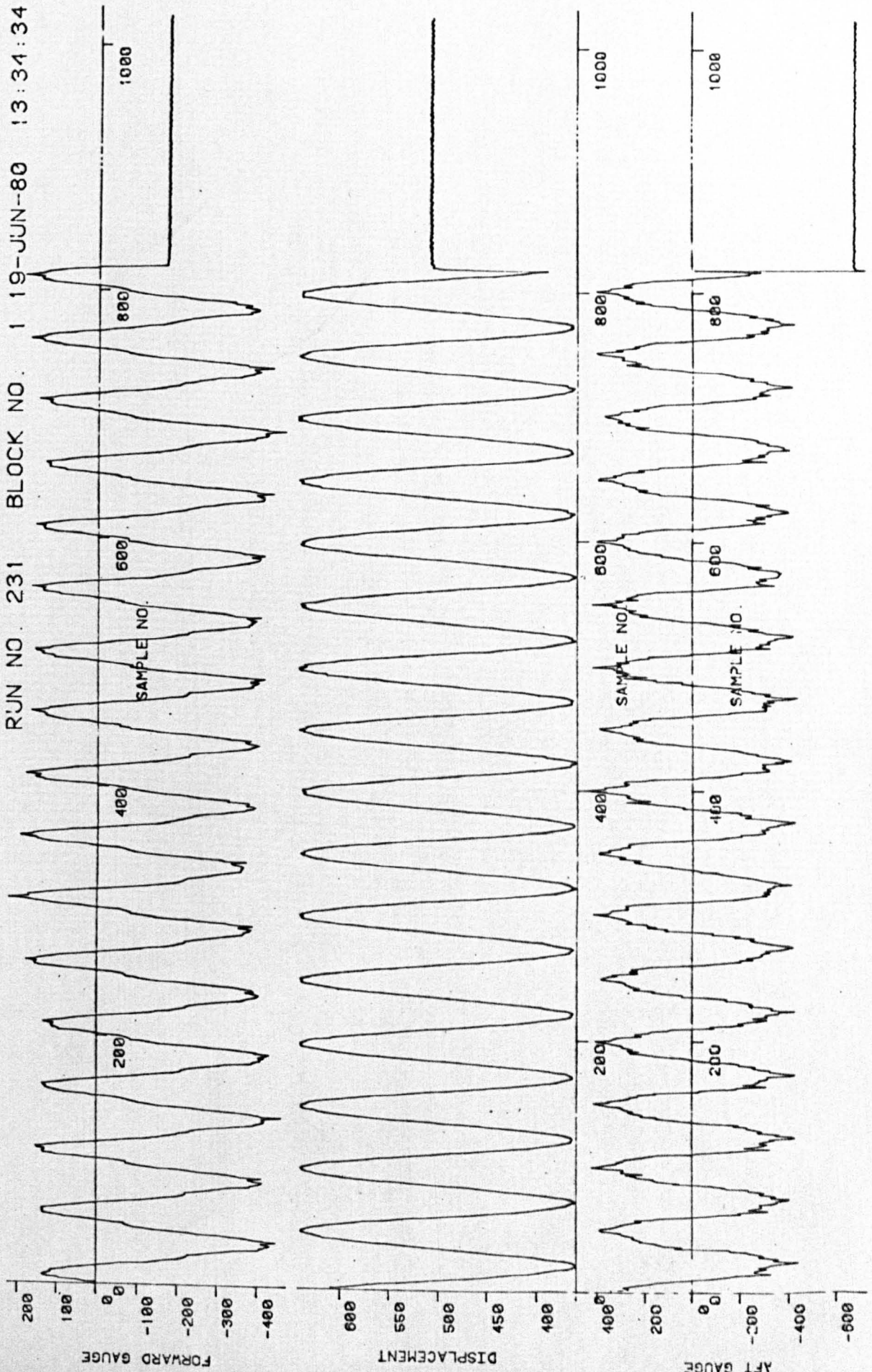


Figure D2 Pure Sway In Calm Water $U_0 = 2.22$ m/s, $w = 1.0$ rads/sec, $y_0 = 0.6$ m

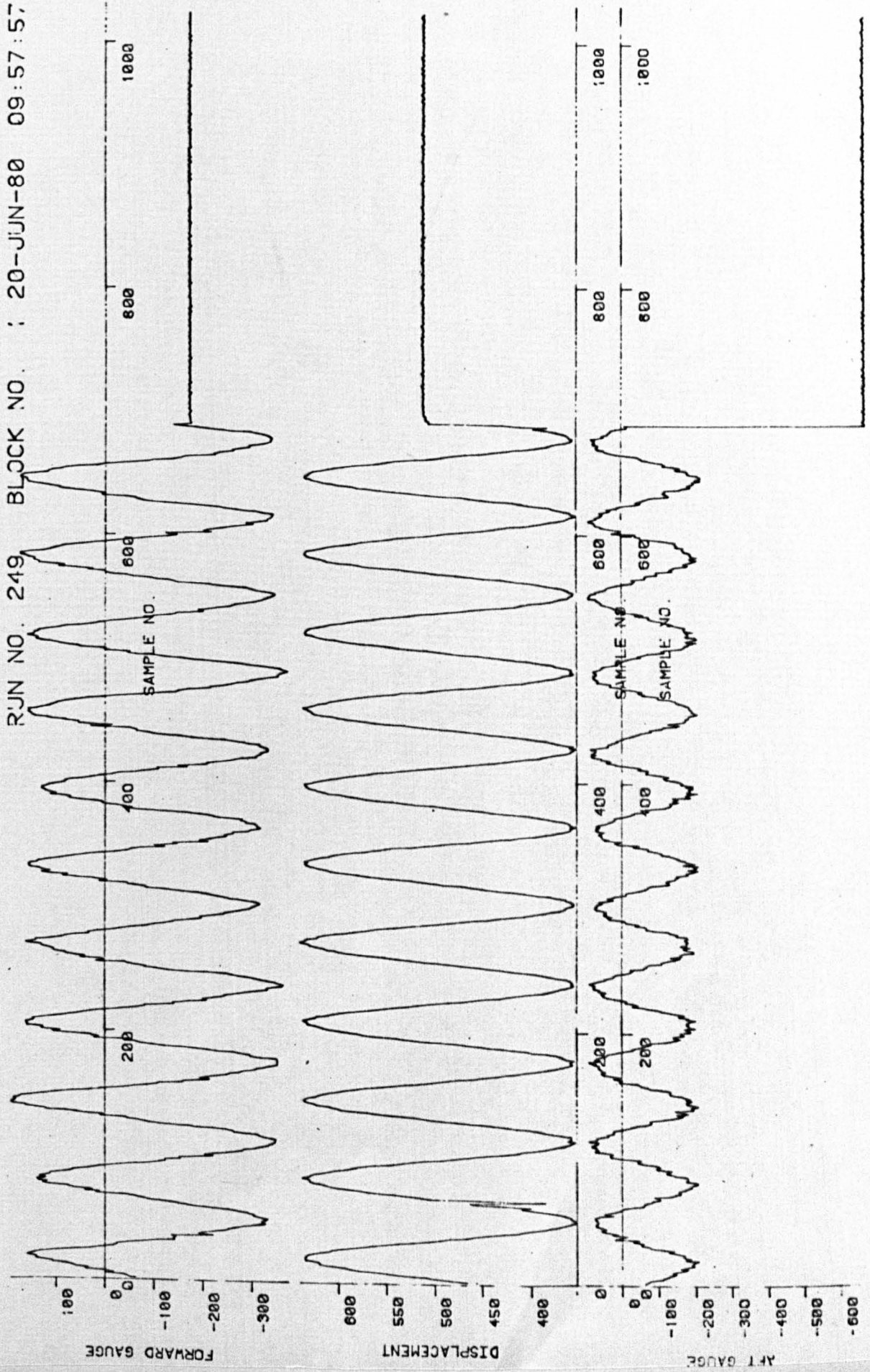


Figure D3 Pure Yaw In Calm Water $U_0 = 2.22$ m/s, $w = 0.8$ rads/sec, $\alpha_0 = 0.216$ rads

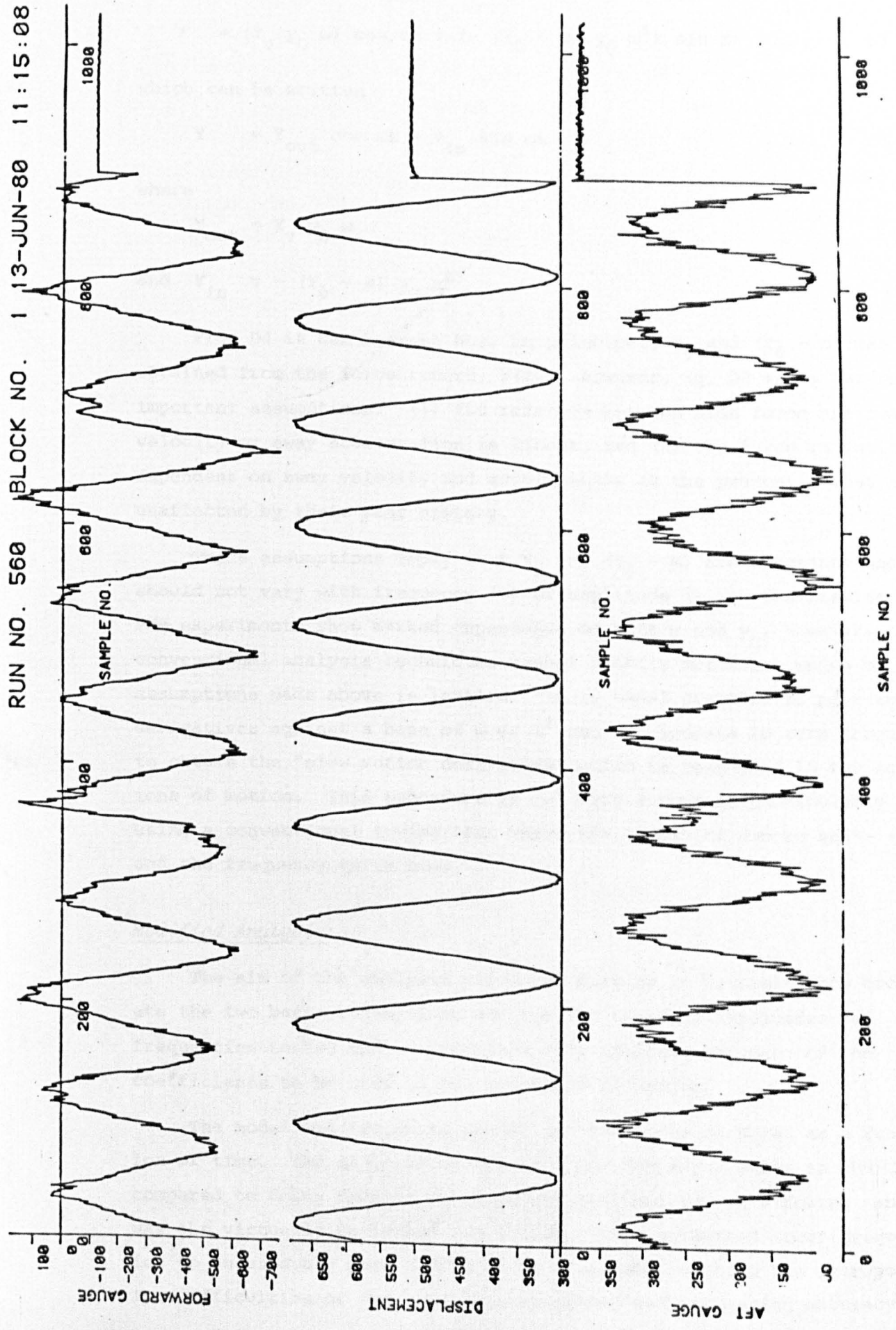


Figure D4 Pure Sway In Waves $U_0 = 2.47 \text{ m/s}$, $\omega = 0.6 \text{ rads/sec}$, $Y_0 = 0.4 \text{ m}$

$$y = (Y_v y_0 \omega) \cos \omega t + (- (Y_v - m) y_0 \omega^2) \sin \omega t \quad \dots \quad D3$$

which can be written

$$Y = Y_{out} \cos \omega t + Y_{in} \sin \omega t \quad \dots \quad D4$$

where

$$Y_{out} = Y_v y_0 \omega$$

$$\text{and } Y_{in} = - (Y_v - m) y_0 \omega^2$$

From D4 it can be seen how, in principal, Y_v and $(Y_v - m)$ can be obtained from the force record, $Y(t)$. However, Eq. D2 makes two very important assumptions: (1) the relation between side force and sway velocity or sway acceleration is linear, and (2) the force is entirely dependent on sway velocity and acceleration at the present moment and unaffected by their past history.

These assumptions imply that Y_v and $(Y_v - m)$ are constants and should not vary with frequency (ω) or amplitude (y_0). The results of PMM experiments show marked dependence on both ω and y_0 , however, and conventional analysis techniques cannot readily determine which of the assumptions made above is invalid. It is usual practice to plot the derivatives against a base of ω or ω^2 and extrapolate to zero frequency to obtain the "slow motion derivative" which is then used in the equations of motion. This procedure is not very accurate, particularly when using a conventional towing tank where the length of run is quite short and the frequency quite high.

Modified Analysis:

The aim of the analysis presented here is to determine how accurate the two basic assumptions are for the range of amplitudes and frequencies tested and to provide a more reliable estimate of the coefficients to be used in the equations of motion.

The model was tested as normal and the force recorded as a function of time. The major advantage of doing PMM experiments in the CWC compared to doing them in the more conventional way in a towing tank was the virtually unlimited run length. This permitted lower frequencies to be used and more cycles to be obtained, reducing the extrapolation difficulties of the conventional method and increasing accuracy.

Rather than assume an equation of the form D2, which immediately invokes the two assumptions to be tested, it is simply stated that the side force will be due to three things: (1) sway velocity, (2) sway acceleration, and (3) memory effects. The make-up of these components is at present unknown and that is what the analysis is directed to determine. The principle behind the analysis technique is to record the force when the contribution of one of the first two of these components is zero and then to vary the contribution of the third (by varying past history) whilst keeping the remaining one constant. The resultant plots give an indication of the importance of the memory effects and the amount of non-linearity separately.

From Eq. D1 it can be seen that at time $t = 0, 2\pi/\omega, 4\pi/\omega, \dots$ the motion becomes

$$v = y_0 \omega$$

$$\dot{v} = 0 = y$$

and at

$t = \pi/\omega, 3\pi/\omega, 5\pi/\omega, \dots$ the motion becomes

$$v = -y_0 \omega$$

$$\dot{v} = 0 = y$$

Thus, any force acting on the model at these times must be due to (1) and (3) above, since there is no sway acceleration. The value of v is easily determined and it is possible to obtain the same value using various combinations of y_0 and ω , i.e. different past histories. Thus, if a plot of this force (denoted $Y^{(v)}$) is made against $v (\pm y_0 \omega)$ for the different amplitudes tested, then the difference between the curves is an indication of the memory effect. The deviation of these curves from a straight line shows the amount of non-linearity. In addition, for the sway velocity only, it is possible to plot the steady state results which have yet another past history. An example of this plot is given in Figure D5, where it can be seen that for this case the memory effect is negligible (at least for the low frequencies), but that non-linearities start to have influence above about $v = 0.2$ m/s. The coefficient, (Y_v) , is obtained by taking the slope of the curve at the origin. The principal objection to this type of analysis is the

fact that by using points much of the data is lost and the result is inaccurate. For the results presented here, the force curves were smoothed using neighbouring samples, reducing irregularities, and the long run time allowed sufficient cycles to be recorded to increase accuracy. If the assumptions discussed above were correct, all the points on Figure D5 would lie on the one straight line and $Y^{(\dot{v})}$ would equal Y_{out} .

It is possible to plot $Y^{(\dot{v})}/y_0 \omega$ against ω^2 as in Figure D6, which corresponds to $Y_{out}/y_0 \omega$ in the conventional analysis and the difficulty of extrapolating to zero frequency can be seen.

If a similar procedure is applied at time $t = 3\pi/2\omega, 7\pi/2\omega, 11\pi/2\omega, \dots$ and at $t = 5\pi/2\omega, 9\pi/2\omega, 13\pi/2\omega, \dots$, then the curve of $Y^{(\dot{v})}$ against \dot{v} can be obtained as in Figure D7. Here it can be seen that both non-linearity and memory effects are negligible over the range tested. This is because all the points lie on one straight line. The slight scatter at the low \dot{v} values is due to the fact that the forces are very small, resulting in a larger percentage error. This is much worse for the plot of $Y^{(\dot{v})}/y_0 \omega^2$ against ω^2 , as the small force is divided by a small number ($y_0 \omega^2$), resulting in a large error. This is shown in Figure D8 where the difficulty of extrapolating the curve to zero frequency can be seen. However, for the more accurate higher frequencies the single straight line parallel to the x-axis can be seen, implying that the coefficient does not vary with frequency or amplitude, i.e. that the two assumptions are correct for this case.

The coefficient ($Y_{\dot{v}} - m$) can be obtained by taking the slope of the line in Figure D7. This line should pass through the origin and the slight offset is attributed to a small error in obtaining $Y^{(\dot{v})}$ from the force record.

Exactly the same procedure can be applied to obtain the moment coefficients from the pure sway records. The pure yawing case is slightly more complex when in the wave condition, due to the dependence of the force on heading angle, as described in Chapter 4. However, the same basic principle holds.

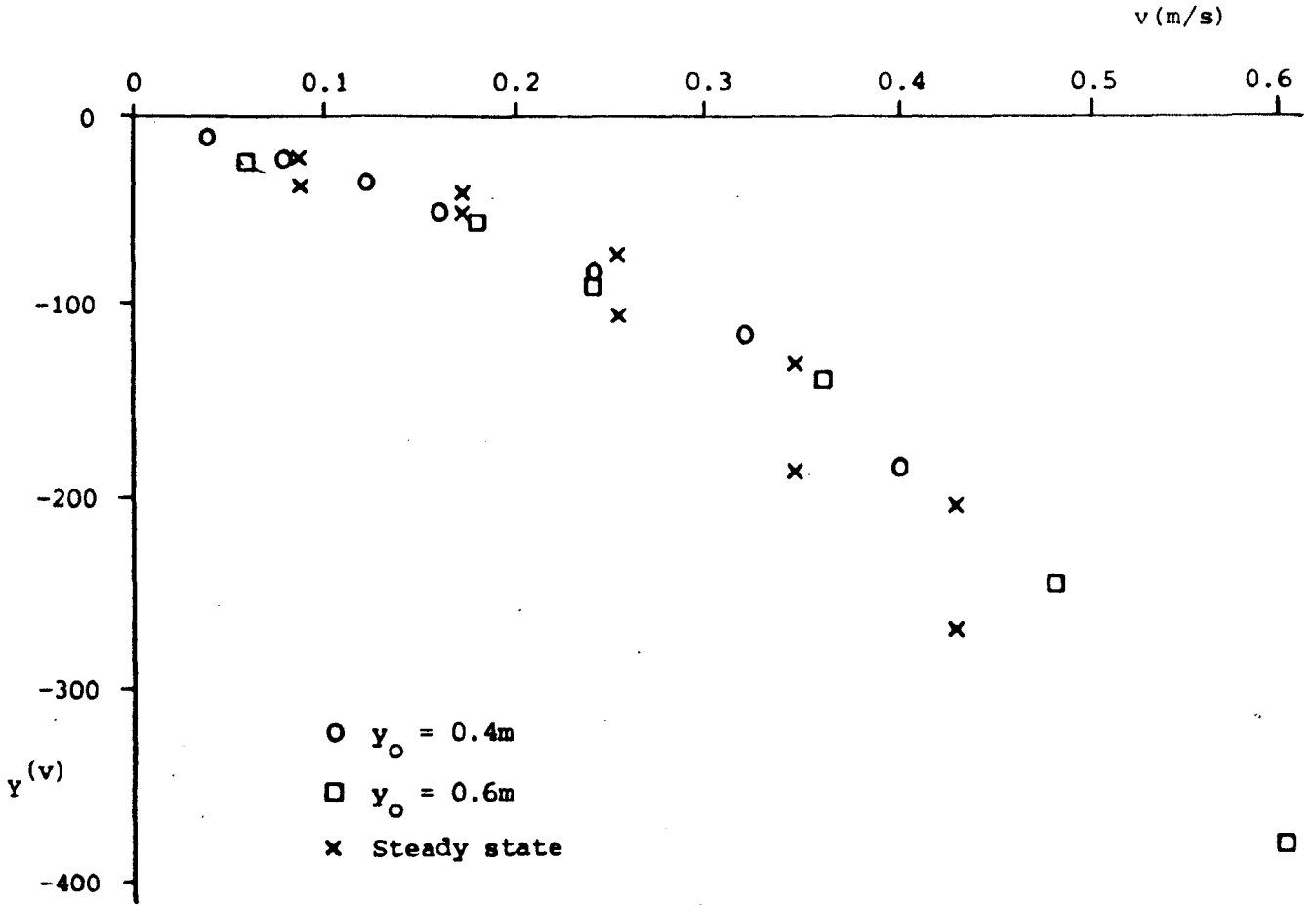


Figure D5 $Y^{(v)}$ for varying v ; high speed calm water

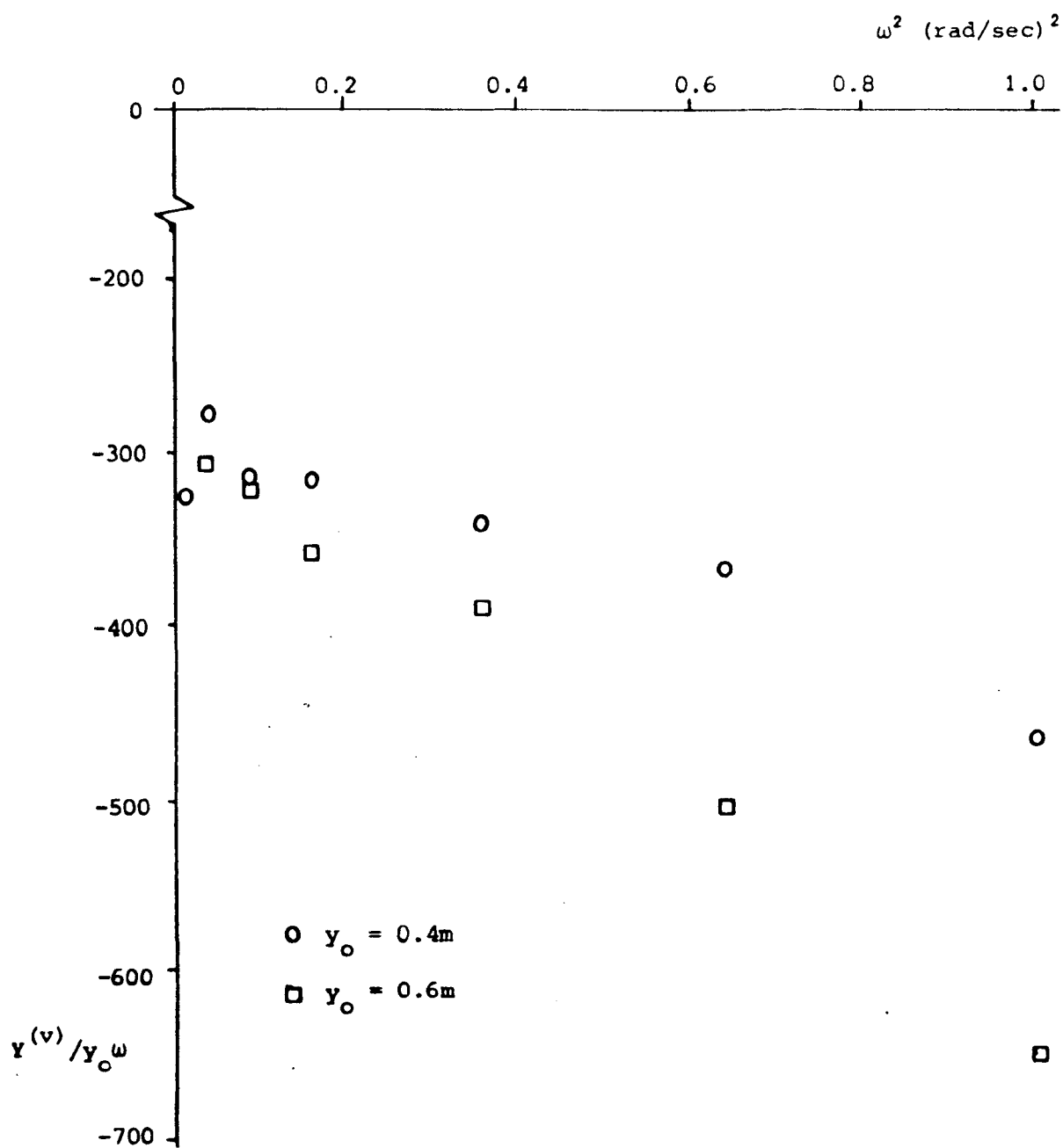


Figure D6 $y^{(v)}/y_0\omega$ for varying ω^2 ; high speed calm water

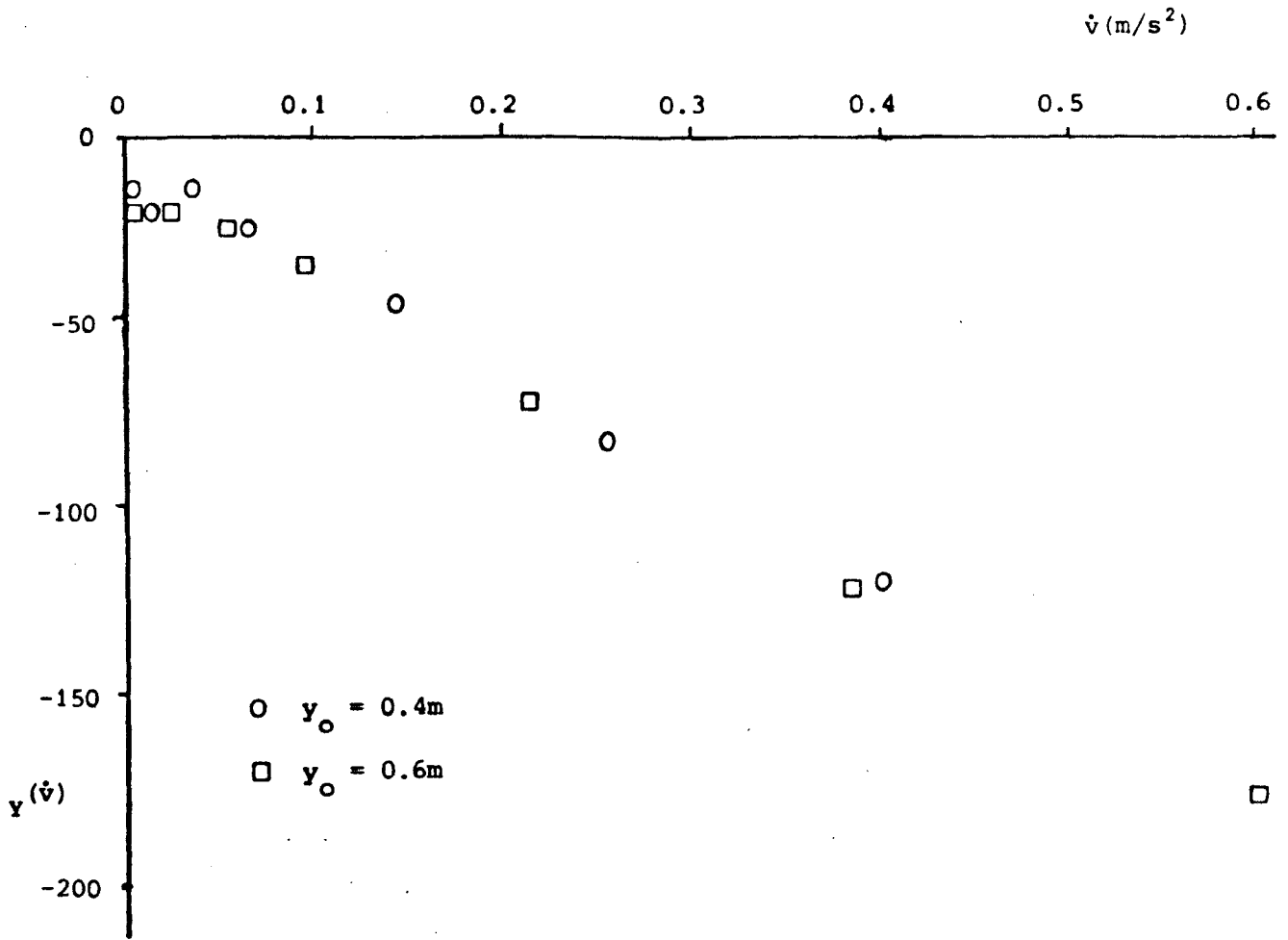


Figure D7 $Y(\dot{v})$ for varying \dot{v} ; high speed calm water

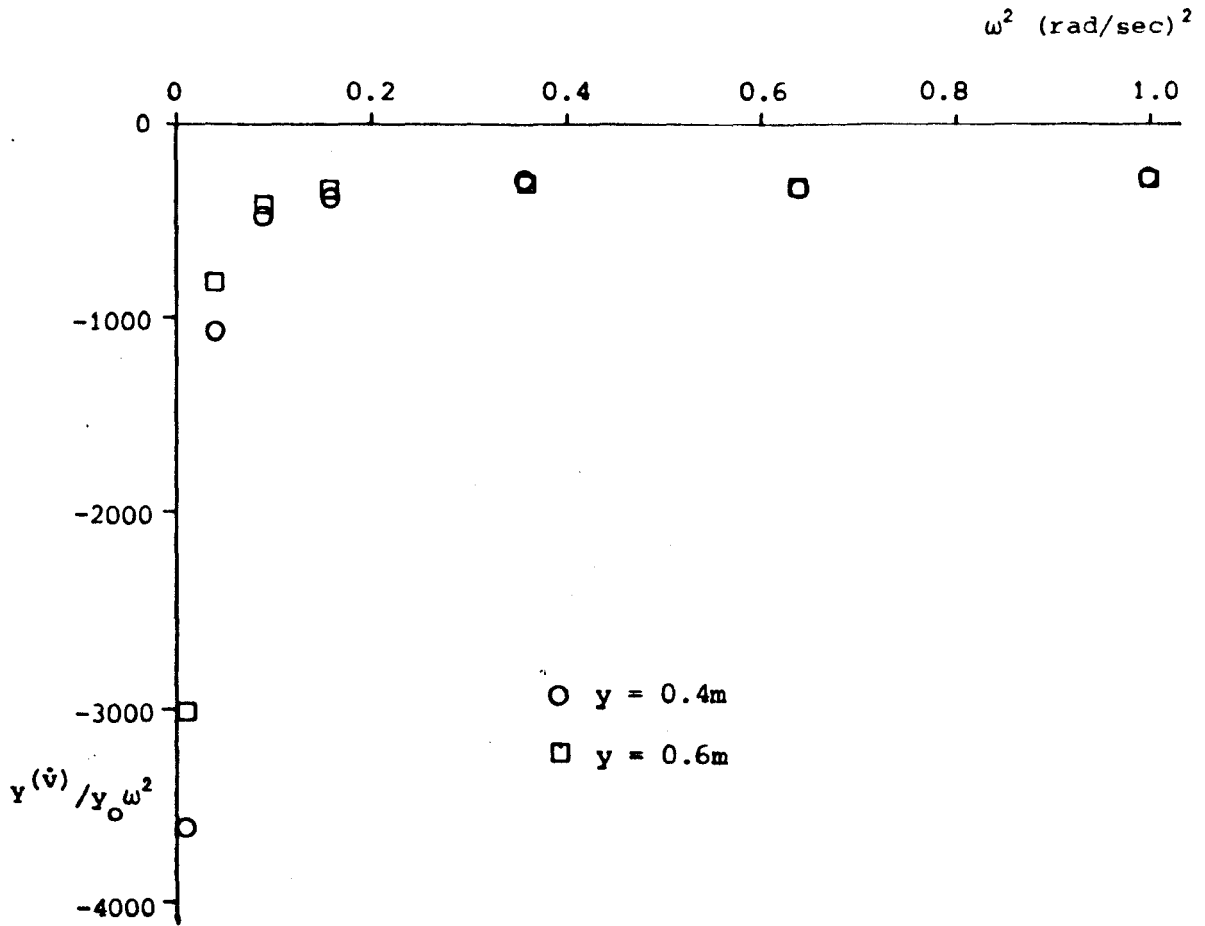


Figure D8 $y(\dot{v})/y_0\omega^2$ for varying ω^2 ; high speed calm water

References

- (1) Du Cane, P., Goodrich, G.J.: "The Following Sea, Broaching and Surging". Trans. RINA Vol.104, April 1962.
- (2) Conolly, J.E.: "Stability and Control in Waves: A Survey of the Problem". Proceedings of Int. Symposium on Directional Stability and Control of Bodies Moving in water, 1972.
- (3) Du Cane, P.: "Model Evaluation of 4 High Speed Hull Forms in Following and Head Sea Conditions". Proceedings Symposium on the Behaviour of Ships in a Seaway, 1957.
- (4) "Fast Container Vessel for Australia". NSMB Report, May 1979.
- (5) Lyster, C.A., Watson, D.G.M. Contributions to reference (24).
- (6) Boese, P.: "Steering a Ship in a Heavy Following Seaway". Institut fur Schiffbau, Hamburg University, March 1970. DRIC Translation No.5700.
- (7) Paulling, J.R., Wood, P.D.: "Numerical Simulation of Large-Amplitude Ship Motion in astern seas". Seakeeping 1953-1973, SNAME Publication, 1974.
- (8) Paulling, J.R., Oakley, O.H., Wood, P.D.: "Ship Capsizing in Heavy Seas; the correlation of theory and experiments". Int. Conf. on Stability of Ships and Ocean Vehicles, University of Strathclyde, 1975.
- (9) Davidson, K.S.M.: "A Note on the Steering of Ships in Following Seas". 7th Int. Congress of Applied Mechanics - London, 1948.
- (10) Eda, H.: "Directional Stability and Control of Ships in Waves". J. of Ship Res., September, 1972.
- (11) Eda, H.: "Yaw Control in Waves". Proceedings of Int. Symposium on Directional Stability and Control of Bodies moving in water, 1972.
- (12) Eda, H., Crane, C.L.: "Steering Characteristics of Ships in Calm Water and Waves". SNAME Vol.73, 1965.
- (13) Rydill, L.F.: "A Linear Theory for Steered Motion of Ships in Waves". Trans. RINA 1959.
- (14) Boese, P.: "Steering a Ship in a Heavy Following Seaway". DRIC Transl. No.2807.
- (15) Wahab, R., Swaan, W.A.: "Course-keeping and Broaching of Ships in Following Seas". J. of Ship Res., April 1964.
- (16) Grim, O.K.: "The Ship in a Following Sea (Das Schiff in von achtern auflaufender See)". DTMB translation 313, February 1965.

- (17) Grim, O.K.: "Surging Motion and Broaching Tendencies in a Severe Irregular Sea". Davidson Laboratory Report R-929, November 1962.
- (18) Hamamoto, M.: "On the Hydrodynamic Derivatives for the Directional Stability of Ships in Following Seas (Part 1)". J. of Soc. of NA of Japan, Vol.130, 1971.
- (19) Hamamoto, M.: "On the Hydrodynamic Derivatives for the Directional Stability of Ships in Following Seas (Part 2)". J. of Soc. of NA of Japan, Vol.133, 1973.
- (20) Nicholson, K.: "Some Parametric Model Experiments to Investigate Broaching-to". International Symposium on the Dynamics of Marine Vehicles and Structures in Waves, London, April 1974.
- (21) Renilson, M.R.: "A Note on the Analysis of AMTE(H) Broaching Records". University of Glasgow, Naval Architecture and Ocean Engineering, Report No. NAOE-HL-80-25, 1980.
- (22) Renilson, M.R.: "Broaching in a Heavy Following Sea". The Motor Ship, September, 1980.
- (23) Hawes, A.P.A.: "Icing and Broaching Experienced Onboard HMS Jaguar off Iceland". AMTE(H) TM80015, 1980.
- (24) Renilson, M.R., Driscoll, A.: "Broaching - An Investigation into the Loss of Directional Control in Severe Following Seas". RINA Spring Meetings, 1981.
- (25) Abkowitz, M.A.: "Stability and Motion Control of Ocean Vehicles". Pub. MIT Press, 1969.
- (26) Principles of Naval Architecture, Ed. J.P. Comstock, SNAME New York.
- (27) Frank, T., Loeser, D.J., Scragg, C.A., Sibul, O.J., Webster, W.C., Wehausen, J.V.: "Transient-Manoeuvre Testing and the Equations of Manoeuvring". 11th Symposium Naval Hydrodynamics.
- (28) Gill, A.D.: "The Analysis and Synthesis of Ship Manoeuvring". Trans. RINA 1979.
- (29) Booth, T.B., Bishop, R.E.D.: "The Planar Motion Mechanism". A.E.W. Crown Copyright, 1973.
- (30) Schiff, L.I., Gimprich, M.: "Automatic Steering of Ships by Proportional Control". Trans. SNAME 1948.
- (31) Wylie, C.R.: "Advanced Engineering Mathematics". Pub. McGraw-Hill Inc.
- (32) Clark, D.: "Some Aspects of the Dynamics of Ship Steering". PhD. Thesis University of London, 1976.
- (33) Atlar, M.: "Frank Close-Fit Computer Program for the

Calculation of Added Mass and Damping Coefficients of Oscillating Cylinders". University of Glasgow, Naval Architecture and Ocean Engineering, Report No. NAOE-HL-81-09, 1981.

(34) Milne-Thompson, L.M.: "Theoretical Hydrodynamics". Pub. Macmillan and Co. Ltd., 1955.

(35) Clark, D.: "A Two-Dimensional Strip Method for Surface Ship Hull Derivatives: Comparison of Theory with Experiments on a Segmented Tanker Model". J. Mech. Eng. Sci. 1972.

(36) Renilson, M.R.: "An Investigation of the Heel-induced Yaw, Moment and Sway Force on a Displacement Vessel Under Way". University of Glasgow, Naval Architecture and Ocean Engineering, Report No. NAOE-HL-79-15, 1979.

(37) Renilson, M.R.: "The Effect of Forward Motion in Following Regular Waves on the Transverse Stability of a Displacement Vessel". University of Glasgow, Naval Architecture and Ocean Engineering, Report No. NAOE-FYP-78-07, 1978.

(38) Renilson, M.R.: "Preliminary Experiments to Investigate Heel Induced Yaw Moment on a Displacement Vessel Under Way". University of Glasgow, Naval Architecture and Ocean Engineering, Report No. NAOE-HL-79-07, 1979.

(39) Hogben, N.: "The 'Wavedozer': a Travelling Beam Wavemaker". 11th Symposium on Naval Hydrodynamics, 1976.

(40) Standing, R.G.: "Proving Trials of the Wavedozer, a Travelling Beam Wavemaker". NPL Report Ship 195, 1976.

(41) Driscoll, A., Renilson, M.R.: "The Wavedozer, a System for Generating Stationary Waves in a Circulating Water Channel". AMTE(H) TM 80013, 1980.

(42) Steele, B.N., Turner, R.T.: "Design and Construction of the NPL Circulating Water Channel". Symposium on the Expt. Facilities for Ship Research in Great Britain, May 1967.

(43) Gill, A.D., Price, W.G.: "Determination of the Manoeuvring Derivatives of a Ship Model Using a Horizontal Planar Motion Mechanism in a Circulating Water Channel". Trans. RINA, 1977.

(44) Smith, R.: "Analogue Computer Programming Manual Vol. II Advanced Techniques". Pub. Electronic Associates Limited Burgess Hill, Sussex.

(45) Chapman, R.B.: "Prediction of Free Surface Effects on Ship Manoeuvring". Eleventh Symposium on Naval Hydrodynamics, London 1976.

(46) Chapman, R.B.: "Numerical Solution for Hydrodynamic forces on a Surface-Piercing Plate Oscillations in yaw and sway". 1st Int. Conf. on Numerical Ship Hydrodynamics,

October 1975.

(47) Chapman, R.B.: "Free-Surface Effects for Yawed Surface-Piercing Plates". J. of Ship Res. Vol.20, 1976.

(48) Kasai, H.: "A Semi-empirical Approach to the Prediction of Manoeuvring Derivatives (1st Report)". Trans. of the West Japan Soc. of NA's, No.58, August 1979.

(49) Yumuro, A.: "Influences of Propeller and Rudder on Manoeuvring Stability Derivates". Naval Architecture and Ocean Engineering, Vol.16, 1978.

Bibliography

The following is a general bibliography of some of the work made use of that is not directly referred to in the Text. It is grouped alphabetically by first named author in general subject headings.

General Seakeeping

Bishop, R.E.D., Price, W.G., Tam, P.K.Y.: "A Unified Dynamic Analysis of Ship Response to Waves". Trans, RINA 1977.

Brooks Peters, J.: "Digital Synthesis of Modelled Irregular Seaway Time Histories". Proceedings 18th General Meeting of the ATTC Vol.2, Annapolis, Maryland, 23-25 August, 1977.

Faltinsen, O.M.: "Theoretical Seakeeping, A State of the Art Survey". Int. Symposium on Advances in Marine Technology; at the Norwegian Institute of Technology, June 1979.

Fein, J.A., McCreight, K.K., Kallio, J.A.: "Seakeeping of the SSP Kaimalino". AIAA/SNAME Advanced Marine Vehicles Conference, 1978.

Grim, O.K.: "Motions of a Ship in a Head or Following Wave". Hamburg Model Basin Report 1303.

Grim, O.K.: "The Influence of Speed on Heaving and Pitching Motions in Smooth Water and on the Forces Generated in Head Seas". Hamburg Model Basin, HSUA Report No.1197, October 1959.

Grim, O.K.: "A Method for a More Precise Computation of Heaving and Pitching Motions both in Smooth Water and in Waves". 3rd Symposium on Naval Hydrodynamics, Scheveningen, September 1960.

Heather, R.G., Nichololson, K., Stevens, J.S.: "Seakeeping and the Small Warship". Symposium on Small Fast Warships and Security Vessels Paper 3, March 1978.

Hosoda, R.: "The Added Resistance of Ships in Regular Oblique Waves". Selected Papers from the Journal of the Society of Naval Architects of Japan, Vol.12, 1974.

Kjeldsen, S.P., Myrhaug, D.: "Breaking Waves in Deep Water and Resulting Wave Forces". Norwegian Maritime Research, No.2, 1979.

Lloyd, A.R.J.M.: "The Hydrodynamic Performance of Roll Stabiliser Fins. AEW Report 8/73 (Unclassified).

Lloyd, A.R.J.M., Brown, J.C., Anslow, J.F.W.: "Motions and Loads on Ship Models in Regular Oblique Waves". RINA Spring Meeting, 1979.

Loukakis, T.A.: "Computer Aided Prediction of Seakeeping Performance in Ship Design". MIT Department of N.A. and M.E. Report No.70-3, August 1970.

McCreight, W.R.: "Exciting Forces on a Moving Ship in Waves". MIT Phd Thesis, September 1973.

Murdey, D.C.: "Experimental Techniques for the Prediction of Ship Seakeeping Performance". Int. Symposium on Advances in Marine Technology June 1979.

Odabasi, A.Y., Hearn, G.E.: "Seakeeping Theories: what is the choice?" NECIES, November 1977.

Ogilvie, T.F.: "Fundamental Assumptions in Ship-Motion Theory". International Symposium on the Dynamics of Marine Vehicles and Structures in Waves, 1974.

Ogilvie, T.F., Beck, R.F.: "Transfer Functions for Predicting Ship Motions: A review of the theory". Seakeeping 1953-1973, SNAME Pub., 1974.

Salveson, N.: "Second-Order Steady-State Forces and Moments on Surface Ships in Oblique Regular Waves". International Symposium on the Dynamics of Marine Vehicles and Structures in Waves, 1974.

Salveson, N.: "Ship Motions in Large Waves". Symposium on Applied Maths dedicated to the late Professor R. Timman, 11-13 January, 1978.

Schmitke, R.T.: "Comparisons of Theory with Experiment for Ship Rolling in Oblique Seas". Proceedings of 18th General Meeting of the ATTC, Vol.2, 23-25 August, 1977, Annapolis, Maryland.

Schmitke, R.T.: "Ship Sway, Roll and Yaw Motions in Oblique Seas". Trans. SNAME, 1978.

Standing, R.G.: "Application of Wave Diffraction Theory". Int. Journal for Numerical Methods in Engineering, Vol.13, pp.49-72, 1978.

Sugai, K.: "A Model Test on Hydrodynamic Pressures Acting on an Ore-Carrier in Oblique Waves". Int. Symposium on the Dynamics of Marine Vehicles and Structures in Waves, 1974.

Takagi, M.: "An Examination of the Ship Motion Theory as Compared with Experiments". International Symposium on the Dynamics of Marine Vehicles and Structures in Waves, 1974.

Tasai, F.: "On the Swaying, Yawing and Rolling Motions of Ships in Oblique Waves". Selected papers from the Journal of the Society of Naval Architects of Japan.

Tasai, F., Sugimuru, Y., Abe, M., Arakawa, A., Kobayashi, M.: "Model Experiments and Theoretical Calculations in Waves on an Ultra-High Speed Container Ship with Triple Screws". (1972) DRIC Translation No.4832.

Transverse Stability and Capsizing

Baker, G.S., Keary, E.M.: "The Effect of the Longitudinal Motion of a Ship on its Statical Transverse Stability". Trans. RINA 1918.

Barr, R.A.: "Dynamic Stability and Capsizing". Proceedings of the 18th General Meeting of the A.T.T.C. Vol.2, Annapolis, Maryland, 23-25 August, 1977.

Bird, H., Odabasi, A.Y.: "State of Art; Past, Present and Future". International Conference on Stability of Ships and Ocean Vehicles, 1975.

Ferguson, A.M., Conn, J.F.C.: "The Effect of Forward Motion on the Transverse Stability of a Displacement Vessel". Trans. IESS Vol.113, January 1970.

Marwood, W.J., Bailey, D.: "Transverse Stability of Round-Bottomed High Speed Craft Underway". Ship Div., NPL, Report 98, 1968.

Miller, E.R.: "A Scale Model Investigation of the Intact Stability of Towing and Fishing Vessels". International Conference on Stability of Ships and Ocean Vehicles, University of Strathclyde, Glasgow, March 1975.

Millward, A.: "Transverse Stability of a Fast Round Bilge Hull". University of Liverpool Report.

Morrall, A.: "Capsizing of Small Trawlers". Trans. RINA 1979.

Obrastsev, W.B.: "Method of Calculating the Restoring Moment of a Moving Ship". Proceedings of the Leningrad Shipbuilding Institute, translated by the University of Michigan, March 1970.

Obrastsev, W.B.: "Experimental Investigation of Influence of Ship's Speed on its Transverse Stability". Proceedings of the Leningrad Shipbuilding Institute, translated by the University of Michigan, March 1970.

Sobolov, G.V., Obrastov, W.B.: "The Calculation of the Righting Moment of a Moving Ship with an Initial Angle of Heel". Proceedings of the Leningrad Shipbuilding Institute, Translated by the University of Michigan, March 1970.

Suhrbier, K.R.: "An Experimental Investigation on the Roll Stability of a Semi-Displacement Craft at Forward Speed". Symposium on Small Fast Warships and Security Vessels Paper 9, March 1978.

Tsakonas, S.: "Effect of Appendage and Hull Form on Hydrodynamic Coefficients of Surface Ships". SIT Report No.740, July 1959.

Watanbe, I.: "On the Effect of the Forward Velocity on the

Roll Damping Moment". Papers of Ship Research Institute No.51, Tokyo, Japan, February 1977.

General Manoeuvring

Astrom, K.J., Kallstrom, C.G., Norrbin, N.H., Bystrom, L.: "The Identification of Linear Ship Steering Dynamics Using Maximum Likelihood Parameter Estimation". Pub. of the Swedish State Shipbuilding Experiment Tank, No.75, 1975.

Burcher, R.K.: "Developments in Ship Manoeuvrability". Trans. RINA 1972.

Burcher, R.K.: "Model Testing". Proceedings of Int. Symp. on Directional Stability and Control of Bodies Moving in Water, 1972.

Crane, C.L.: "Manoeuvring Trials of 278000-Dwt Tanker in Shallow and Deep Waters". SNAME Annual Meeting, 15-17 November, 1979.

Davidson, K.S.M., Schiff, L.I.: "Turning and Course-Keeping Qualities". Trans. SNAME Vol.54, 1946.

Eda, H., Falls, R., Walden, D.: "Ship Manoeuvring Safety Studies". SNAME Annual Meeting, 15-17 November, 1979.

Fujino, H.: "Directional Stability and Control of a Vessel in Restricted Waters". Proceedings of Int. Symposium on Directional Stability and Control of Bodies Moving in Water, 1972.

Gill, A.D., Price, W.G.: "Experimental Evaluation of the Effects of Water Depth and Speed on the Manoeuvring Derivatives of Ship Models". Trans. RINA 1977, (Supplementary Paper).

Lewison, G.R.G.: "The Development of Ship Manoeuvring Equations". NPL Report SHIP 176, December 1973.

McVoy, J.L.: "Prediction of a Submarines Trajectory by an Approximate Solution to its Equation of Motion". Naval Engineers Journal, August 1979.

Martin, M.: "Analysis of Lateral Force and Moment caused by Yaw during Ship Turning". Davidson Laboratory Report No. R792, March 1961.

Newman, J.N.: "Some Theories for Ship Manoeuvring". Proceedings of Int. Symposium on Directional Stability and Control of Bodies Moving in Water, 1972.

Newman, J.N.: "Theoretical Methods in Ship Manoeuvring". Int. Symposium on Advances in Marine Technology, June 1979.

Newman, J.N.: "Marine Hydrodynamics". MIT Press, 1977.

Nomoto, K.: "Problems and Requirements of Directional Stability and Control of Surface Ships". Proceedings of Int. Symposium on Directional Stability and Control of Bodies Moving in Water, 1972.

Norrbin, N.H.: "Circle Tests with a Radio-Controlled Model of a Cargo Liner". Pub. of the Swedish State Shipbuilding Experiment Tank, No.57, 1965.

Sutherland, W.H., Korvin-Kroukovsky, B.V.: "Some Notes on Directional Stability and Control of Ships in Rough Seas". SIT Report Note No.91, October 1948.

Thurman, G.D.: "Yaw Motion Stability; Twin-Screw Twin-Rudder Ships - Some Model and Ship Results". Proceedings of Int. Symp. on Directional Stability and Control of Bodies Moving in Water, 1972.

Autopilots and Control Theory

Afremoff, A.Sh., Nikolaev, E.P.: "Yawing of a Ship Steered by an Automatic Pilot in Rough Seas". Proceedings of Int. Symposium on Directional Stability and Control of Bodies Moving in Water, 1972.

Fuwa, T., Nimura, T.: "A Consideration on the Extraordinary Response of Model Ship's Automatic Steering System in Following Sea (English Abstract)". 26th General Meeting of Ship Research Institute, 1975.

Koyama, T., Kose, K., Hasegawa, K.: "A Study on the Instability Criterion of the Manual Steering of Ships". Naval Architecture and Ocean Engineering Vol.16, 1978.

Whyte, P.H.: "A Note on the Application of Modern Control Theory to Ship Roll Stabilisation". Proceedings of the 18th General Meeting of the ATTC Vol.2, 23-25 August, 1977, Annapolis, Maryland.

Calculation of Manoeuvring Derivatives

Aklurst, R.: "Calculation of Stability and Control Derivatives for Surface Ships and Application to Ship Design". A.E.W. Technical Memorandum No.26/67, September 1967.

Dawes, J.E.: "Calculation of Slow Motion Derivatives for a Surface Ship Using the IBM 1130 Computer". AMTE Report R41804.

Fedayevsky, K.K., Sobolev, G.V.: "Application of the Results of Low Aspect-Ratio Wing Theory to the Solution of Some Steering Problems". Proceedings Symposium on the Behaviour of Ships in a Seaway, 7-10 September, 1957.

Fuwa, T.: "Hydrodynamics Forces Acting on a Ship in Oblique Towing". J. of the Soc. of NA's of Japan, Vol.134,

December 1973.

Jacobs, W.R.: "Method of Predicting Course Stability and Turning Qualities of Ships". Davidson Laboratory Report 945, March 1963.

Jacobs, W.R.: "Estimation of Stability Derivatives and Indices of Various Ship Forms, and Comparison with Experimental Results". J. of Ship Res., September 1966.

Sundstrom, O.: "Experiments with a Surface-Piercing Flat Plate". Symposium on Small Fast Warships and Security Vessels Paper 9, March 1978.

Sundstrom, O.: "Measurements of Side Forces and Moments on a Ship Model and a Comparison with Some Simplified Theories". The Royal Institute of Tech. in Stockholm - Dept. of Hydrodynamics - TRITA-HYD-78-03. August 1978.

Wu, T.Y., Newman, J.N.: "Unsteady Flow Around a Slender Fish-Like Body". Proceedings of Int. Symp. on Directional Stability and Control of Bodies Moving in Water, 1972.

Planar Motion Mechanism

Bishop, R.E.D., Parkinson, A.G.: "On the Planar Motion Mechanism Used in Ship Model Testing". Trans. R.Soc. Lond. (A), Vol.266, February 1970.

Bishop, R.E.D., Burcher, R.K., Price, W.G.: "The 5th Annual Fairey Lecture, On the Linear Representation of Fluid Forces and Moments in Unsteady Flow". J. of Sound and Vibrations, 29(1) pp113-128, 1973.

Bishop, R.E.D., Burcher, R.K., Price, W.G.: "The Uses of Functional Analysis in Ship Dynamics". Trans. R.Soc. Lond. (A) Vol.332, 1973.

Bishop, R.E.D., Price, W.G., Tam, P.K.Y.: "A Unified Dynamic Analysis of Ship Response to Waves". Trans. RINA, 1977.

Chislett, M.S., Smith, L.W.: "A Brief Description of the HyA Large Amplitude PMM System". Proceedings of Int. Symposium on Directional Stability and Control of Bodies Moving in Water, 1972.

Grim, O.K., Ottmann, P., Sharma, S.D., Wolff, K.: "CPMC - A Novel Facility for Planar Motion Testing of Ship Models". 11th Symposium on Naval Hydrodynamics UCL London, 29th March - 2nd April, 1976.

Zunderdorp, H.J., Buitenhek, M.: "Oscillator-Techniques at the Shipbuilding Laboratory Tech. University - Delft Report No.111, November 1963.